

UNIVERSITÀ DEGLI STUDI DI PADOVA

SCUOLA DI SCIENZE

Dipartimento di Geoscienze
Direttore Prof. Fabrizio Nestola

TESI DI LAUREA MAGISTRALE IN GEOLOGIA E GEOLOGIA TECNICA

FACTORS CONTROLLING THE THICKNESS OF FAULT DAMAGE ZONES IN CARBONATES (CENTRAL APENNINES, ITALY)

Relatore: Prof. Giulio Di Toro
Correlatore: Dott. Michele Fondriest

Laureando: Fabio La Valle

ANNO ACCADEMICO 2018-2019

Contents

RIASSUNTO **5**

ABSTRACT **8**

1 INTRODUCTION AND STATE OF THE ART **11**

1.1 FAULTS IN CARBONATES 13

1.2 FAULT ZONE ROCKS AND FAULT ARCHITECTURE 13

1.2.1 Pulverized rocks and In-situ Shattered Rocks (ISRs) *15*

1.2.2 Mirror-like fault slip surfaces *17*

1.2.3 Fault damage zones *19*

1.2.4 Fault zones scaling laws *21*

2 METHODS **25**

2.1 REMOTE SENSING ANALYSIS 25

2.1.1 Landsat 8 Images *26*

2.1.2 Aster Images *27*

2.2 FIELD GEOLOGY SURVEY TECHNIQUES 27

2.3 KINEMATIC ANALYSIS 28

2.4 OPTICAL AND FIELD EMISSION-SCANNING ELECTRON MICROSCOPY 28

2.4.1 Optical Microscope (OM) *29*

2.4.2 Field-Emission Scanning Electron Microscope (FE-SEM) *29*

3 GEOLOGICAL SETTING **31**

3.1 TECTONIC EVOLUTION OF THE CENTRAL APENNINES 31

3.2 GEOLOGY AND STRUCTURAL SETTING OF THE CENTRAL APENNINES 34

3.2.1 Stratigraphy *37*

3.3 ACTIVE FAULTS IN CENTRAL APENNINES 38

4 RESULTS **43**

4.1 STRUCTURE OF THE DAMAGE ZONE OF THE PIZZOLI-MONTE MARINE FAULT 43

4.1.1 The overstep sector of the Monte Marine Fault zone *50*

4.2 MICROSTRUCTURES OF FAULT ZONE ROCKS 62

4.3 CATALOGUE OF FAULT DAMAGE ZONES IN THE CENTRAL APENNINES 70

4.3.1 Middle-Aterno Valley Fault zone (MAVF) *71*

4.3.2 Morrone Fault zone (MF) *72*

4.3.3 Pescasseroli Fault zone (PF) *74*

4.3.4 Venere Fault zone (VF) *74*

4.3.5 Campo Imperatore Fault zone (CIF) *75*

5 DISCUSSION **77**

5.1 ROLE OF GEOMETRICAL COMPLEXITIES IN CONTROLLING THE ISRS DISTRIBUTION 77
5.2 ROLE OF COMPRESSIVE STRUCTURES IN CONTROLLING THE ISRS DISTRIBUTION 79
5.3 SEISMOGENIC BEHAVIOUR OF THE MONTE MARINE FAULT AND SIMPLE MODEL FOR THE FORMATION OF ISRS 83
5.4 SCALING LAWS OF FAULT DAMAGE ZONES IN THE CENTRAL APENNINES 85
6 CONCLUSIONS 91
6.1 FUTURE RESEARCH 93
REFERENCES 95
References of the catalogue 107
APPENDIX 110
ACKNOWLEDGMENTS 113

Riassunto

Gli Appennini centrali sono una delle aree più sismicamente attive del Mediterraneo (p.e., terremoti storici e strumentali di L'Aquila-Pizzoli Mw 6.7, 1703; Avezzano Mw 7.1, 1915; L'Aquila Mw 6.1, 2009) e la loro continua sismicità è prodotta dalla propagazione di rotture sismiche lungo faglie normali in carbonati (sia dolomie che calcari).

Alcune di queste zone di faglia attive sono ben esposte lungo la catena appenninica all'interno di morfologie calanchive. La più impressionante caratteristica strutturale di queste zone di faglia è la presenza di rocce esplose *in-situ*. Si tratta di rocce ridotte in frammenti con taglia media <1cm e non disturbate da deformazioni per taglio e che, di conseguenza, preservano in alcuni casi strutture sedimentarie quali stratificazione, laminazione etc. La geometria di questi corpi rocciosi "esplosi" *in-situ* e il loro meccanismo di formazione (p.e., durante la propagazione della rottura sismica o durante altre fasi del ciclo sismico) rimangono ancora sconosciuti, anche per la mancanza di dati geologico-strutturali quantitativi. Tra questi ultimi, la distribuzione e i volumi delle rocce esplose *in-situ* lungo faglia ma anche rispetto al rigetto, lunghezza e geometria della faglia. Una più approfondita conoscenza di come vengono prodotte le rocce esplose *in-situ* impatterebbe sulla nostra comprensione della meccanica dei terremoti in carbonati e sugli studi di pericolosità sismica.

Data la mancanza di dati quantitativi sulle rocce "esplose" *in-situ*, gli scopi di questa tesi sono:

1. il rilevamento geologico-strutturale di dettaglio per quantificare la distribuzione e lo spessore delle rocce esplose *in-situ* all'interno delle zone di danneggiamento di faglie attive in carbonati e,
2. l'analisi di telerilevamento associata ad una revisione dei dati da letteratura per determinare le relazioni di scala tra la lunghezza e rigetto di una faglia da un lato, geometria e spessore delle rocce esplose *in-situ* dall'altro.

Questi dati sono indispensabili per costruire qualsiasi interpretazione riguardo la formazione delle rocce esplose *in-situ*. Per raggiungere tali obiettivi:

1. Ho condotto rilievi geologico-strutturali di dettaglio della faglia di Monte-Marine (Appennini Centrali), la cui zona di danneggiamento è caratterizzata dalla presenza di dolomie esplose *in-situ*,

2. Ho effettuato osservazioni microstrutturali al microscopio ottico e a scansione elettronica sia di rocce esplose *in-situ* che di zone di scivolamento di faglie,
3. Ho prodotto un catalogo di sei tra le principali faglie normali e attive degli Appennini Centrali, caratterizzate tutte da zone di danneggiamento spesse fino a centinaia di metri e dalla presenza di rocce esplose *in-situ*.

In particolare, ho cartografato (alla scala 1:500) il settore della faglia di Monte Marine (comuni di Pizzoli e Arischia in provincia de L'Aquila) dove due segmenti della faglia si sovrappongono (zona di possibile *overstep*) e raccolto dati in 26 stazioni strutturali. In quest'area il nucleo della faglia è spesso circa 30 metri mentre la zona di danneggiamento raggiunge quasi 1000 metri di spessore e comprende grandi volumi di rocce esplose *in-situ*, oltre che faglie estensionali minori sintetiche e antitetiche, faglie minori trascorrenti e faglie inverse. Queste ultime sono da me interpretate come strutture Mioceniche-Plioceniche riattivate durante la fase estensionale quaternaria e che hanno interferito con le faglie normali post-orogenetiche di neo-formazione, facendo aumentare il volume delle rocce cataclastiche nelle zone di intersezione. Le sezioni geologiche fornite in questa tesi evidenziano la complessità strutturale dovuta sia al collegamento di due segmenti maggiori della faglia di Monte Marine, che all'eredità dell'inversione tettonica, da compressiva ad estensiva.

Attribuisco il grande spessore della zona di danneggiamento della faglia di Monte Marine ad una combinazione di:

1. complessità geometrica del settore di *overstep*,
2. presenza di strutture compressive ereditate (*thrusts*) e
3. al comportamento sismogenetico della faglia di Monte Marine.

Le cataclasiti e le rocce "esplose" *in-situ* sono infatti attribuite all'effetto cumulativo di fenomeni di esplosione della roccia incassante avvenuti fino a centinaia di metri dalla faglia principale. L'esplosione della roccia è dovuta alla perturbazione del campo di sforzi locale e all'emissione di onde sismiche nel "*near-field*" associati alla propagazione di rotture sismiche sia nella faglia principale (*main shock)* che nelle faglie secondarie che tagliano la zona di danneggiamento (*foreshocks* e *aftershocks*).

Per produrre il catalogo di faglie ho utilizzato immagini satellitari e carte geologiche pubblicate, così da riconoscere dove le morfologie calanchive potessero essere legate alla presenza di rocce esplose *in-situ*. Oltre al caso della faglia di Monte Marine, il catalogo include le zone di faglia della Media Valle dell'Aterno, del Morrone, di Venere, di Campo

Imperatore e di Pescasseroli. Le interpretazioni delle immagini satellitari sono state supportate da rilievi geologico strutturali preliminari.

I principali risultati della tesi includono:

1. la prima determinazione della distribuzione delle rocce della zona di faglia di Monte Marine nel settore di *overstep* e la ricostruzione dell'architettura di faglia;
2. il primo riconoscimento di strutture compressive ereditate nel settore di *overstep* della faglia di Monte Marine e,
3. sfruttando il catalogo delle zone di faglia da me prodotto, la determinazione di una legge di potenza tra lo spessore della zona di faglia, il rigetto e la lunghezza della faglia. In particolare, lo spessore della zona di danneggiamento incrementa con il rigetto ma decresce con la lunghezza della faglia, suggerendo che complessità geometriche di prim'ordine (e.g., *step-overs*) condizionano lo spessore della zona di danneggiamento e la distribuzione delle *in-situ shattered rocks*.

Abstract

The Italian Central Apennines are one of the most seismically active areas in the Mediterranean (e.g., L'Aquila-Pizzoli Mw 6.7, 1703; Avezzano Mw 7.1, 1915; L'Aquila Mw 6.1, 2009). Most of this continuous seismicity is produced by earthquake ruptures propagating along normal faults hosted in carbonate rocks (dolostones and limestones). Some of these active fault zones are well-exposed in the mountain belt within badlands exposures.

The most impressive structural feature of these exposed fault zones is the occurrence of up to hundreds of meters thick *in-situ* shattered rocks (fault rocks reduced in fragments < 1 cm in size on average and affected by negligible shear strain, i.e. they may preserve original sedimentary fabrics such as bedding, laminations etc.). However, both the geometry of these shattered rock bodies and how they have been produced (during seismic rupture propagation or other stages of the seismic cycle) remain largely unknown, also because of the lack of quantitative fault zone structural data (e.g., how shattered fault rocks are distributed along fault strike, how their thickness varies with fault length, displacement, geometry, etc.). A deep understanding of how *in-situ* shattered carbonate rocks are produced may impact our understanding of earthquake mechanics in carbonates and seismic hazard studies.

Given the lack of quantitative data about *in-situ* shattered fault rocks in active fault zones in carbonates, the main goals of this thesis are:

1. the detailed field structural survey to quantify the distribution and thickness of *in-situ* shattered rocks and,
2. the remote-sensing analysis coupled with literature data review to determine, if any, scale relations between fault zone length, displacement, geometry and thickness of *in-situ* shattered fault rocks in carbonates.

Indeed, such dataset is at the base of any model about the formation of the *in-situ* shattered rocks. To achieve these goals:

1. I conducted detailed field structural geology survey of the Monte Marine fault zone (Central Apennines), whose damage zone is characterized by *in-situ* shattered dolostones,

2. I conducted Optical and Scanning Electron Microscopy microstructural investigations of both *in-situ* shattered fault rocks and fault slipping zones,
3. I produced a *catalogue* which includes six main active normal fault zones of the Central Apennines characterized by up to 100s m thick damage zones with *in-situ* shattered carbonates.

In particular, I mapped at 1:500 scale the Monte Marine fault zone (between the villages of Pizzoli and Arischia, 10 km NE of the town of L'Aquila, Italy) where two fault strands overlap and collected data in 26 structural stations. Here, the fault core is ~ 30 m thick while the damage zone reaches ~ 1000 m in thickness and hosts *in-situ* shattered rocks, plus hundreds of minor synthetic and antithetic extensional faults, strike-slip and thrust faults. The latter are interpreted as Miocene to Pliocene structures reactivated during the Quaternary extensional phase and that interfered with newly formed post-orogenic normal faults, thus increasing the cataclastic rock volume in the intersection areas. The geological cross sections provided in this study underlie structural complexities due to the linkage of different fault segments and to the inherited compressional-to-extensional tectonic inversion.

Based on the field observations, I propose that the extraordinary volumes of damage zone in the studied area of the Monte Marine Fault zone result from a combination of

1. geometrical complexities associated to the overstep sector,
2. presence of inherited compressional structures (thrust faults) and
3. seismogenic behaviour of the Master and minor faults.

Cataclasites and *in-situ* shattered rocks are inferred to be the result of shattering up to hundreds of meters far from the Master Fault due to the stress perturbations and the near-field elastic waves induced and released by the propagation of seismic ruptures both along the Master Fault (main shocks) and minor faults cutting the damage zone (aftershocks).

To produce the fault catalogue I used satellite images coupled with published geological maps to recognize where badland-type exposures could be related to the presence of *in-situ* shattered rocks. The Middle-Aterno Valley, the Morrone, the Venere, the Campo Imperatore and the Pescasseroli fault zones were also selected for less detailed structural geology survey to determine the fault damage zone thickness.

The main results of the thesis include:

1. the first description of fault zone rocks distribution of the Monte Marine Fault and the reconstruction of the fault architecture in the overstep sector,
2. the first description of inherited compressional structures within the Monte Marine Fault zone,
3. exploiting the still limited fault catalogue, I find power-law relations between *fault damage zone thickness, fault displacement* and *fault length*. In particular, the thickness of the damage zone increases with fault displacement and slightly decreases with fault length suggesting that first order geometrical complexities (e.g., presence of step-overs) control the thickness of *damage zones*.

1 INTRODUCTION AND STATE OF THE ART

Earthquakes result from ruptures which nucleate and propagate mostly on pre-existing faults with catastrophic strain energy release and radiation of seismic waves (Scholz, 2019). In the last two decades, a lot of attention was spent to investigate on-fault deformation processes within localized fault slip zones, but less was done to characterize off-fault volumetric deformation in seismogenic fault zones (e.g., Cowan, 1999; Faulkner et al., 2008; Wibberley et al. 2008; Rowe and Griffith, 2015). In this thesis I study off-fault damage in seismogenic fault zones cutting carbonates, which are the rocks where most of the seismicity striking the Mediterranean area is hosted.

The occurrence of thick belts (10–100s m) of poorly distorted breccias with an exploded jigsaw textures (i.e., evidence of no shear strain) and cm-to-μm in size rock fragments is common within exhumed carbonate fault zones of various kinematics and becomes almost ubiquitous in seismically active regions such as the Central Apennines of Italy (Agosta et al., 2006; Billi et al., 2003; Demurtas et al., 2016). These fault zone rocks were defined by Fondriest et al. (2015) as *in-situ shattered rocks (ISRs)*. ISRs in carbonates, as other fault zone rocks (e.g., pulverized rocks, Dor et al., 2006a), may represent a potential marker of coseismic damage and a unique source of information regarding earthquake rupture dynamics and energy partitioning (Shipton et al., 2006a).

Nevertheless, till today the spatial distribution of ISRs has been poorly investigated and their occurrence tentatively associated to the quasi-static growth of fault zones during a polyphasic deformation history (i.e., sequential formation and activation of joints, shear fractures, etc.) (e.g., Billi et al., 2003; Agosta and Aydin, 2006). Thus, a deeper understanding of how ISRs are produced in carbonates host rocks and the identification of dynamic signatures within fault zones may (1) impact on our understanding of earthquake and rupture mechanics, (2) constrain earthquake energy budgets (how much energy is dissipated in off-fault damage vs. on-fault slipping processes?) and (3) contribute to seismic hazard studies.

Given the lack of quantitative data about ISRs, in my thesis:

a) I conducted detailed field structural geology survey (1:500 scale) of the fault entire overstep sector of the well-exposed Monte Marine Fault zone (MMF) located near

the village of Pizzoli in the Central Italian Apennines and characterized by the exposure of *in-situ* shattered rocks in dolostones (Fig. 1.1);

b) Starting from aerial and satellite images, I produced a *catalogue* of the main active normal fault zones of the Central Apennines characterized by thick (up to 100s m) damage zones with *in-situ* shattered carbonates. I collected from the literature as much information as possible (e.g., length, total displacement, host rock, historical seismicity) for each fault zone. Of these, four fault zones (Middle Aterno Valley Fault, Morrone Fault, Venere Fault, Pescasseroli Fault) were selected for structural geology surveys, determination of the fault zone thickness in the field and fault rock sampling.

In chapter 5 of the thesis, I also discuss scaling laws among geometrical (fault length, presence of step-overs, thrusts, etc.), lithological (carbonates vs. other lithologies) and seismological (e.g., maximum expected earthquake magnitude) parameters and their relations with the thickness of the *in-situ* shattered rocks.

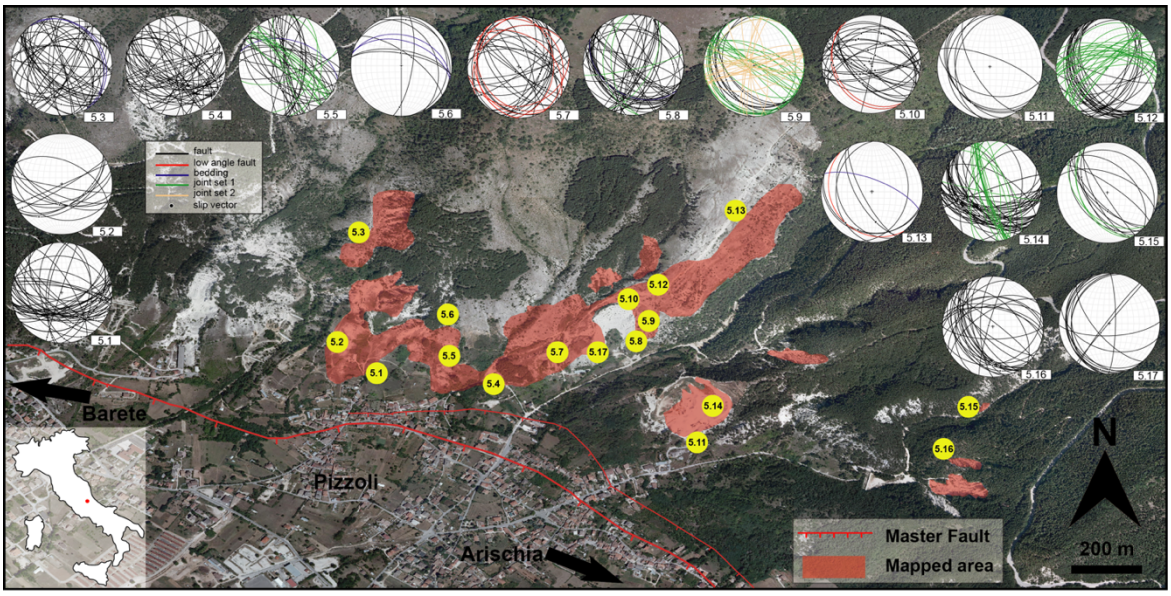


Fig. 1.1 The Monte Marine Fault (MMF). The aerial photo includes the overstep sector of the MMF, with structural stations (yellow in color dots) made during fieldwork and related stereoplots. In red the surveyed area.

1.1 *Faults in carbonates*

Thick carbonates sequences are common within the upper continental crust (< 10 km depth) and many seismogenic sources producing destructive earthquakes worldwide are hosted in such lithologies, especially in the Mediterranean area (Italy, Greece, Turkey; Billi and Di Toro, 2008). In addition, carbonate-hosted fault damage zones are also of great economic and societal interest for their exploitation of natural resources such as oil, gas and water.

Carbonates-hosted fault zone architecture is strictly linked to type of deformation mechanisms and fault slip behaviours (e.g., seismic vs. aseismic) and might be markedly different from the architecture of fault zone cutting siliciclastic rocks. In fact, rock forming carbonate minerals, especially calcite, may easily deform by both cataclastic and especially crystal-plastic processes (e.g., twinning, fluid assisted pressure-solution) also at very shallow depths (<3 km) (Delle Piane et al., 2017 and reference therein). Importantly, and perhaps differently to fault zones cutting siliciclastic or crystalline rocks, faults in carbonates usually include a fault core and a up to hundreds of meters thick damage zone. Here, intensely fractured rock strata occur, including fragmented rocks cut by mirror-like surfaces, possibly associated to seismic ruptures (Billi and Di Toro, 2008).

Because of relevant interest for society (exploitation of hydrocarbon and water reservoirs, earthquake hazard, etc.), an increasing volume of experimental work has been recently dedicated to investigate the frictional properties of carbonate fault rocks and to study the sealing processes in carbonate hosted fault zones. The following sections review the major features of carbonated-hosted faults, focusing on those structures whose knowledge can lead to an improved understanding of earthquake mechanics.

1.2 *Fault zone rocks and fault architecture*

Fully developed fault zones typically include one or more fault cores sandwiched by a damage zone and surrounded by country rocks (Caine, et al., 1996; Wibberley et al., 2008: Faulkner et al., 2010) (Fig. 2a). The *fault core* is the zone where most of fault displacement is accommodated, it can be continuous or patchy and it is commonly composed by fault rocks such as breccias, cataclasites and gouges (Sibson, 1977; Woodcock and Mort, 2008). Conversely, the sandwiching *damage zone* accommodates a limited amount of slip, though fracturing and deformation can be intense.

Mature fault zones are not simple planar features but typically they consist of multiple, usually < 1 cm thick, discrete slip surfaces and slip zones within which displacement and strain are localized. Geometrical complexities in the fault core and the damage zone result from the presence of fault bumps, step-overs and other irregularities inherited from the initial stages of fault evolution and from the host rocks (bedding, stylolitic surfaces, etc.). The rock volumes between adjacent fault segments are referred to as *transfer zones*, *relay ramps*, *fault bridges* and *steps* (Peacock et al., 2000). These high strain zones are supposed to strongly influence the type of fault rocks and their volumetric distribution. In addition, the fault zone architecture seems to vary with the grade of maturity (i.e., displacement) of the fault and with increasing depth (Savage and Brodsky, 2011; Faulkner et al., 2011). Furthermore, mechanical stratigraphy (Michie et al., 2014), porosity and permeability (Caine, et al., 1996; Micarelli et al., 2006; Agosta et al., 2007, 2015), lithologies and lithofacies (Agosta and Aydin, 2006) can play an important role in the heterogeneity of fault zone architecture.

Lastly, even though theoretical (e.g., Fang and Dunham, 2013), seismological (e.g., Chiaraluce, 2012; Valoroso et al., 2013) and seismotectonics (e.g., Lavecchia et al., 2012) studies conclude that the fault zone architecture is a fundamental factor in controlling the evolution of a seismic sequence, to date few attempts have been made to quantify in detail the geometrical complexity and off-fault damage distribution of exhumed seismogenic fault zones (e.g., Faulkner et al., 2003; Dor et al., 2006a, Dor et al., 2006b, Smith et al., 2013; Fondriest et al., 2015; Schröckenfuchs et al.,2015; Demurtas et al., 2016; Billi et al., 2003; Cortinovis et al., 2018).

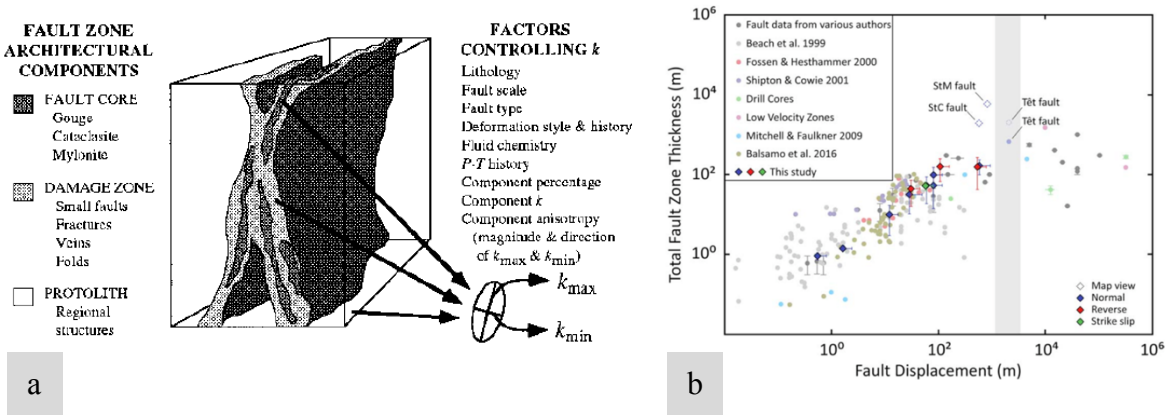


Fig. 1.2 Fault structure: (a) Conceptual model of fault zone with protolith removed. Ellipse represents relative magnitude of the permeability tensor (k) (from Caine et al., 1996). (b) Total fault zone thickness vs. fault displacement: scaling laws define linear scaling for displacement <100, while over 100 m the trend saturates (from Mayolle et al., 2019).

1.2.1 Pulverized rocks and *In-situ* Shattered Rocks (ISRs)

Pulverized rocks are fault zone rocks found up to 100 m away from the fault core of major (i.e., hundreds to thousands kilometers long) strike-slip seismogenic faults cutting silicate-built rocks (e.g. Brune et al., 2001; Dor et al., 2006a). Pulverized rocks are very fine in grain size (<1 mm on average) and show evidence of being shattered *in-situ*. In fact, they do not record evidence of (1) significant shear strain (both at the macro- and micro-scale), (2) grain rotation and (3) wear and rounding, so that the original texture (i.e., grain boundaries in crystalline rocks and foliation surfaces in metamorphic rock) can be preserved (Dor et al., 2006a; Wechsler et al., 2011). Grain size reduction is due to the abundance of tension fractures down to the micrometer in size range, often exploiting mineral cleavage surfaces, while still maintaining the original grain boundaries and rock fabric (Mitchell et al., 2011). Notably, crystals in pulverized rocks yield a powdery rock-flour texture that can be mashed with ones' fingers (Sisk 2007).

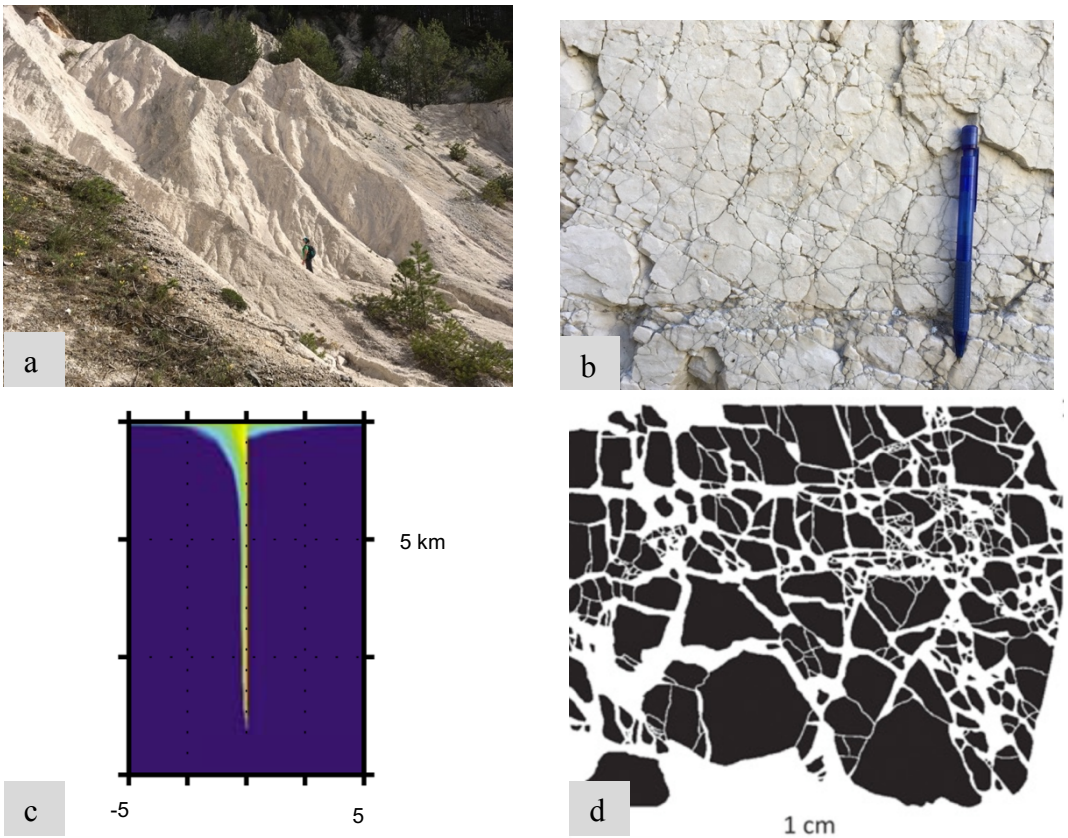


Fig. 1.3 *In-situ* shattering at different scales: (a) ISRs from the footwall of the Monte Marine Fault Zone, Italy. Typical fault zone badland exposure of ISRs in dolostones. (b) Detail of the pervasive fractures of ISRs. (c) Vertical section across the coseismic damage zone of a left-strike slip fault, perpendicular to the fault strike, adapted from Ma and Andrews, (2010). The Damage zone is predicted to have a flower-like shape, broader near the surface and narrow at depth. (d) Tracing of the clasts borders at the thin section scale of an *in-situ* shattered rock, from Fondriest et al., (2017).

In-situ shattered rocks (ISRs) are fault breccias with an exploded jigsaw textures (i.e., evidence of no shear strain) proposed as an equivalent to pulverized rocks for carbonates lithologies, since they are reduced in fragments too (< 1 cm in size on average) but still preserving their original sedimentary fabric (Fig 1.3d) (Fondriest et al., 2015). The ISRs were first recognized in dolostone and limestone both in the Italian Southern Alps and Central Apennines (Agosta and Aydin, 2006; Fondriest et al., 2012; 2015; Demurtas et al., 2016). Indeed, the pervasive fracturing of this fault zone rock is accountable for faster erosion rate resulting in badlands morphology (Fondriest et al., 2012; Demurtas et al., 2016) (Fig. 1.3a).

Sibson (1986) provided a genetic classification of the incohesive faults rocks and proposed that implosion breccia (i.e., breccia with jigsaw texture, low clast deformation, "well sorted" clasts of one composition and an exotic hydrothermal cement), which are the fault product most similar to the ISRs, were produced at dilational jogs by the sudden creation of extra void space during earthquake rupture. However, alternative formation mechanisms for implosion breccias can be envisaged, involving slower aseismic processes (e.g., Cowan, 1999) like the quasi-static growth of fault zones characterized by the sequential formation and activation of joints, pressure solution seams, veins and shear fractures during prolonged polyphasic deformations (e.g., Salvini et al., 1999; Billi et al., 2003; Agosta and Aydin, 2006). Similarly, pervasive fracturing can also occur in the outer, stretched arc of folded competent layer (Fossen, 2016).

Even though the action of water and frost weathering can produce a loose cover of regolith over the outcrops, microstructural evidence (e.g., radial arrangement of fractures) clearly shows that pulverized rocks are the result of mechanical processes rather than a weathering product (Fondriest et al., 2015). However, the specific processes producing pulverized rocks in granitoids and ISRs in carbonates remain debated. Pulverized rocks have an asymmetric distribution along fault strike (Dor et al., 2006a, Mitchell et al., 2011), consistently with the "wrinkle-like pulse" model proposed by Andrews and Ben-Zion (1997). According to the "wrinkle-like pulse" model, pulses of slip velocity can propagate on a planar interface which separates different elastic materials. The strong dynamic reduction of normal stress associated to the propagation of the seismic rupture produces larger displacement in the softer medium resulting in the asymmetric distribution of

pulverized rocks (Andrews and Ben-Zion, 1997). Other mechanism that can produce dynamic reduction of normal stress during earthquakes include acoustic fluidization, collision of rough surfaces and various fluid effects (see Ben-Zion, 2001 for more details). Importantly, the association of pulverized rocks with dynamic rupture propagation during earthquakes has been proposed also by Doan et al., (2009) and Yuan et al., (2011), who experimentally demonstrated that pulverized rocks generation may require very high strain rates (>150 s^{-1}), typically achieved along faults during the propagation of seismic ruptures (rupture velocity ca. 3 km/s).

In addition, rock shattering and pulverization should occur at shallow crustal depths (< 4 km), where confining pressures are low enough to be exceed by off-fault stress perturbations induced by the radiated seismic field. This is confirmed by both field studies (Dor et al., 2009) and experimental observations (Yuan et al., 2011). Similar processes were proposed for the formation of ISR by Fondriest et al. (2015; 2017). The *in-situ* shattered dolostones of the Foiana Fault Zone, for example, are considered the result of off-fault coseismic damage due to the propagation of multiple earthquake ruptures in a relative fluid-poor environment (Fondriest et al., 2017). Nevertheless, several unknowns remain regarding the distribution of pulverized rocks and especially of the ISR, including:

- ISRs distribution along fault strike,
- ISRs petrophysical properties (elastic properties, fracture toughness etc.),
- ISRs distribution, fault geometry and host rocks (presence of step-overs, fault bends, type of host rock lithology, bedding etc.),
- depth at which ISRs were produced.

Importantly, these geological and petrophysical information might unravel the mechanism of formation of ISRs, to which phase of the seismic cycle ISRs are associated, the role of ISRs in the evolution of seismic sequences (foreshocks, mainshock and aftershocks) and, maybe, better constrain the energy budget of earthquakes (e.g., off-fault damage vs. on-fault processes).

1.2.2 Mirror-like fault slip surfaces

Slickensides are the most common marker of fault zones providing, together with slickenlines, the slip direction. Particular kind of slickensides are naturally polished, smooth and glossy surfaces, commonly referred as *fault mirrors* (or *mirror-like slip surfaces)* because of their high visible-light reflectivity (Siman-Tov et al., 2013; Fig. 1.4). Fault mirrors are found in most of fault zones of any tectonic environments and lithology

(e.g., Power and Tullis, 1989 for silicates; Jackson and McKenzie, 1999 and Siman-Tov et al., 2013 for limestones; Fondriest et al., 2012 and Demurtas et al., 2016 for dolostones). In the last years, particular attention has been given to fault mirrors developed in carbonate-bearing rocks. Here, fault mirrors are often lined by brownish flames (typically Fe-oxides and -hydroxides) with lateral continuity in the range 1–20 m (Fondriest et al., 2013). Thanks to laboratory experiments, it has been shown that fault mirrors can form in calcitic and dolomitic gouges when sheared at seismic rates (slip rate > 0.07 m/s under low normal stresses ~1 MPa according to Siman-Tov et al., 2015, up to 20 MPa according to De Paola et al., 2011; 2015; Fondriest et al., 2013; Pozzi et al., 2018) accompanied with thermal decomposition, nanograin coating and sintering or recrystallization reactions (Han et al., 2007; Smith et al., 2013; Siman-Tov et al., 2015). Under these deformation conditions the friction coefficient drops from 0.8 to 0.2 or less and faults are lubricated during earthquakes (Di Toro et al., 2011; De Paola et al., 2011; Fondriest et al., 2013; Smith et al., 2013; 2015; Pozzi et al., 2018). However, tiny structures similar to fault mirrors (10 to 100 μm in length) form also at very low, sub-seismic, slip velocity (~10^{-6} m/s) but large normal stresses (50 MPa) (Verberne et al., 2014).

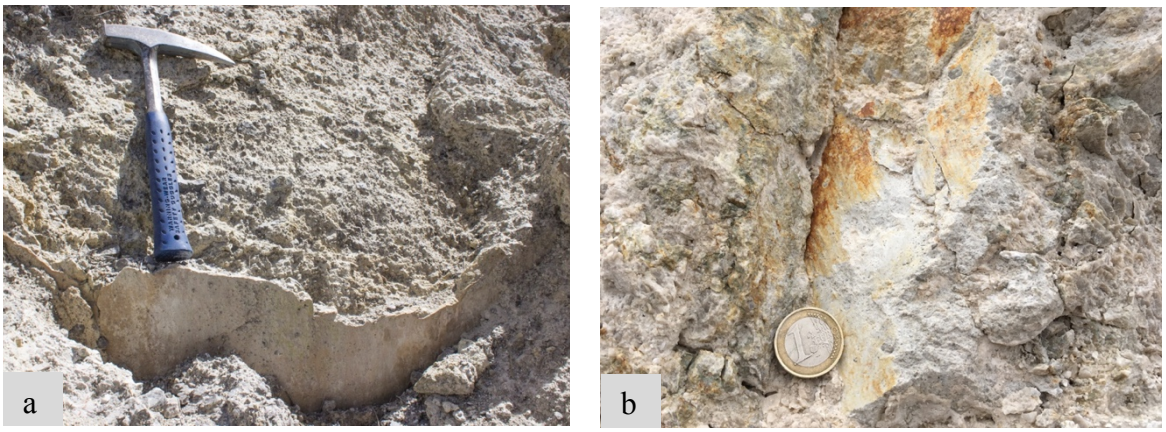


Fig. 1.4 Mirror-like surfaces. (a) Mirror-like slip surfaces from the Monte Marine Fault zone (Central Apennines, Italy). (b) Slip surfaces are typically lined with brownish in colour flames of Fe-oxides and Fe-hydroxides

Atomic force and high resolution scanning and transmission electron microscopy investigations show that the glossy-like slip surface is made by a thin (< 1μm) layer of highly packed particles with a sharp contrast with respect to the deeper layer made by micron-size calcite crystals (Siman-Tov et al., 2013; De Paola et al., 2015; Demurtas et al., 2019a; 2019b). The formation and presence of calcitic or dolomitic nanograins may result in the activation of grain-size and temperature-dependent deformation mechanisms (mainly grain-boundary sliding aided by diffusion creep) which would result in the large decrease

of the friction coefficient measured in the experiments (De Paola et al., 2015; Spagnuolo et al., 2015; Green et al., 2015; Demurtas et al., 2019b).

As stated above, fault mirrors have been produced also in experiments performed at sub-seismic slip rates (~10^{-6} m/s, Verberne et al., 2013), but these fault mirrors do not cut grains. Therefore, the presence of fault mirrors truncating clasts of a carbonatic gouge made also by *in-situ* fragmented ("exploded") grains could provide a criteria for the association of the mirrors to the propagation of seismic ruptures (Fondriest et al., 2015). However, a recent model proposed by (Pozzi et al., 2018) refers to fault mirrors, still produced at seismic slip rates, not as frictional slip surfaces, but rather as a surface that marks a rheological contrast. In fact, according to Pozzi et al. (2018), a sharp strain gradient exists between the zone where slip localizes in the gouge and the outer or deeper layers of the sheared gouge. Clearly, further field and experimental studies are required to constrain better the mechanism of formation of the mirror-like surfaces and if the latter are associated to seismic or aseismic slip (or both) in upper crustal faults.

1.2.3 Fault damage zones

A fault damage zone is defined as *''the volume of deformed wall rocks around a fault surface that results from the initiation, propagation, interaction, and build-up of slip along faults''* (Kim et al., 2004). This definition includes both pre- and syn-faulting damage. Instead, the *seismological damage zone* is the width perpendicularly to the fault surface where 95% of the aftershocks are localized (e.g., Valoroso et al., 2013).

The fault zone, conventionally considered as a planar (tabular in 3-dimension) structure, include volumes of damaged rocks where shear deformation is less intense compared to the fault core (Caine et al., 1996; Shipton and Cowie, 2003). Structures typically occurring within damage zones include secondary antithetic and synthetic faults, folds, deformation bands, veins, breccias, minor fault gouges and cataclasites, joints and stylolites (Agosta and Aydin, 2006; Agosta and Kirschner, 2003; Billi et al., 2003; Billi, 2010). These structures, together with the width of the damage zone, give valuable information about the mode of fault propagation and growth, earthquakes rupture propagation and rock permeability. The latter holds practical applications regarding water and hydrocarbon extraction and the storage of hydrocarbons and CO_2 (Kim et al., 2004; Wibberley et al., 2008; Choi et al., 2016; Peackock et al., 2017)

The formation and evolution of fault damage zones, commonly supposed to occur by means of quasi-static progressive growth and linkage of fractures, is controlled by a

variety of factors including lithology, dip of bedding relative to fault slip direction and principal stress axis, etc. (Kim et al., 2004 and discussion in section 5.3). The spatial distribution of damage zones in fault zones often has lateral asymmetry (e.g. Shipton and Cowie, 2001) and asymmetry between hangingwall and footwall damage distribution (e.g., Demurtas et al., 2016). Asymmetry could be related to different rock properties and different stress conditions during faulting. Given these complexities, several classifications have been proposed in order to group damage zones which share similarities. For instance, Kim et al., (2004) provided a broad classification defining *Tip*, *Wall* and *Linking* damage zones around segmented faults (Fig. 1.5) which was further implemented by (Peacock et al., 2017), who defined the *Interaction* damage zones between two faults with any orientation.

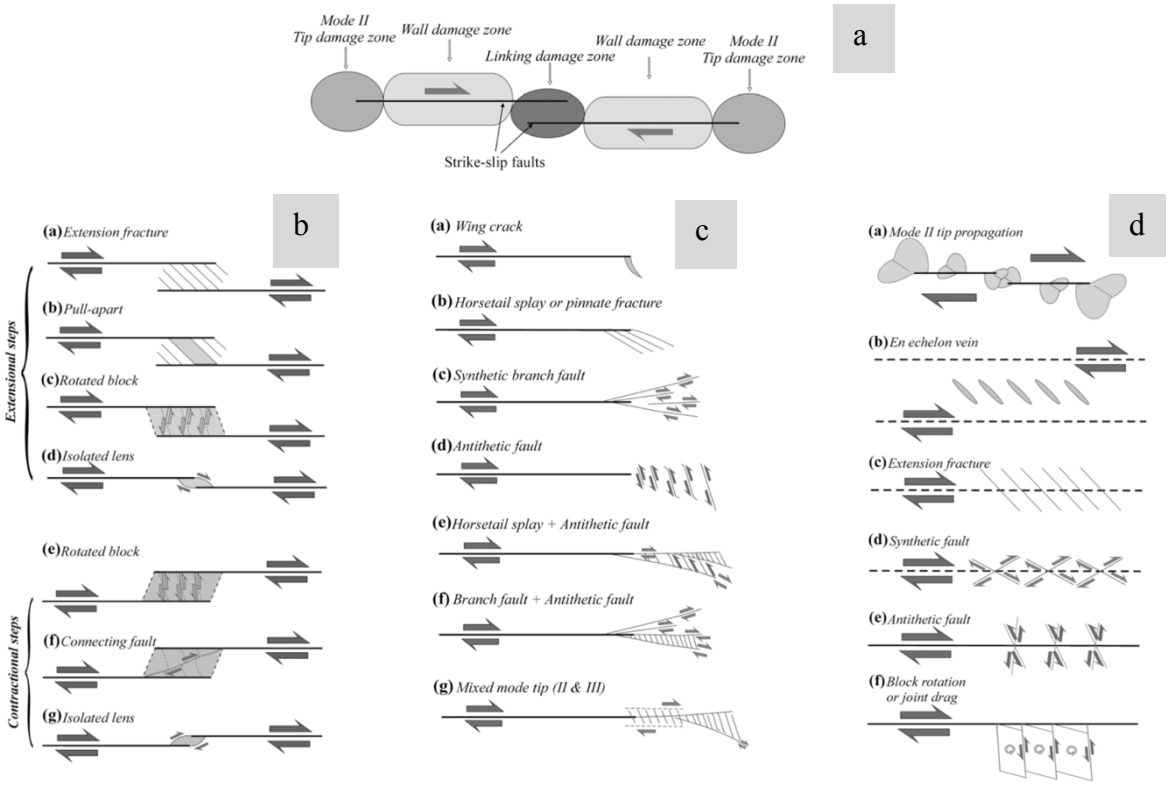


Fig. 1.5 Type of damage zones: Classification of damage zones provided by Kim (2004): (a) Schematic diagram of the principal locations of damage zones around strike-slip fault in map view. Main type of (b) linking damage zone, (c) tip damage zone, (d) wall damage zone.

Observations of damage zones are usually limited to 2-Dimensional outcrop exposures, with the exception of mines, which restrict the possibilities to make inferences about the 3D geometries of damage zones. Dynamic rupture simulations can give relevant information about the expected thickness of damage zones and its dependence with depth (e.g. Ma and Andrews, 2010). However, though Ma and Andrews, (2010) model shows a narrower damage zone at increasing depth, Scholz, (2019) suggest that the fault thickness should theoretically increase with depth. (Fig. 1.3c). Unfortunately, 3D seismic inversion data still do not have enough resolution to detect many of the typical damage zones structures (Peacock et al., 2017).

1.2.4 Fault zones scaling laws

An important question in fault and earthquake mechanics is how damage zones form and whether the same mechanisms govern the development of different damage zones throughout the evolution of the fault zone (Savage and Brodsky, 2011). One way to approach this question is through the study of how fault damage zones scale with displacement (e.g., Shipton et al., 2006b; Childs et al., 2009; Faulkner et al., 2011; Savage and Brodsky, 2011; Mayolle et al., 2019), fault length (e.g., Vermilye and Scholz, 1998) and how the structures of damage zones vary along-strike (e.g., Shipton et al., 2005).

A key factor in scaling laws is the damage zone thickness: it is defined as the total adjacent rock volume around the fault core which shows brittle damage structures related to the fault (Shipton and Cowie, 2001; Berg and Skar, 2005). In field observations, the greatest difference between the fault core and damage zone is strain localization and then the preservation of the original fabric of wall rocks. In damage zones, even if deformation structures develop, the original fabric of the wall rock is locally preserved (e.g. Gudmundsson et al., 2010). This difference makes it easy to detect the inner boundary of damage zones. However, it is relatively difficult to detect precisely the outer boundary of the damage zone because all physical properties change gradually (Choi et al., 2016). Thus, methodologies used to measure or quantify the thickness of the damage zones do not find general consensus (e.g., Kim and Sanderson, 2005). A definition of the outer limit of the damage zone is the point where the fracture frequency reaches the background frequency of the host rocks located at significant distance from the fault core (Berg and Skar, 2005; Mitchell and Faulkner, 2009; Smith et al., 2013; Rempe et al 2018). This last definition is often used even though the background fracture frequency is usually difficult to determine,

adding errors in the assessment of thickness value (Savage and Brodsky, 2011). Given the wide area of field-work of this thesis, I never constrained the outer limit of the damage zones and the intensity of fracture in damage zones has always been recognized (qualitatively, by expeditious observations) as higher than the host-rock background fracture frequency value. All measurements of the damage zone thickness are thus considered minimum estimates.

Importantly, in the scaling laws analysis, together with the different definition of the thickness of the damage zones, factors such as (1) fault damage types (tip damage, wall damage, link damage, (*sensu* Kim et al., 2004), (2) depth of formation, (3) tectonic regime and (4) wall rock lithologies are usually not considered. Since the thickness of the damage zone is strongly related to these factors, this approach introduces a large scattering in the data (up to two orders magnitude: Savage and Brodsky, 2011) (Fig. 1.2b). For instance, the type of rock alone would produce a strong effect on fault zone architecture and potentially on the *fault displacement – damage zone thickness* scaling (e.g. Soliva et al., 2006; Ballas et al., 2014; Mayolle et al., 2019). In fact, the development of the initial microfracture pattern (i.e., the process zone) is rock-type dependent (Scholz et al., 1993). However, despite the issues discussed above, data compilations of the thickness of the damage zones with fault displacement follow a power law of the type:

$$y = Cx^a$$

with y the fault damage zone thickness, C a pre-exponential factor, x displacement and a the power law exponent. Field data show that the damage zone thickness evolves with the net fault displacement (e.g., Evans, 1990; Manighetti et al., 2004; Mitchell and Faulkner, 2009; Faulkner et al., 2011; Savage and Brodsky, 2011; Torabi and Berg, 2011; Perrin et al., 2016).

However, most of the displacement vs. thickness scaling laws are based on faults cutting siliciclastic lithologies (e.g. Berg and Skar, 2005; Mitchell and Faulkner, 2009). According to these dataset, for fault displacements ranging from 0 - 100 m, the damage zone thickness scales linearly with displacement (a = 0.95 Mayolle et al., 2019); for displacements greater than 100 m, the damage zone thickness tends to saturate (Savage and Brodsky, 2011; Mayolle et al., 2019; Fig. 1.5b). Nevertheless, several field studies (e.g., Shipton and Cowie, 2001) and numerical models (Ben-Zion and Zaliapin, 2019) show that damage zones do not grow linearly with fault displacement at all locations along the fault; instead, damage zones are asymmetrically distributed along fault strike and, since displacement varies along the length of the fault and diminishes to zero at the fault tips,

also the damage zone thickness should drop to zero at the fault ends (Walsh and Watterson, 1988). The asymmetric distribution of the damage zone thickness with respect to the fault core could be due also to local geometrical complexities, such as fault linkages, which are highly variable along strike and independent of displacement (Shipton et al., 2005).

As discussed in this introduction, despite their geological importance, the structure of fault damage zones and their displacement-thickness relations remain poorly known (e.g., large scattering of data), and, also because of these limitations in the dataset, the processes responsible for the formation of fault damage zones remains debated.

2 METHODS

2.1 *Remote sensing analysis*

I performed remote structural analysis to identify the major active tectonic lineaments of the study area and, where possible, the associated fault damage pattern based on the effects of weathering (e.g., formation of badlands). In doing so, I combined the use of the databases Ithaca (ITaly HAzard from CApable faults, Michetti et al., 2000) and DISS (Database of Individual Seismogenic Source, Basili et al., 2008), Digital Elevation Model (DEMs) and the available geological maps. For higher resolution investigations, I used orthorectified photographs (spatial resolution of ~20cm) available at the geological portal of the Regione Abruzzo (www.regione.abruzzo.it/xcartografia), captured with aerial survey performed in summer 2010. All these datasets were combined through a multilayer analysis with software ArcGIS 10.6.1. The following digitalized geological maps were imported in an ArcGis project to trace the tectonic lineaments and were also used during the fieldwork:

- Vezzani et al. Geological-Structural map of the Central-Southern Apennines (Italy) (2010, scale 1:250.000)
- Foglio 349 "Gran Sasso d'Italia" (CARG project, scale 1:50.000)
- Foglio 358 "Poscorecchiano" (CARG project, scale 1:50.000)
- Foglio 359 "L'Aquila" (CARG project, scale 1:50.000)
- Foglio 360 "Torre de' Passeri" (CARG project, scale 1:50.000)
- Foglio 367 "Tagliacozzo" (CARG project, scale 1:50.000)
- Foglio 368 "Avezzano" (CARG project, scale 1:50.000)
- Foglio 369 "Sulmona" (CARG project, scale 1:50.000)
- Foglio 378 "Scanno" (CARG project, scale 1:50.000)
- Ghisetti, Vezzani et al., Geological map of "Gruppo M. Siella-M. Camicia-M. Prena-M. Brancastello (Gran Sasso d'Italia, Abruzzo), (1986, Scale 1:15.000)
- Ghisetti, Vezzani et al., Carta Geologica del Gran Sasso d'Italia (da Vado di Corno al Passo delle Capannelle),(1990, scale 1:25.000)

Digital Elevation Models (DEMs) with a 10 m-cell size grid, available in the geological portal of Regione Abruzzo and a second DEM available from INGV (courtesy

of Ph.D. Marco Moro) with a higher resolution (5 m-cell size grid) were used mainly for the construction of topographic profiles and hillshaded images were created for a sounder interpretation of fault scarps.

Lastly, during the course of *Remote sensing for geology* (held by Prof. Matteo Massironi) that I attended for my M.Sc. degree, I applied remote sensing techniques to verify the possibility of recognizing carbonate hosted fault damage zone from medium resolution satellite images. In the sections 2.1.1 and 2.1.2 below I will describe the applied procedure and briefly report the main conclusions of this latter study, since this approach was not further implemented during my M.Sci. thesis.

I used Landsat 8 L1T (LC08_L1TP_190031_20180718_20180731_01_T1, 11 bands, 15m/px PAN; 30 m/px VIS, NIR, SWIR; 100 m/px TIR) and ASTER L1T images (AST_L1T_00309192003100403_20150430222120_97140 14 bands, 15 m/px VIS and NIR; 20 m/px SWIR; 90 m/px TIR). Level 1T it is the highest quality level for Landsat and Aster images, which are radiometrically calibrated and orthorectified with ground control point and DEM. Images pre-processing, using software ENVI, consisted in:

- stacking of Visible (VIS), Near-infrared and Short-wave infrared (NIR e SWIR), Panchromatic (PAN) and Thermal-wave infrared (TIR) bands with a spatial subset on the study area, with resampling resolution at 15m/px.
- log-residual with dark subtraction atmospheric correction, to remove solar irradiance, atmospheric transmittance, instrument gain, topographic effects, and albedo effects from radiance data (Green and Craig, 1985). Both Aster and Landsat images were then exported in TIFF format.

2.1.1 Landsat 8 Images

In the Landsat 8 image I applied Intensity-Hue-Saturation (IHS) sharpening with a subsequent Normalized Difference Vegetation Index (NDVI) mask (value from -0.504052 to -0.190474) to remove clouds related pixels. Different image classifications were tested, (K-mean, 7 classes and 10 iteration; Maximum Likelihood, 7 classes; Minimum Distance) with and without applying Principal Component Analysis (PCA). The chosen classes were: water, woods, meadows, highly fragmented carbonates, carbonate massifs, cultivated land, buildings. Several Region of Interest (ROI, on which the un-supervised classifications are based) pixels were selected based on dedicated field checks performed during the summer geological surveys. Each classification yielded an image with different colours for pixels

belonging to different classes. However, the classification allowed me to recognize only few isolated pixels pertaining to the carbonates classes, which were rarely and by chance pertaining to areas in which carbonates effectively crop out. Based on this work, I concluded that the spatial resolution of the Landsat images is too low for an efficient image classification of the damage zone fault rocks. In fact, the high variability of land uses in this area that underwent intense anthropization invalidates these remote sensing techniques (IHS, NDVI and classifications).

2.1.2 Aster Images

Given the higher spectral resolution (14 bands) of the Aster sensors, I applied three selected band-depth ratios (BDR 7, BDR 8 and band depth ratio 3/2) to emphasize highly-fragmented carbonate spectral signature. I associated these bands ratios to visualize a false colour composite image. Aster bands were previously resampled on a laboratory-obtained spectral signature of calcite and dolomite at micron-size grain scale (Traforti et al., 2017). Aster images analysis did not give any useful result, since the spectral resolution of laboratory-obtained spectral signatures (~50 nm) and Aster sensors (~800 nm) are too different. Any classification applied to the false colour composite images with band ratios failed.

2.2 *Field geology survey techniques*

We performed most of the geological surveys in September 2018 and April 2019, within the MMF footwall block between the villages of Pizzoli and Arischia ("Provincia" de L'Aquila, Abruzzo Region, Italy). During April 2019, we conducted preliminary geological-structural surveys of other selected fault zones (Venere Fault, Morrone Fault, Middle Aterno Valley Fault, Pescasseroli Fault) previously studied by means of remote sensing analysis (see section 2.1) to check for the presence of fault-associated damage. In all cases, the surveys (about one day per each fault) were conducted in the fault footwall, since these high-displacement (>100 m) active faults put in contact Mesozoic carbonate footwall with the hangingwall terrigenous Quaternary deposits.

We mapped the footwall block in the Pizzoli sector of the MMF at 1:500 scale (mapped area c. 0.6 km^2) using, as a topographic basis, orthorectified aerial photographs (aerial acquisition performed in 2010, spatial resolution 0.2 m) downloaded from the Regione Abruzzo website. Using geological compasses, we collected structural data

(attitude and dip angle) of faults, fractures, veins and stylolites for the reconstruction of the architecture of this sector of the fault zone. When possible, we collected also the sense of shear on lineated fault surfaces. When doubtless recognizable, we collected bedding attitudes.

In previous geological surveys conducted in other sectors of the Monte Marine fault zone by M. Sci. Silvia Cortinovis and Prof. Fabrizio Balsamo, specific fault zone rock facies were recognized (see section 4.1). Further laboratory analysis (i.e., grain-size and grain-shape analysis on fault core cataclasites and breccia) were performed by Silvia Cortinovis. Their fault zone rock classification was used in my surveys and, as a consequence, in the geological cross sections and in the high-resolution geological structural maps of my thesis. These latter original research products report also the structural data, structural stations and samples locations (see section 4.1). All structural elements and lithologies were digitalized using software ArGIS 10.6.1

2.3 *Kinematic analysis*

A total of 933 structural data were taken in 26 structural stations to characterize the structural domains within the fault zone. The structural data (e.g., dip, dip azimuth) were elaborated using Stereonet 10 software (Marrett and Allmendinger, 1990; Cardozo and Allmendinger, 2013) to produce stereoplots and pole projections (equal area, lower hemisphere plots). Structural data included fault planes attitude, bedding attitudes, slip directions and, when possible, the sense-of-slip. For non-planar faults, several measurements were collected. Qualitative and quantitative kinematic analysis of fault-slip data were made following the method proposed by Marrett and Allmendinger (1990) while contouring of pole-to-fault data were calculated following Kamb (1959) (i.e. contouring interval of 2sigma and significance level of 3sigma). P&T (shortening and extension) axes were determined using FaultKin 7 software (Allmendinger et al., 2011).

2.4 *Optical and Field Emission-Scanning Electron Microscopy*

Twenty-three samples were collected at different sites within the footwall of the MMF (for the sample location see Poster 1). Of these, eight samples of fault slip zones were selected (see sections 2.4.1 and 2.4.2) for optical and scanning electron microstructural observations. The samples were first consolidated with epoxy resin and

then cut to obtain 30 micrometres thick polished thin sections at the department of Geosciences of the university of Padua) (see appendix A for table of samples).

2.4.1 Optical Microscope (OM)

Thin sections were cut perpendicular to the fault surface and parallel (seven samples) or perpendicular (one sample) to the lineation; in the absence of a lineation the samples were cut parallel to the dip azimuth. The goal was the investigation of the microstructures (from μm- to mm-scale) at increasing distances from the principal slip surface. Sample MM5.3 was the best for this purpose, thus it was the only one which was also cut perpendicular to the lineation. Images of the thin sections were obtained with the Olympus BH-2 optical microscope at Department of Geoscience in Padua University.

2.4.2 Field-Emission Scanning Electron Microscope (FE-SEM)

For higher resolution microstructural investigations, the thin sections from samples MM5.3 and MM5.6 were polished and then coated with a 100 Å thick Chromium layer. Investigations were performed using Field-Emission Scanning electron microscope (resolution 0.6 nm in secondary electrons, and 1.2 nm in back scattered electrons) at the *Ultra-high resolution scanning electron microscopy and ultra/high resolution microanalysis laboratory (CERTEMA, Cinigiano, Grosseto, Italy).* The FE-SEM is a Zeiss Merlin II equipped with WD/ED probe spectrometers and with secondary and backscattered electrons detectors installed in the specimen chamber and in the "electron gun" (or "in Lens"). Operational conditions of the electron beam were 10 kV with ~8.5 mm as working distance. We collected micrographs of the fault zone specimens with Secondary Electron (SE) and Backscattered Electron (BSE) detectors using in-lens detectors. Elemental semi-quantitative point analyses were performed with highly sensitive X-MAX 50 detector (50 mm active area). We also conducted specific elemental composition data analysis (EDS) across the principal slipping zone of sample MM5.3 to obtain the elemental map of the investigated area.

3 GEOLOGICAL SETTING

3.1 *Tectonic evolution of the Central Apennines*

The Apennines are a mountain range ~1200 km long which crosses the Italian peninsula from the Maritime Alps to the Calabrian-Peloritan arc. Together with the Carpathians, the Hellenides, the Apennines-Maghrebides and the Betic-Rif-Tell system, the Apennines belong to the Western-Alpine system and Western-Mediterranean tectonic framework (Malinverno and Ryan, 1986), the latter being one of the most geodinamically complex regions in the world. The Western-Mediterranean evolution and paleogeography is connected with the relative movement and different styles of subduction of three main tectonic plates: Africa, Adria, and Europe. A vast scientific literature is available, including elaborated geodynamic evolutionary models which condense investigations from geology, geophysics, volcanology, seismology, paleogeography, paleomagnetism, geodesy, stratigraphy, etc. (Alvarez et al., 1974; Gasperi, 1995; Vezzani et al., 2010; Carminati et a., 2012; Faccenna et al., 2001).

During the middle Jurassic, the opening of the N-S striking Central Atlantic Ocean and Ligurian-Piedmont Ocean led to the formation of the new continental margin of Adria to the East and of the European Margin to the West (see Fig. 3.1a). Adria is a continental plate where essentially shallow to deep marine carbonates were deposited from the Mesozoic to the Early Paleogene (Vezzani et al., 2010). Adria had a fundamental role in the evolution of central Mediterranean but some aspects remain debated, namely the presence of a single plate rather than a collage of continental plates and the Adria crustal continuity with the Africa mainland (Carminati et al., 2012). During the Late Cretaceous, the opening of the Southern-Atlantic Ocean led to the slow convergence of Africa (and its promontory Adria) towards NE. According to the most accepted interpretation, the Ligurian-Piedmont Ocean was subducted beneath the Adria Plate with a E-directed subduction which flipped into the present W-directed subduction (Carminati et al., 2012). Timing and kinematics of the later W-directed Apennine–Maghrebide subduction onset are not well constrained and range from Late Cretaceous (~ 80 Ma) to Early Oligocene (~ 33 Ma) (Doglioni et al., 1999; Lustrino et al., 2009, Doglioni, 1991; Gueguen et al., 1998). During the flip, the Alpine slab was truncated by the new Apenninic slab, which in turn was characterized by a continuous roll-back, with an eastward migration of the fold-and-

thrust belt and related foredeeps (1-7 cm/yr, Doglioni et al., 1994). The maximum North-South Africa/Europe convergence was estimated in 135 km, while the eastward migration of the Apennine arc was more than 700 km (Faccenna et al., 2001) (Fig 3.1c-f). Remnants of the former Alpine orogens were boudinaged and passively incorporated into the accretionary wedges (i.e., crystalline and metamorphic units of the Calabria nappes) (Alvarez et al., 1974; Morelli et al., 1976; Alvarez, 1976).

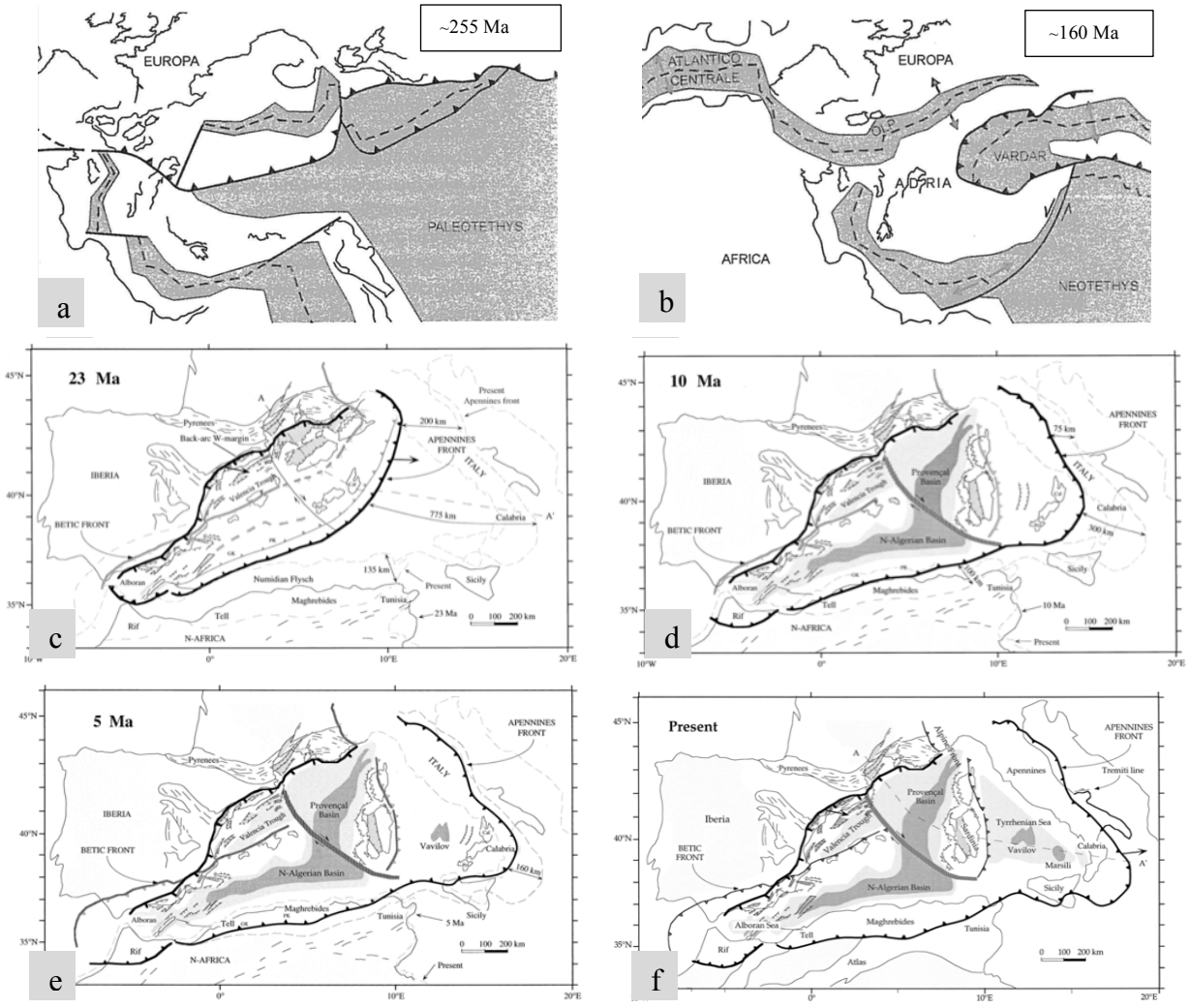


Fig. 3.1 Paleotectonic reconstruction of the western Mediterranean area at different stages of its evolution, showing the eastward retreating Apenninic slab and subsequent eastward migration of the belt-front, from Gueguen et al., (1998).

The fast radial roll-back and crustal thinning processes led to the formation of the Liguro-Provençal Basin (30-15 Ma) and the Sardinia–Corsica continental blocks moved radially with a counter-clockwise rotation of about 60° until Northern Corsica and Adria collided (20-22 Ma) forming the so-called Ancestral Apennines (Fig. 3.1c). The flexure-

hinge retreat continued and from the late Miocene (Tortonian-Messinian) the orogenic front and foredeep-foreland system eastward migration was accompanied by synchronous extensional collapse of the inner domains of the Apenninic thrust belt (Fig. 3.1d). Slab roll-back culminated with the formation of new oceanic crust in the Tyrrhenian (Vavilov and Marsili basins, Late Pliocene), which is thus interpreted as a back-arc basin to the west of the eastward retreating slab (Patacca et al., 1990; Vezzani et al., 2010) (Fig.3.1e, f). Differences in thicknesses of the Adria lithosphere (70km) with respect to the thicker Puglia continental lithosphere (110km) resulted in the lower penetration of the slab and lithosphere buckling. In fact, after the Pliocene-Early Pleistocene, the Puglia region and the Bradanic Foredeep underwent uplift, while subsidence continued in the northern and central Apennines. These different tectonic realms are separated by the Tremiti Line, a E-W trending transfer zone with right-lateral sense of motion (Fig. 3.2) (Doglioni et al., 1994).

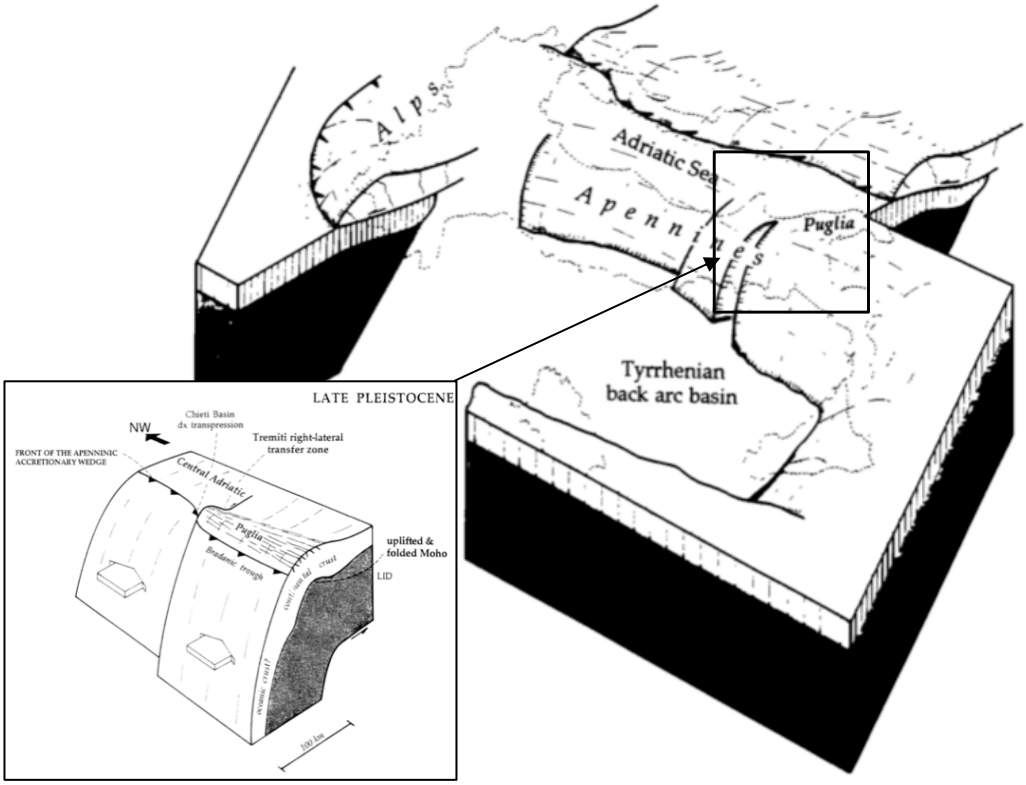


Fig. 3.2 Tectonic framework of Italy, with the Adria Plate subducting westward underneath the Apennines and eastward below the Dynarides. The inset shows the different behaviour of the thinner plate Adria (70km) in respect to the thicker Puglia lithosphere (110km), the latter being uplifted. The two domains are divided by the Tremiti right-lateral transfer zone (modified from Doglioni et al., 1994).

3.2 *Geology and structural setting of the Central Apennines*

The Apennines are a fold-and-thrust belt that can be subdivided into the arcuate segments of Northern and Southern Apennines, with the intermediate pivot segment of the Central Apennines, the latter being bounded by the Ancona-Anzio Line to the NW and by the Volturno-Sangro Line to the SE (Ghisetti and Vezzani, 2010). The actual lithotectonic assemblage of Apennines results from the interaction between the African and European plates through (1) the Mesozoic development of Ligurian-Piedmont Ocean domain, the Cretaceous-Eocene Adria westward subduction, (2) subsequent Oligocene-Miocene continental collision/shortening and (3) Miocene-to-present extension following the eastward migration of the chain front (Vezzani et al., 2010). Nowadays, the northern sector of the Apennines consists of a series of in-sequence N-NE verging imbricate thrusts while the Central-Southern consists of ENE-E verging thrusts with duplex geometry and out-of-sequence thrusting. The major structural domains are:

- Extensional Tyrrhenian domain, with thinned crust overlaying the W-dipping Benioff Zone,
- The extensionally downfaulted inner (with respect to the Ligurian-Piedmont Ocean) thrust belt (i.e., Calabride, Liguride and Sicilide Units),
- The Adria-Bradanic Foredeep, developed above the continental margin of the Adriatic-Apulia foreland,
- The Adria-Apulia Foreland.

During the continental collision between the Adria and Europa plates, the thrust-belt inner units were transported with NE vergence onto the outer units, building a 7-8 km thick imbricate stack of thrust sheets that tectonically overlies the Adriatic-Apulia Foreland (Vezzani et al., 2010). In particular, in the Central Apennines, the large-exposure of carbonate massifs are indicative of the past depositional environment: from the upper-Triassic the western margin of Adria was a shallow-water environment with a carbonate megabank covering much of the western Mediterranean area. During the rift phase (early Jurassic), normal listric faults striking parallel and oblique to the Adria margin (Bernoulli, 2001), dissected the wide pre-existing Triassic- Lower Jurassic carbonate platforms forming a number of smaller ones (e.g., the Latium-Abruzzi area) separated by pelagic basins (e.g., the Umbria-Marche area), and slope domains (e.g., the Gran Sasso Massif area; Pace et al., 2014; Fig 3.3a). Extensional tectonics associated to rifting halted during the

oceanic convergence which was instead driven by favourably-oriented pre-existing Jurassic main structural elements, such as the Ancona-Anzio and Volturno-Sangro lines (Centamore et al., 2002).

At the start of the continental collision between Africa and Europe (from Oligocene to Pliocene) the eastward-shifting thrust system incorporated more and more external sectors of the foreland. Here, westward-dipping low-angle listric faults have been reactivated firstly in their deeper parts as thrusts (e.g., Velino fault and Fiamignano Fault; Bigi and Pisani, 2003). Also Jurassic-in-age oblique faults have been reactivated as transpressive ramps (e.g., the Ancona-Anzio and Velino-Magnola faults; Centamore et al., 2002 and reference therein) (Fig 3.3c).

Since late Miocene (Tortonian), in the wake of eastward advancing thrust fronts, post-collisional rifting affected the Tyrrhenian domain and soon (late Tortonian) extensional faulting affected the inner sectors of the Apenninic chain. The Apennines are currently bounded to the east by the outer extensional front, which largely coincides with the Apenninic drainage divide (Ghisetti and Vezzani, 2002 and reference therein). Further to the east, the early-middle Pleistocene fold-and-thrust belt overrides the Adriatic foredeep-foreland system and which in turn is still subjected to active shortening (Fig 3.3b). The post-orogenic Quaternary extension is characterized by mainly NW-SE trending normal/transtensive active fault systems with associated seismicity. These normal faults bound Quaternary intramountain basins in their hangingwall-blocks and consist of an array of en-echelon SW dipping high-angle segments with lengths ranging from a few kilometres to ca. 35 km and with downthrows up to several hundreds of meters. Fault slip data measured along Quaternary/active fault planes and earthquake focal mechanisms reveal an ongoing extension with a sub-horizontal NE trending σ_3 axis (Pizzi and Galadini, 2009, Pace et al., 2014). There are different interpretations about this Quaternary extension. In particular, Ghisetti and Vezzani (1999) relate the current extensional collapse to a thin-skinned gravitational tectonics induced by strong components of regional uplift in which normal faults are rooted in shallow detachments. These authors propose that the extensional regime is entirely disconnected from the rifting mechanism that operated in the Tyrrhenian domain.

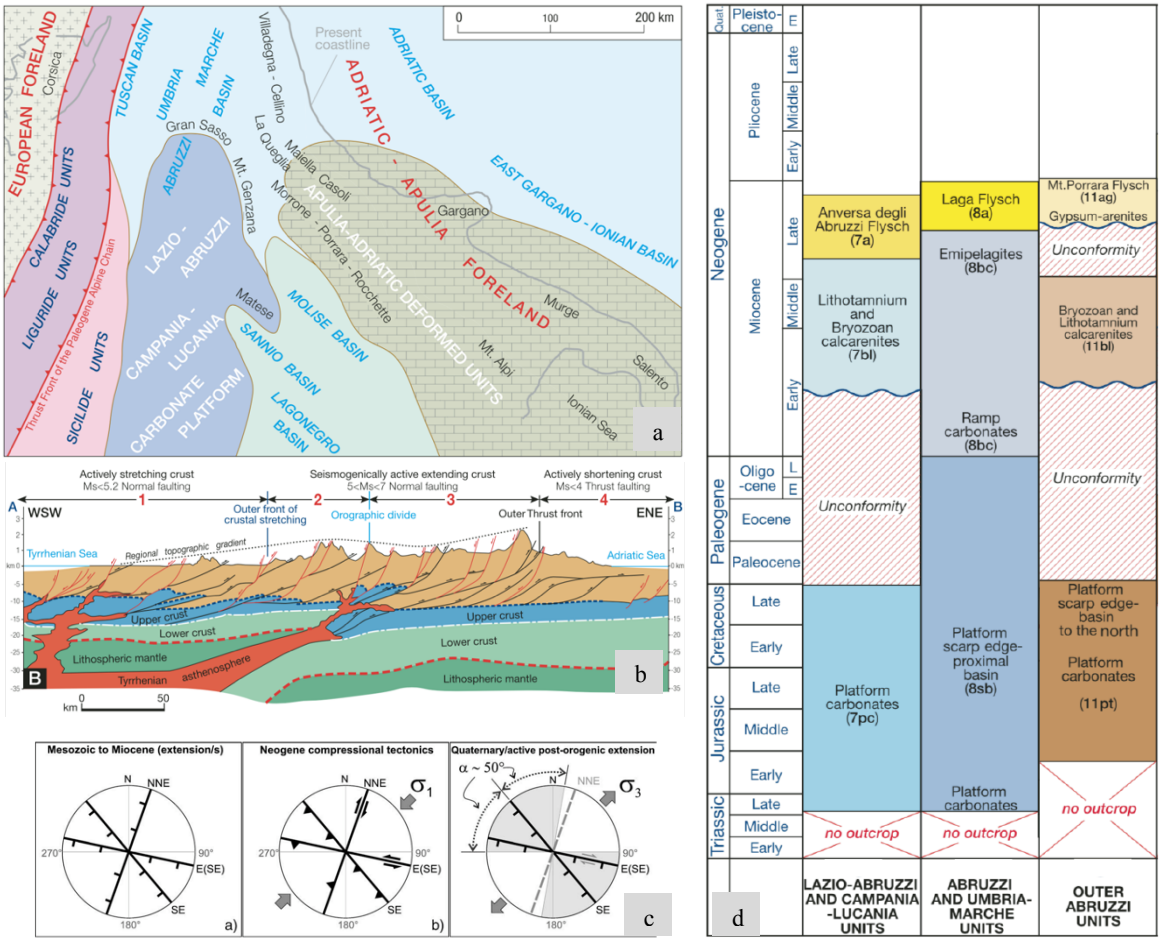


Fig. 3.3 Geological and structural setting of Central Apennines. (a) Restoration of the paleogeography and distribution of carbonate platform and relative pelagic basins in the Central Apennines during the Paleogene, from Ghisetti and Vezzani (2010). (b) Cross section from the Tyrrhenian to the Adriatic Sea in which the extensional stretching of Tyrrhenian hinterland and the active shortening in the outer Adriatic zones are evident, from Ghisetti and Vezzani, (2010). (c) Kinematic history of the three major structural trends of the present structural framework of Central Apennines. Since Neogene compression and post-orogenic extension were co-axial, faults trending NNE, E(SE) and SE were reactivated with different kinematics during from the Neogene to the Quaternary (from Pizzi and Galadini 2009). (d) Main stratigraphic units of the outermost external domain of the Central Apennines area (modified from Ghisetti and Vezzani, 2010).

3.2.1 Stratigraphy

All the faults in the catalogue presented in this thesis cut through to the so-called stratigraphic Outer Units, which derive from the progressive deformation of the outermost external Apenninic domains. These stratigraphic succession were originally deposited in domains of carbonate platforms and interposed pelagic basins along the Adria passive margin and are now tectonically overlain by the Liguride and Sicilide Units (Vezzani et al., 2010).

Within the Outer Units, Ghisetti and Vezzani (2010) recognized the main stratigraphic successions and subdivided them in further Units: the Middle-Aterno Valley Faults, the Venere Fault and the Pescasseroli fault cut through the *Lazio-Abruzzi and Campania-Lucania Units*, the Pescasseroli fault cut through the *Outer Abruzzi Units*. The Monte Marine Fault and the Campo Imperatore fault cut through the *Abruzzi and Umbria-Marche Units*. The latter stratigraphic successions include Upper Triassic–lower Jurassic shallow-water carbonates overlain by platform scarp-edge proximal basin deposits, with variable amounts of platform-derived sediments (Fig 3.3d). These deposits are conformably covered by the lower Messinian siliciclastic turbidites of the Laga and Gran Sasso Flysch. The main geological formations of the *Abruzzi and Umbria-Marche Units* outcropping in the Monte Marine fault area are (Vezzani et al., 1998; Fig. 4.1b):

- Calcare Massiccio Fm. (Hettangian – Lower Sinemurian). It is a typical Carbonate paleoplatform Mesozoic succession made of white to brownish limestone in which oolitic levels and fenestrae are common. The succession is organized in a typical ciclothemic succession with basal strata partially dolomitized. The depositional environment is a peritidal carbonate platform. Strata thickness ranges from 5-50 cm to 1-5 m while the maximum thickness of the formation is ca. 600 m. In the MMF area the Calcare Massiccio Fm. appears totally dolomitized and rarely original features like laminations and fossils are preserved.

- Corniola Fm. (Upper Sinemurian – Toarcian p.p.). It is a scarp Meso-Cenozoic succession made of brownish to greyish carbonate-rich mudstones organized in thin (10-50 cm) strata, commonly with grey, dark or red chert lenses; the depositional environment is the toe of the slope. The transition with the Calcare Massiccio Fm. is characterized by a sharp stratigraphic discontinuity, usually a vertical

superposition and the basal part is often dolomitized and recrystallized. Thickness of this formation ranges from few tens of meters up to ca. 600 m.

Marls and arenaceous limestone (E2-0 Fm., Eocene in age, Carta Geologica d'Italia, 1955) crops out both at the hangingwall and at the footwall of the Monte Marine fault. The E2-0 Fm. was thus exploited to estimate the total displacement for the Monte Marine fault (e.g., Roberts and Michetti, 2004).

3.3 *Active faults in Central Apennines*

From the Quaternary period, the Central Apennines have been affected by intense seismicity resulting, in historical times, in moderate to large in magnitude earthquakes (e.g., **1349**, L'Aquila Mw= 6.8; **1456**, Molise Mw = 7.19; **1654** Marsica Me = 6.1; **1703** L'Aquila-Pizzoli Mw = 6.7; **1706** L'Aquila Me = 6.7; **1915** Avezzano Mw = 7.1; Rovida et al., 2016). Most of the fault structures responsible for these and other destructive historical earthquakes are not well-constrained. This fact, associated with the present strong seismicity of the entire peninsula (L'Aquila, April 9, **2009**, M_w6.1; Emilia, May 12, **2012**, M_w6.1; Amatrice-Norcia, October XX, **2016** M_w6.6; Chiaraluce, 2012; Valoroso et al., 2013), and in particular in the Central Apennines framework, has prompted Italy to develop research methods in the seismological and geological fields for an effective hazards seismic assessment.

Research on active tectonics in the Central Apennines began in the 1970s (Bosi, 1975) mainly through the application of geomorphological criteria; the first main publication was the *Neotectonic Map of Italy* (Ambrosetti, 1983). At that time, however, investigations were purely geological and the relations between Apennine seismicity and active structures were missing (Galadini and Galli, 2000a). In the late 80s and 90s, further investigations of the Quaternary geological evolution and the first paleoseismological studies brought quantitative data on the characteristics and kinematics of some active faults. Based on these studies, a fault is defined as:

- ***active*** and therefore of interest for Seismic Hazard Assessment if "*it has an established record of activity in the Late Pleistocene (i.e. in the past 125 ka) and a demonstrable or inferable capability of generating major earthquakes"* (Boschi, 1996).

- ***capable*** if the fault shows evidence of repeated reactivation during the last 40.000 years (Late Pleistocene-Holocene) and *capable* of rupturing the ground surface (Michetti et al., 2000).

However, Machette (2000) states that, to be useful for seismic-hazards analysis, fault maps should encompass a time interval that includes several earthquake cycles; in doing so, the term *active* is valid for different time periods. Fault activity is strictly connected to the morphologic expressions (i.e. normal faulting-generated mountain front, intramountain basins, fault scarps, etc.) and still nowadays geomorphic analysis remain an important tool for the identification of geological fault segments (Blumetti and Guerrieri, 2007) even though not always diagnostic of Late Pleistocene–Holocene activity. In fact, due to convergence of forms (land-sliding, morphoselection processes), bedrock scarps have also been detected along inactive faults (Galadini and Galli, 2000a).

Thanks to technological advances, in recent years several other methods have been applied to gather active faults data, including:

- Ground penetrating radar (GPR) and terrestrial laser scanning (TLS) coupled to field mapping measurement of faulted of geomorphic offsets (Bubeck et al., 2015; Wilkinson et al., 2015);
- Geomorphological studies on displaced post-glacial sediments and slopes associated with the last major glacial retreat to get deformation-rate data (Papanikolaou et al., 2005);
- Geodetic and GPS data for the fault slip-rate data, (D'agostino et al., 2001; Papanikolaou et al., 2005; Faure Walker et al., 2010);
- High resolution (double-difference methods) fore-shock and after-shock distributions to "illuminate" the geometry at depth of the seismogenic structure (Chiaraluce, 2012; Valoroso et al., 2013);
- Paleoseismological studies coupled with geochronological analysis made from trenches excavations. (Saroli et al., 2008; Galli et al., 2011; Moro et al., 2016; Maceroni et al., 2018);

- Cosmogenic isotopes concentrations measured on bedrock scarps to constrain fault slip-rates (Cowie et al., 2017).

The data derived from these new methods are a fundamental step towards the identification of primary seismogenic sources and for a more accurate assessment of regional seismic hazard, thus they are a major tool for efficient urban planning and for developing suitable risk mitigation plans (Basili et al., 2008). For these purposes and to synthetize all the available data, two main database were created, namely DISS (The Database of Individual Seismogenic Sources; Basili et al., 2008) and ITHACA (Italy Hazard from Capable Faults: a database of active faults of the Italian onshore territory; Michetti et al., 2000). These databases are a repository of geologic, tectonic, and active fault data for the whole Italian territory and include fault geometrical features (coordinates, length, dip angle, kinematics, depth if possible) and energetic-kinematic features (slip-rate, slip/event associated maximum or characteristic earthquake magnitude data; Barchi et al., 2000). These databases are constantly updated and thus may contain errors (e.g., fault traces length, Roberts and Michetti, 2004). However, the intense and rich work made resulted in the following main conclusions regarding the seismicity of the Central Apennine:

- Inner Apennines are going through **active extension** at regional extensional rate of 2.5-5 mm/yr (Hunstad et al., 2003), horizontal strain-rate ca. 1.18×10^{-8} yr^{-1} parallel to the regional principal strain direction (Faure Walker et al., 2010) and, within the Apennines, this present-day active extension is **accommodated by young NW-SE faults** (Morewood and Roberts, 2000; Chiarabba et al., 2009), revealing a nearly horizontal **NE trending σ3 axis** (Pizzi and Galadini, 2009, Pace et al., 2014);

- Strain-rates vary spatially on the length scale of individual faults and on a timescale between 10^2 yr and 10^4 yr (Faure Walker et al., 2010);

- **Several active faults systems** are present within Central Apennine framework (Fig. 3.4; at least seventeen, as reported by Roberts and Michetti, 2004), NW–SE to NNW–SSE trending and 16 to 33 km-long, **with mean fault-slip direction of 222°± 4°**, consistent with almost pure dip-slip faulting. Nevertheless, the number of active faults could be in the order of tens and it is difficult to constrain exactly

this number since, for instance, a single seismogenic source could be associated to multiple nearby fault segments at the surface. It is up to seismology and geophysics, through fore-shock and after-shock localization analysis, the determination of the number of activated fault segments during an earthquake (e.g.,Valoroso et al., 2013)

- Some **geomorphic features** such as fault scarps and intramountain basins (e.g., L'Aquila intramountain basin) are well **correlated with the activity of the normal active faults**, whose geometry at depth is well-constrained by seismological data (Chiarabba et al., 2009).

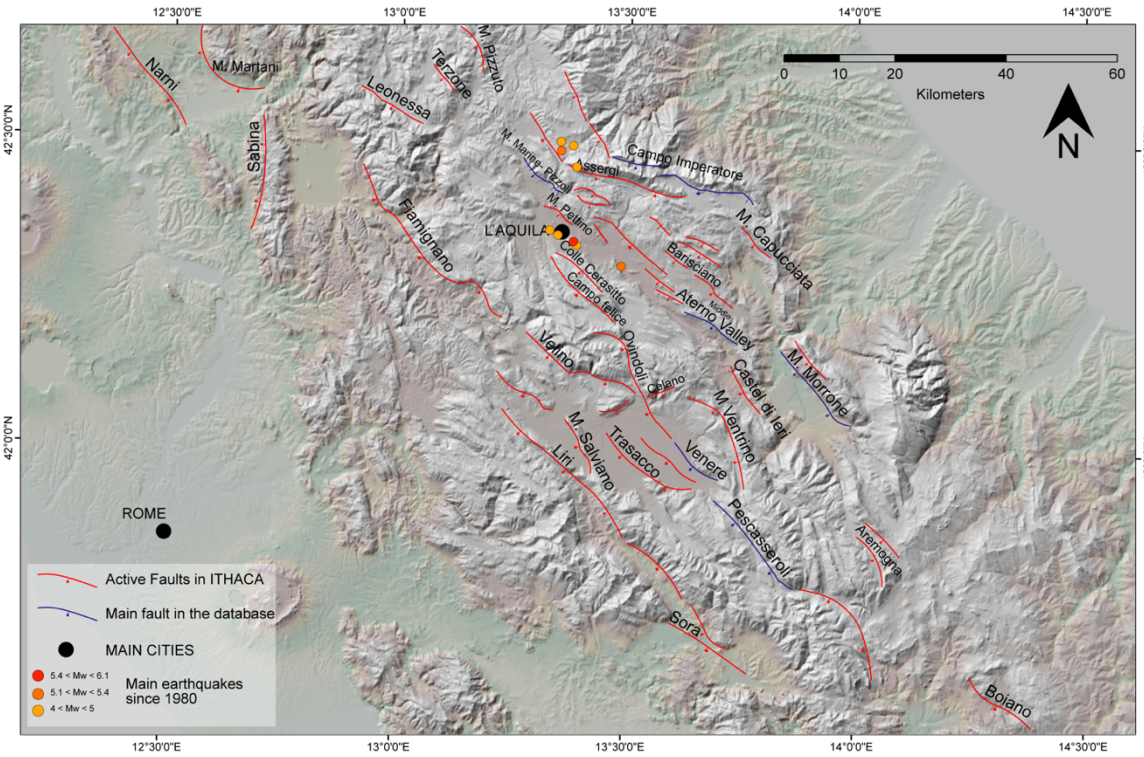


Fig. 3.4 Main active faults in central Apennines: Map with the main active faults within the Central Apennines framework and with the main earthquakes from 1980 to 2015 (data collected from ITHACA database).

4 RESULTS

The core of this thesis was the field work. We performed a preliminary field survey in Abruzzo in July 2018 where we established to focus on the **Monte Marine Fault zone (MMF)**, both for its extraordinary footwall-block exposure and because in the same period geological surveys were conducted by researchers from the University of Parma. I collected the first geological and structural data in that period. I surveyed the area in September 2018 and April 2019 for a total of 16 days of field work. The surveys were conducted in collaboration with Ph.D. Michele Fondriest, Prof. Giulio Di Toro, M.Sci. Luca Del Rio and B.Sci. Miriana Chinello from University of Padua, M.Sci. Silvia Cortinovis and Prof. Fabrizio Balsamo from University of Parma. The data presented here were discussed, in the field, with Ph.D. Marco Moro, Ph.D. Emanuela Falcucci, Ph.D. Stefano Gori (INGV) and Prof. Michele Saroli (University of Cassino). All the data (geological maps, structural data, rock specimens, etc.) presented in this section of the thesis were collected by myself if not specified.

The aims of this thesis are:

1. detailed field structural survey to quantify the distribution and thickness of *in-situ* shattered rocks (ISRs) within the damage zones of active fault zones in carbonates;
2. remote-sensing analysis coupled with literature data review to determine, if any, scale relations between fault length, displacement, geometry (e.g., presence of step-overs, other major faults) and thickness of *in-situ* shattered fault rocks in carbonates.

In this section I will show the results obtained from the fieldwork and from microstructural analysis. They will be used in chp. 5 to discuss the architecture of the MMF and the factors controlling the ISRs distribution in the other faults of the catalogue.

4.1 *Structure of the damage zone of the Pizzoli-Monte Marine Fault*

The Monte Marine Fault (MMF) is the main segment of the Upper Aterno Fault system, which is composed of four main dextral faults arranged in an *en-echelon* array (from South to North: Mt. Pettino (MPF), Mt. Marine (MMF), San Giovanni (SGF), and Capitignano (CAPF) faults) bordering the L'Aquila, Arischia and Capitignano basins (Galadini and Galli, 2000b; Galli, 2011; Fig. 4.1a). The four faults drove the Quaternary evolution of the intramountain basins (Galadini and Messina, 2001). The MMF is about 14

km long but evidences of recent activity are only observed along the 9-km-long south-eastern segment which crops out at the Barete, Pizzoli and Arischia villages (Fig 4.1b-c). Trenches excavations report evidences for five seismic re-activations during the last 15.000 years, and the historical earthquake sequences of the 1315, 1349, 1461, 1762 (IX-X of the Mercalli Scale) have been attributed to the Upper Aterno Fault system (Moro et al., 2002, 2016; Galli et al., 2011). The most recent faulting event recognized from paleosismology is ascribable to the Mw 6.7 February 02, 1703 event (Moro et al., 2016). This earthquake caused more than 5,000 casualties, and produced open fractures, chasms, associated to sulphurous gas emission and white water escape (Blumetti, 1995; Moro et al., 2002; Blumetti and Guerrieri, 2007). The February 02, 1703 earthquake was generated by a ca. 30-km-long fault rupture (i.e. the whole Upper Aterno Fault System was activated) with fault surface displacements of the order of 0.10-0.60 m (Moro et al., 2002).

Focal mechanisms of the moderate and minor in magnitude earthquakes associated to the MMF are consistent with dominant normal (dip-slip) faulting, and accommodate the ongoing extension in the inner Apenninic domain which started in the early Pleistocene. At present, minimum vertical slip rate is in the order of 0.25–0.43 mm/yr (Galadini and Galli, 2000) and the fault accumulated a total displacement of ca. 1700 m (Roberts and Michetti, 2004).

Along the southern MMF segment, the trace of the fault surface was mainly detected during investigations aimed at realizing the "Prototipe Geological Map" (National Geological Service of Italy). The average attitude of the fault surface is N204/65° (dip azimuth/dip) corresponding to a strike of N114, but in the central sector (near Pizzoli village), probably because of structural geometrical complexities, the surface of the main fault bends to strike ca. N90 (Fig. 4.1c). The MMF could be interpreted as consisting of two hardly or softly linked left-stepping segments, namely the Barete-Pizzoli segment to the northeast and the Arischia segment to the southwest (Fig 4.1b-c) (Cortinovis et al., 2018). The overstepping area and the fault scarps are poorly exposed and they might have been extensively modified by bi-millenarian human activities. Because of these limitations, in the structural map produced in this thesis, the trace of the main fault surface is the one proposed by Moro et al., (2016) based on trench data, and the geometry of the overstepping sector is discussed in detail in section 5.1.

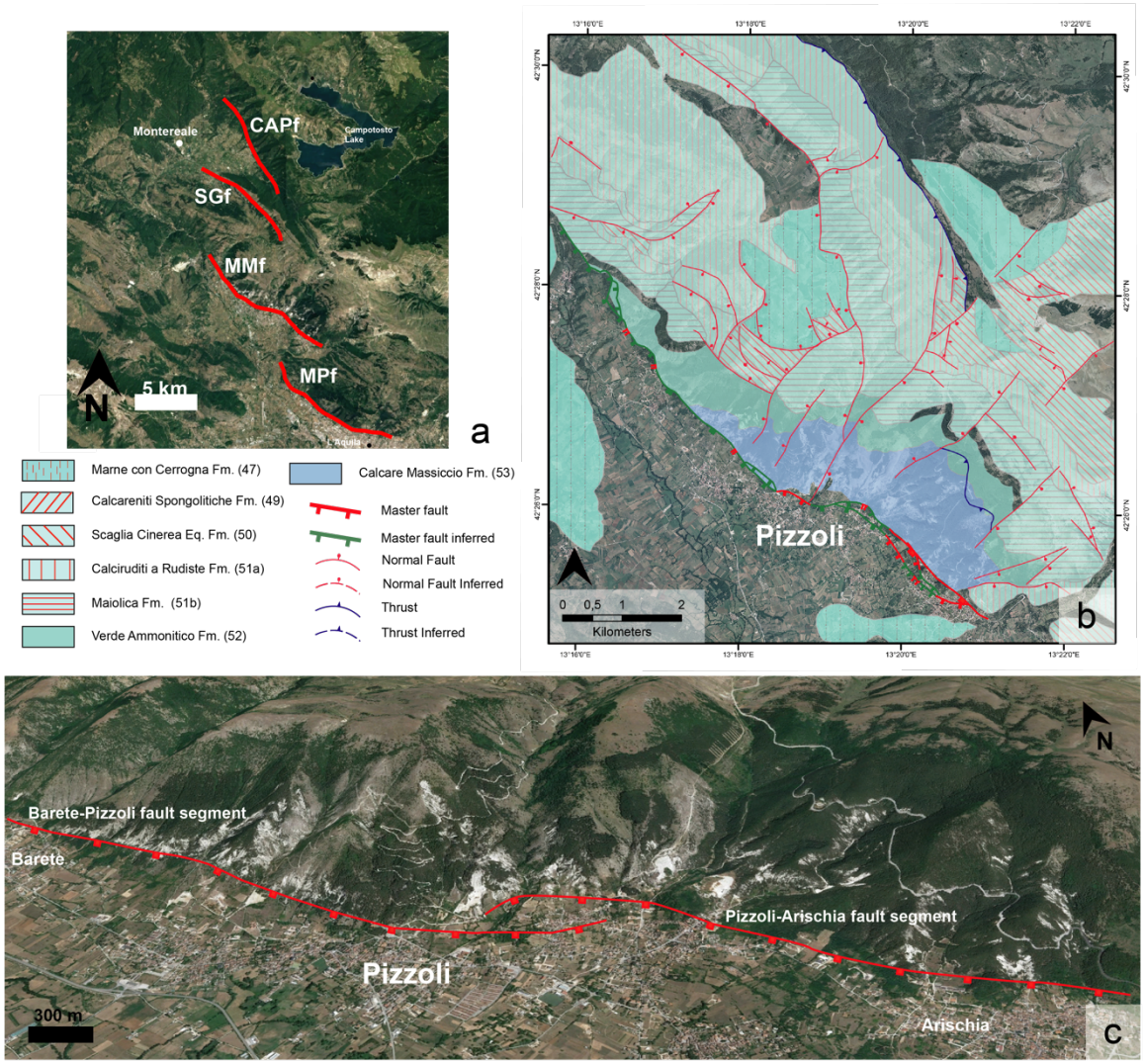


Fig. 4.1 (a) Setting of Monte Marine Fault Zone within the Upper Aterno en-echelon fault system: Monte pettino fault (MPf), Monte Marine fault (MMf), San Giovanni fault (SGf) and Capitignano fault (CAPf) . (b) Geological map of the MMF area. (c) View of the 9-km long exposed part of the MMF: the fault damage zone became hundreds of meters thick in the sector where the two fault segments overlap.

Starting from the southern sector, the MMF footwall rocks are the Mesozoic carbonate rocks of the Calcare Massiccio Fm. and, going towards the northern sector (near Barete), of the Corniola Fm. The MMF puts them in contact with hangingwall Late Pleistocene layered slope deposits (Galadini and Galli, 2000; Fig 4.1b). Beside the fault trace, the most impressive feature of the MMF is the thickness of the fault damage zone: going from the southern sector (Arischia) towards the northern sector (Barete) the hangingwall block is exposed within badlands morphologies ranging from 100s to 10s of meter in thickness (Fig 4.1c). The fault damage zone of the northern Barete segment was mapped by Silvia Cortinovis for her Ph.D. project. She characterized and classified the

fault zone rock types (ultracataclasites, cataclasites and breccias), determined the grain size and shape distributions of these fault rocks, and produced geological cross sections of the fault zone of the northern sector near Barete and of the central sector near Pizzoli village (Fig 4.2). In the northern sector (Barete) the Master slip surface is very smooth and quasi-planar, cuts the Corniola Fm. with an average attitude of 204/65 (dip azimuth/dip), the fault core is ~5m thick and the damage zone hosts secondary synthetic faults almost parallel to the Master Fault. In the central sector (Pizzoli) the fault core is wider (30 m) and the transition between fault core and footwall damage zone is marked by the presence of m-thick blocks (i.e. lithons) of cemented cataclastic rocks which are also offset by subsidiary normal faults.

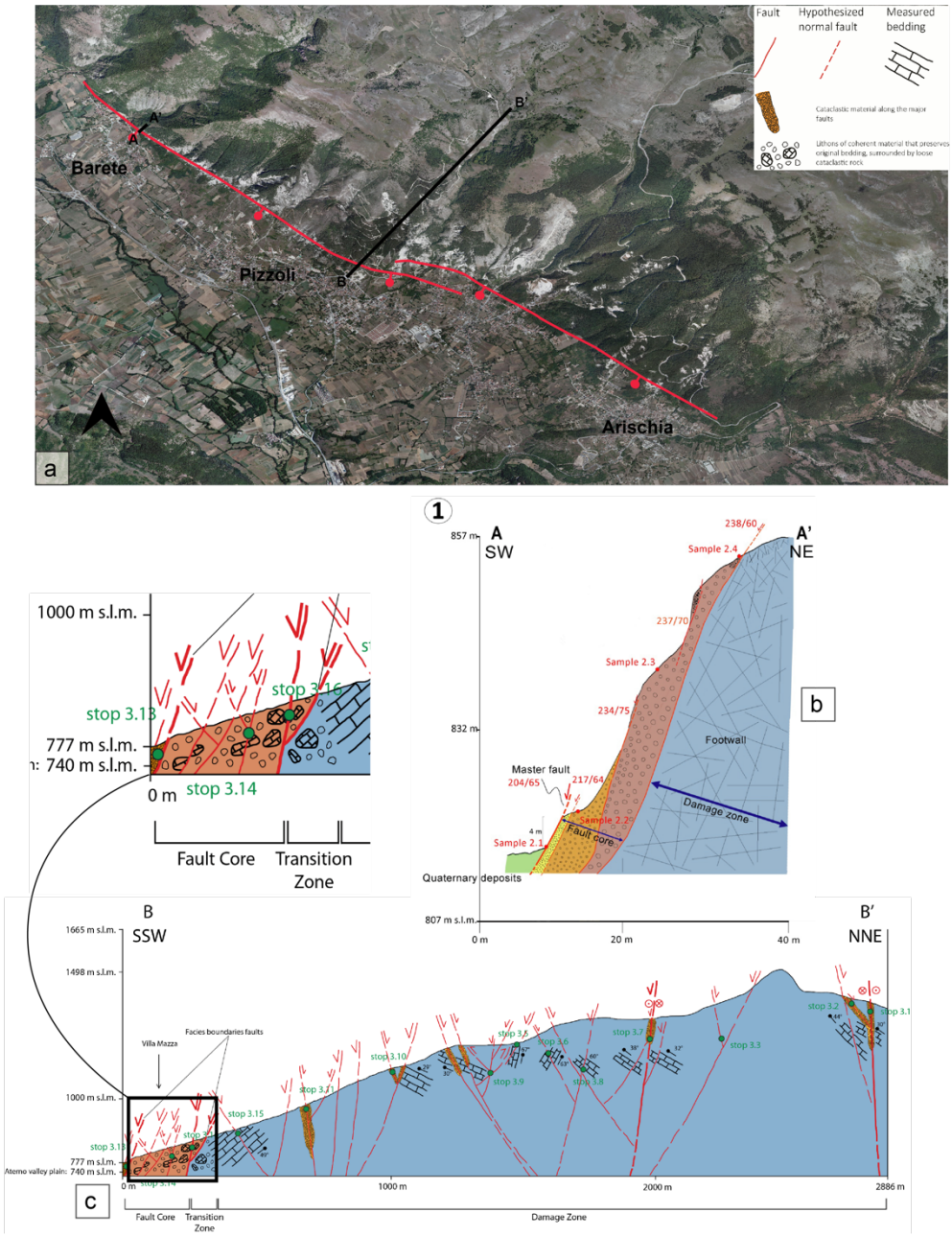


Fig. 4.2 Structure of the Monte Marine Fault Zone (from the Ph.D. thesis of Silvia Cortinovis) (a) Two geological cross sections through the MMF zone, (b) the first in the Barete sector and (c) the second in the Pizzoli sector.

In my thesis, with respect to the classification proposed by Cortinovis in her Ph.D. thesis, the fault rock classification has been improved and used for the structural geology map of the central and southern sector (Pizzoli). In fact, if the facies of the fault core were already well-characterized in the norther sector (Barete), for the damage zone facies characterization we exploited the better exposures in the Pizzoli area:

Fault core facies:

- **Facies 1**: ultracataclasites with sub-rounded grains < 63 μm in diameter lining the Master fault surface of the MMF (Fig 4.3a);

- **Facies 2**: coarser cataclasite with sub-rounded grains 0.063- 2 mm in diameter and proto-cataclasites with angular clasts (Fig 4.3b);

Damage zone facies:

- ***In-situ* shattered rocks**: coarse breccia with an exploded jigsaw textures (i.e., no evidence of relative movement between the nearby fragments), with sub-angular rock fragments up to few centimetres in size (Fig 4.3c-d).

  Facies 3a: coherent/uncoherent loose mosaic breccia with fracture spacing < 1 cm, formed by elongated cm-in-size rock fragments (Fig 4.3c). The pristine sedimentary structures and bedding are not preserved;

  Facies 3c: 3 to 10s of m-in-size blocks (i.e., lithons) with morphological relief, often bounded by secondary faults and pervaded by various sets of joints. The lithons consist of cohesive mosaic breccia with fracture spacing < 1 cm, formed by cm-in-size rock fragments. The higher cohesion of the rock results in the morphological relief of the lithons even if the fracture spacing is the same as in Facies 3a (Fig 4.3d, Fig 4.19 c-d). The pristine sedimentary structures and bedding are rarely preserved;

- **Green Veined Breccia:** green-brownish in colour grain-supported breccia with cm-in-size dolomite angular clasts pervaded by dolomite-filled veins (Fig 4.3 f-h). In the few localities where the Green Veined Breccia crops out, it appears in well-defined domains associated to the presence of thrust faults and fluid circulation (see discussion in section 5.2).
- **Low strain Damage Zone**: host rock cut by regularly spaced (> 30 cm) joints. The pristine sedimentary structures and bedding are well-preserved (Fig 4.3i-k).

The damage zone is also cut by secondary synthetic/antithetic, high/low angle faults with their cataclastic slip zones. The latter are usually mm-thick if filled by ultracataclasites and cm-thick when filled by cataclasites. Where these secondary slip zones are thicker and longer, they were traced in the structural maps as Facies 1 and Facies 2. Furthermore, image analysis investigations showed that Facies 1 and 2 differ primarily for the grain size and grain shape distribution: approaching the main fault surface, the fractal dimension increases while the grain size decreases (Fig 4.3e, Cortinovis et al., 2018;).

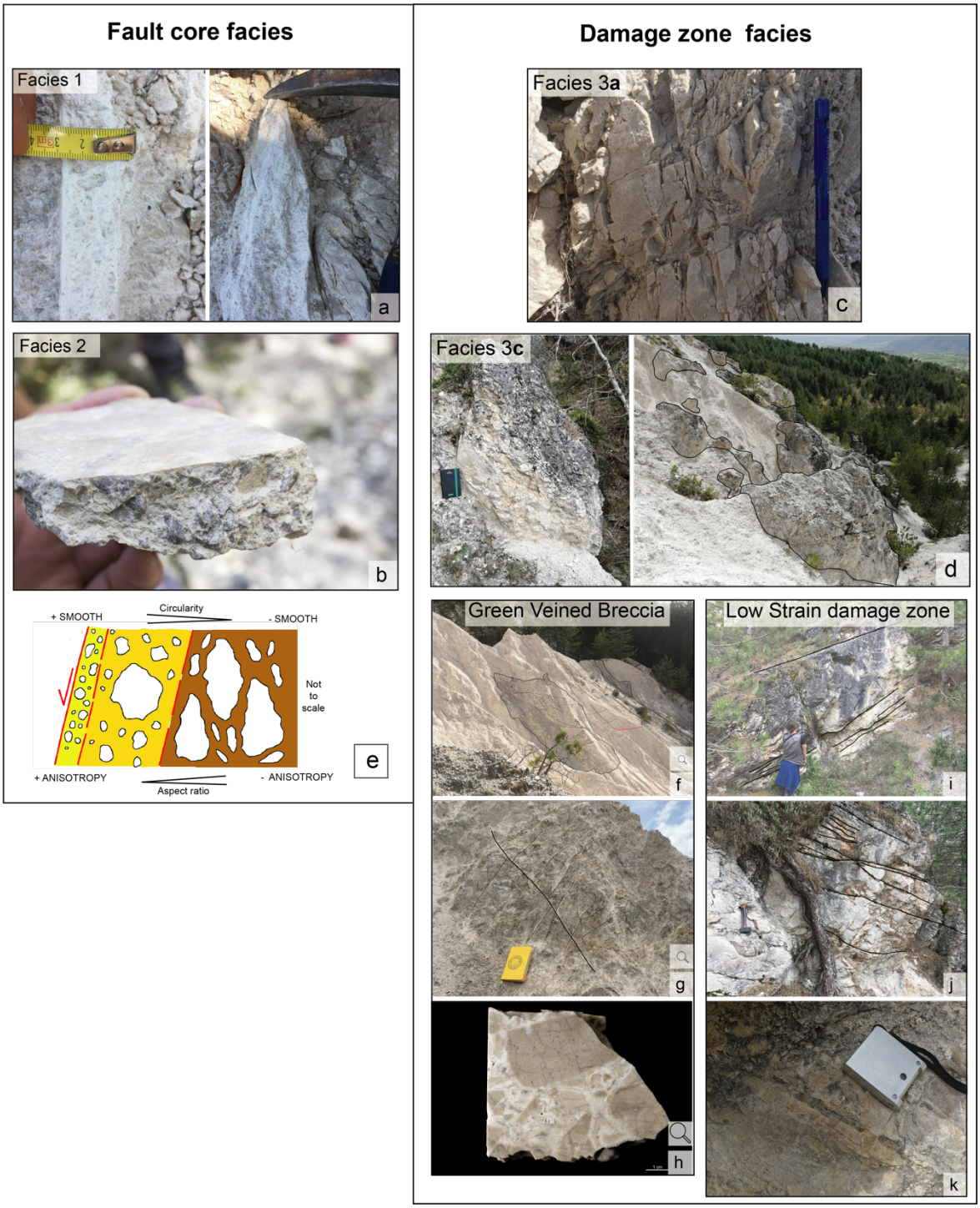


Fig. 4.3 Photographs of the main fault zone rocks facies recognized in the overstep sector of the MMF. (a-b) Facies 1 and 2 (5 m and 30 m thick in the Barete and Pizzoli sections, respectively) belong to the fault core and border the master fault surface. (c) The damage zone ISRs of Facies 3a. (d) The damage zone ISRs of Facies 3c. (e) Fault core rocks in the Barete sector increase in circularity and decrease their aspect ratio approaching the master fault plane (from Silvia Cortinovis Ph.D. Project). (f-h) Green Veined Breccia. (i-k) Low strain damage zone.

4.1.1 The overstep sector of the Monte Marine Fault zone

In the central overstep sector of the MMF, the Master fault surface crops out discontinuously in the village of Pizzoli covered by buildings and roads, and its trace is inferred from the presence of small escarpments (1-3 m high) and from trench excavation data (Moro et al., 2016) (Fig. 4.4). The latter showed evidences for faulting and displacement of the exposed colluvial, organic and "cultural" sediments and palesols (Moro et al., 2016).

Going towards the south from the village of Pizzoli towards Arischia, the fault damage zone increases in thickness up to ~ 1000 m. Structural stations highlighted the presence of at least two sets of joints, secondary normal (synthetic and anthytetic) faults, oblique faults, low angle (dip <45°) and thrust faults (Figs. 4.4-4.8). Thrust faults and major normal secondary faults are often lined by mm-thick ultracataclasites and cm-thick cataclasites, sometimes with the principal slip zone highlighted by a reddish I colour Fe-Oxide coating (Fig 4.6d). Cross-cutting relations show that low-angle (dip <45°) faults (usually with dominant reverse sense of shear) are often cut by normal high-angle (dip ≥45°) faults, particularly by those with the same dip azimuth of the Master Fault of the MMF (e.g., station 5.9 where the normal faults displace the thrust; Fig 4.6a and Fig 4.8). Displacements range mostly from 10 to 50 cm. Moreover, where low-angle faults with dominant reverse sense of shear intersect normal high-angle faults, the thickness of cataclastic products increases and locally the ultracataclasites of the secondary faults reach 10 cm in thickness. In the damage zone, the bedding is still recognizable in very few outcrops: in areas distant (> 200 m) from the Master Fault of the MMF, the bedding mainly dips towards NE. Instead, approaching the Master fault, the attitude of the bedding becomes more scattered. Station 5.13 represent the location at which, in the overstepping sector, we measured the maximum thickness (ca. 1000 m) of the damage zone (Fig. 4.4). The outer domains are composed by the Low strain Damage Zone with largely spaced (>1m) fractures.

The geological-structural map of Monte Marine Fault zone summarizes all the information collected during the surveys. The map contains the distribution of fault rock facies within the damage zone, faults (reverse faults are in blue in colour, normal fault in red and strike-slip faults in black), bedding attitude and the location of the structural stations (see Fig 4.4 and poster n. 1).

A sostituire questa e la prossima facciata va la Fig. 4.4 (Miniatura del Poster 1) stampata in formato A3 e piegata.

4.1.1.1 Structural stations

We measured faults, joints and bedding attitudes in 26 structural stations (Fig 4.5a). The contouring of all normal faults lineation had a peak towards the SW (N210°-220° trend) consistent with the sense of shear of the Master Fault of the MMF, while contouring of the low angle (dip <45°) faults lineation was N206° on average (Fig 4.5b). Though we found several low angle faults, only those exposed at stations 5.7, 5.9, 5.11 and 5.17 were unambiguously identified as thrusts based on kinematic indicators and Riedel-type geometry (Fig 4.6-4.7).

The kinematic inversion of the structural data shows predominance of ca. NE-SW oriented extension especially in the vicinity of the Master Fault (stations 5.1, 5.2, 5.4, 5.14), while in the NW sector the extension rotates to ca. E-W (station 5.3, 5.5). Only at station 5.9 kinematic inversion shows compression (ca. NNE-SSW oriented, Fig 4.8). Only few minor strike-slip faults are present and accommodate limited slip in this area.

4.1.1.2 Geological cross sections

I built four geological cross sections (Fig 4.9):

- 1 parallel to the Master Fault strike (**B-B'**),
- 1 parallel to the Master Fault dip direction (**A-A'-A''**) and
- 2 to illustrate the structure of sites of particular interest (**C-C'** and **R-R').**

In particular, cross section R-R' was built to estimate the displacement cumulated by a set of secondary normal faults within the damage zone and to quantify how strain is partitioned among the fault core and the damage zone. In fact, the hanging wall of MMF is mantled by sparse remnants of slope-breccias Late-Pleistocene in age (Sant'Antonio breccias, *sensu* Bosi et al., 2003; Galadini and Galli, 2000; Galli et al., 2011, see inset in Fig 4.10). R-R' is a 150 m long cross section between two displaced Pleistocene breccia outcrops, located ca. 120 m apart which we interpreted as belonging to the same paleosurface since the dip angles among the two outcrops are almost the same. The vertical throw between the two Pleistocene Breccia outcrops is ~8.4m and could be considered as cumulated from the activity of ~10 normal faults (both synthetic and antithetic) hosted in between the two St. Antonio Pleistocene Breccia outcrops (Fig 4.10).

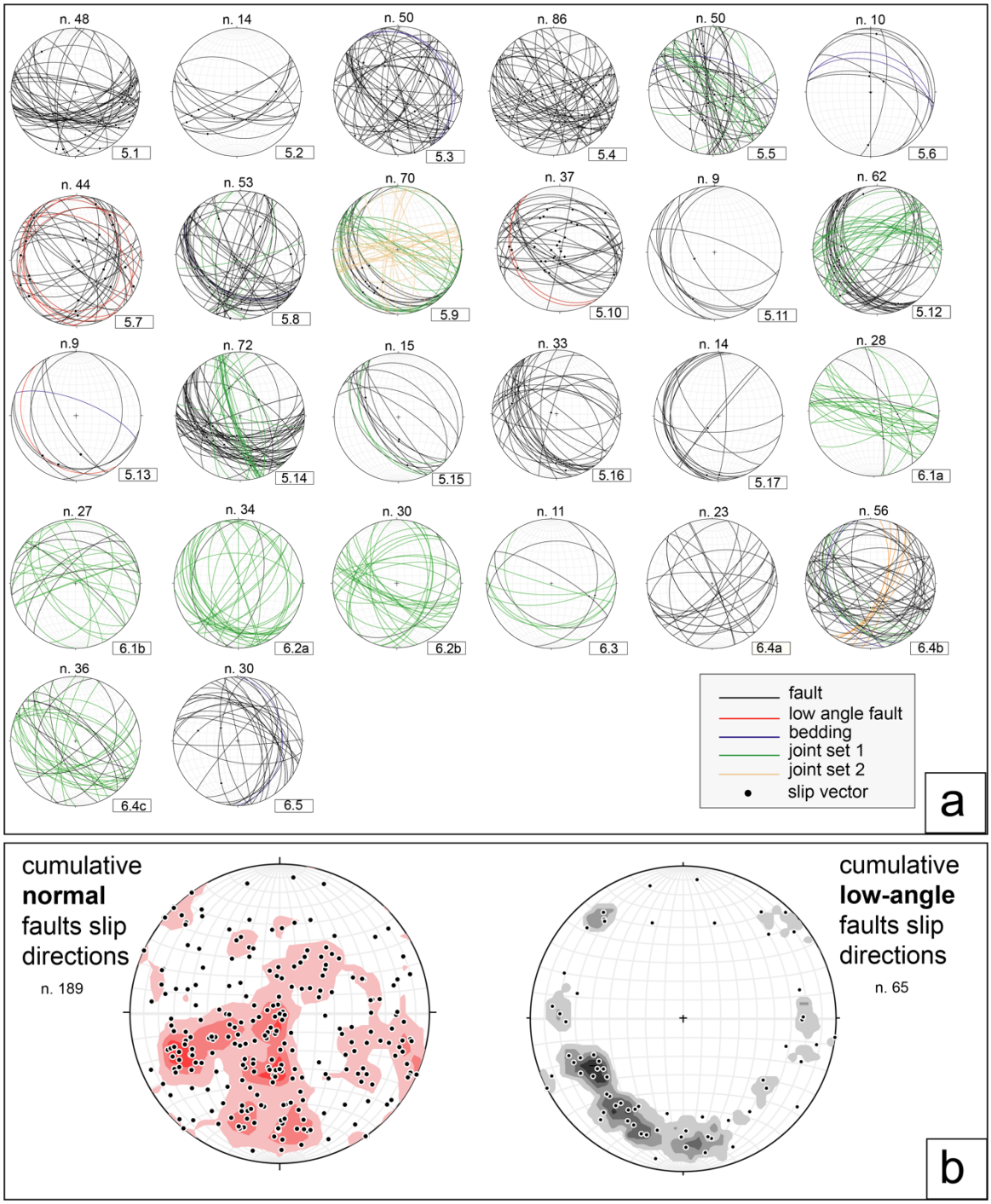


Fig. 4.5 Structural data from the overstep sector of Monte Marine Fault Zone (see Fig. 4.4. for location of the stations). (a) Stereoplots of the 26 structural stations. (b) Attitude of the fault lineations divided between those pertaining to high-angle (dip ≥ 45°) and low-angle (dip< 45°) faults.

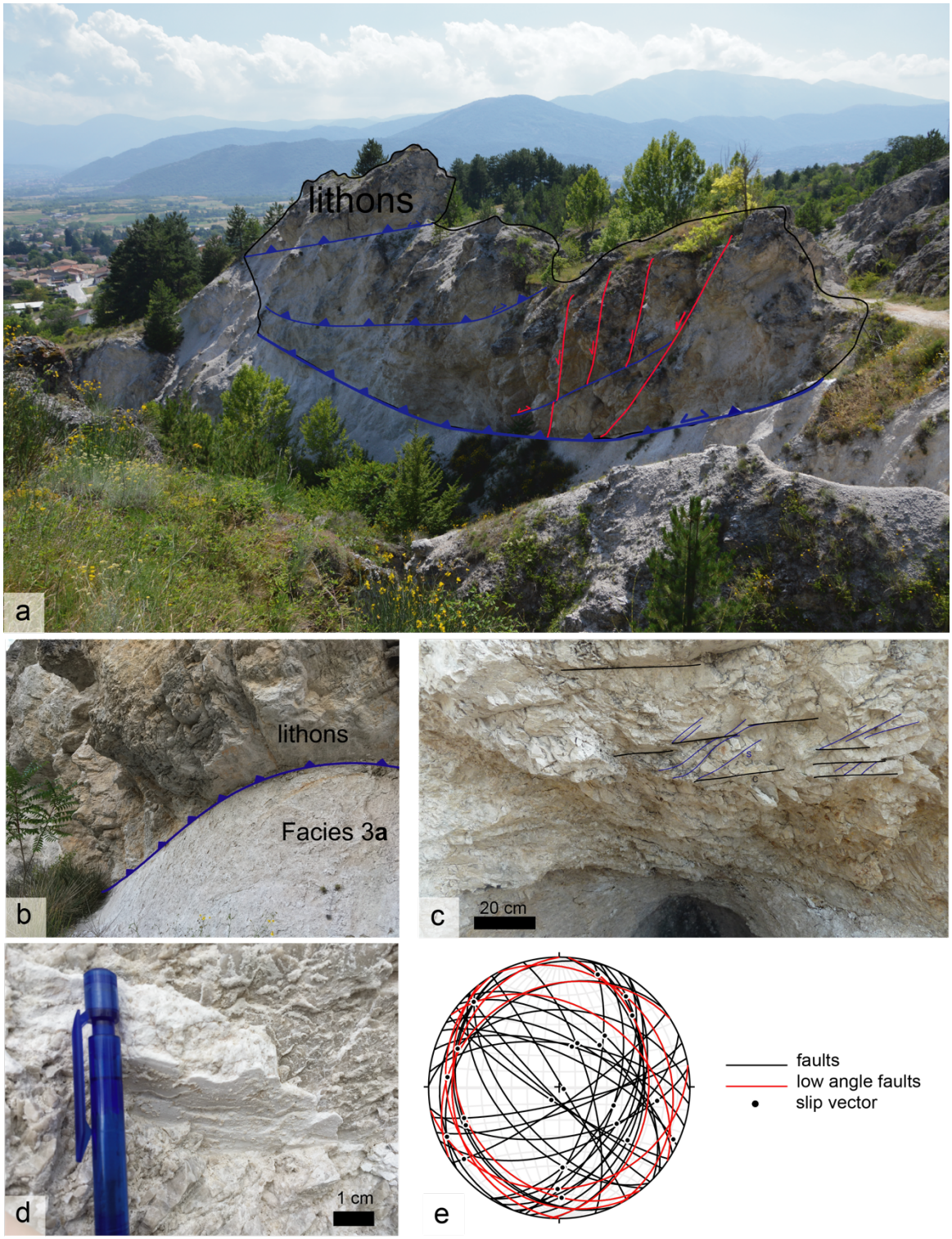


Fig. 4.6 Example of low-angle fault exposure and fault rock distribution (structural station 5.7). (a) Panoramic view of the outcrop which includes one of the best-exposed low-angle faults. (b) Cataclastic Facies 3a and Facies 3c are dominant at the footwall and at the hangingwall, respectively, of the low angle fault. (c) In the hangingwall of the low angle fault, a S-C foliation consistent with top to SW shear normal fault is recognisible. (d) Polished secondary fault surfaces are often lined by cm-in-thickness ultracataclasites. (e) Stereoplot of the faults measured in this structural station.

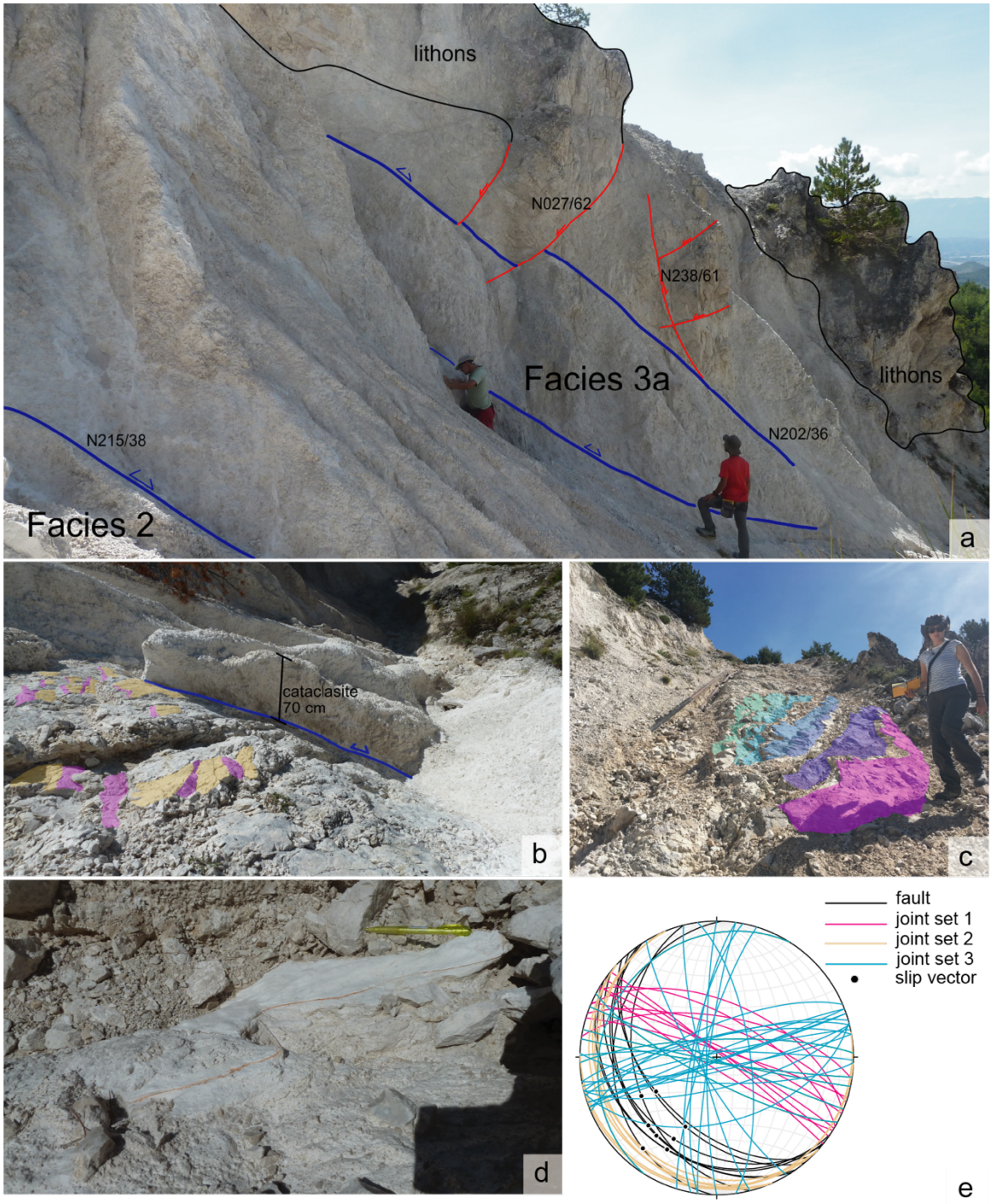


Fig. 4.7 Example of intersection between high-angle normal faults and low-angle faults (structural station 5.9). (a) High-angle normal faults cutting low-angle faults. (b) The thickness of the cataclastic materials (Facies 2) increases up to 70 cm at the intersection of the faults. The different colours highlight the sets of very minor faults and joints cutting the footwall. These joints are arranged as R and R' Riedel shears. (c) Detail of the very minor faults and joints cutting the footwall. (d) Cm-thick ultracataclasite of a low-angle faults principal slip zone. (e) Steroplot of the structural data from station 5.9.

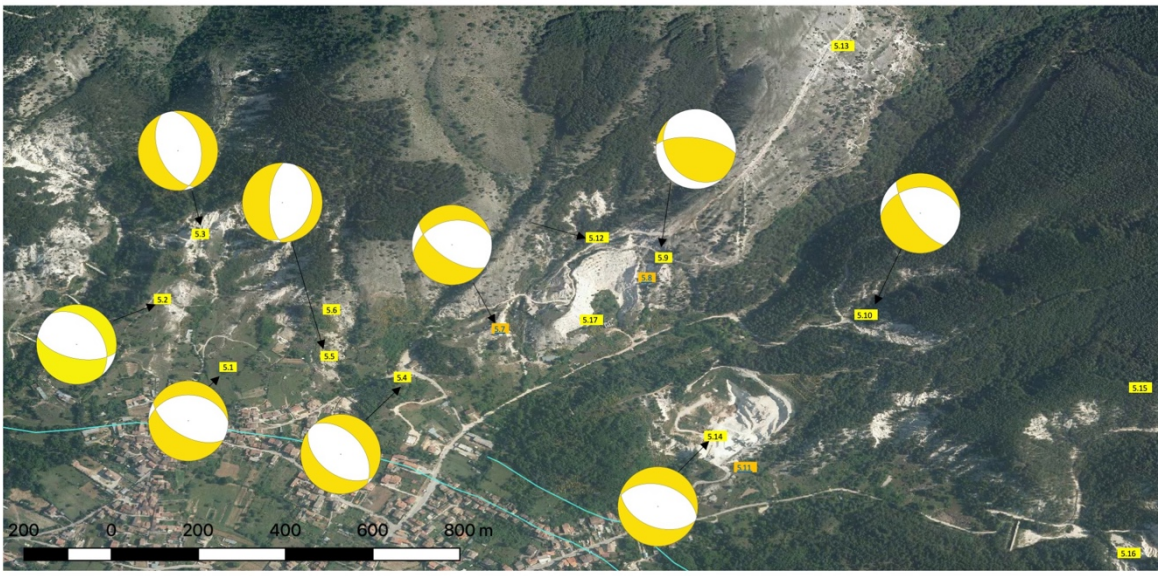


Fig. 4.8 Kinematic inversion of slip vector data are presented in the form of *beach balls,* with the compressive quadrant in yellow.

A sostituire questa e la prossima facciata va la Fig. 4.9 (Sezioni geologiche) stampata in formato A3 e piegata.

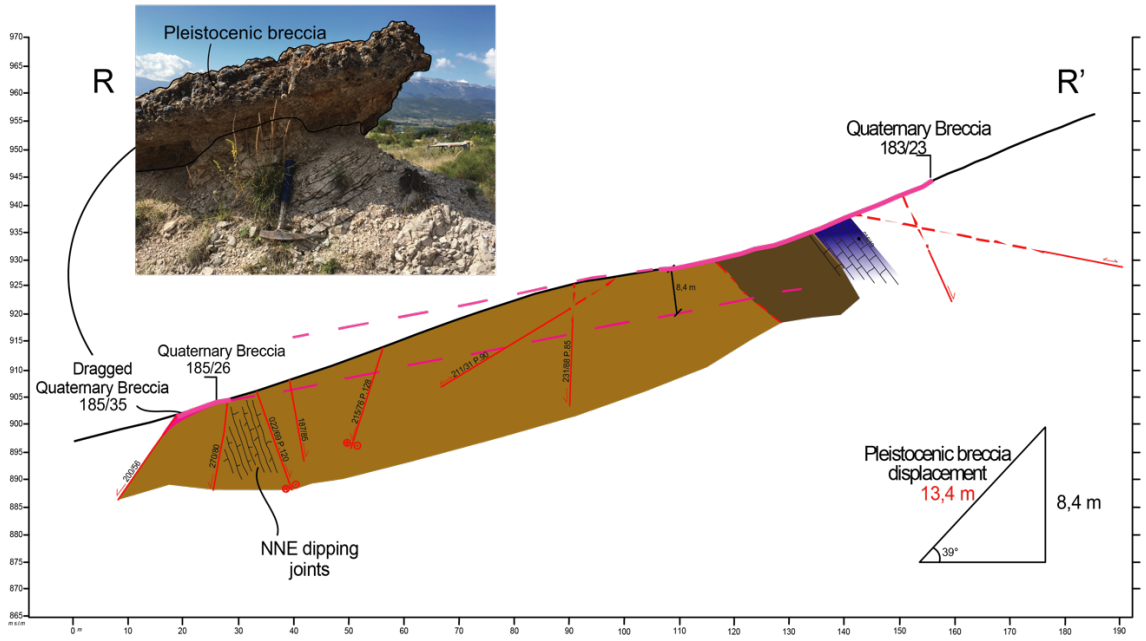


Fig. 4.10 Geological cross section R-R' is built to calculate the displacement cumulated by ten secondary faults in the damage zone. Constraints are offered by the Pleistocene-in-age slope breccia (see the inset) which mantles the badland slope. The dip angle of the slope reflect the original dip of the paleosurface.

4.2 *Microstructures of fault zone rocks*

Under the optical and scanning electron microscopes, the studied faults are characterized by the occurrence of mirror-like slip surfaces cutting a slip zone which ranges from ~2 mm to ~5 cm in thickness. The slip surface corresponds to the fault ‘‘plane’’, while, as it is the case of shallow-seated brittle faults hosted in carbonate-bearing rocks, the slip zone contains gouges, cataclasites, ultracataclasites and, in some cases, dynamically recrystallized calcitic in composition nano- and micro-grains (Siman-Tov et al., 2013; Smith et al., 2011; 2013; Fondriest et al., 2013; Demurtas et al., 2016). Collectively, the slip surface and the slip zone accommodate the bulk of coseismic displacement during individual seismic rupture events (Sibson, 2003). Here below I describe fault core rocks of a major (sample MM5.3, thrust cut by normal fault) and a minor (sample MM5.6, fault hosted in Facies 3) fault hosted in the damage zone. I selected samples MM5.3, which include a slip zone from a thrust structure, and MM5.6, which include a slip zone from a secondary normal fault, because they include both footwall and hangingwall of the slip surfaces. In addition, the thrust is a relevant structure in the architecture of the overstep sector of the MMF, hence the comparison of the microstructures in thrusts vs. minor normal faults could reveal differences in their deformation mechanisms.

Sample MM5.3 includes the principal slip zone of the thrust fault from station 5.9 (Fig. 4.7). The several centimetre-thick principal slip zone is cut by a sharp and sub-planar slip surface which separates a fine grained cataclasite in the hangingwall from an ultrafine ultracataclasite in the footwall (Fig. 4.11a). The cataclasite in the hangingwall includes a porous 50% to 90% in volume matrix made of randomly oriented angular grains of dolomite wrapping larger clasts of reworked cataclasite up to several mm-in-size (Fig. 4.11a-b). The dolomite grains split along cleavages resulting in the formation of a fine matrix made of dominant < 5 μm in size and tabular dolomite in shape grains (Fig. 4.11c). Approaching the principal slip surface (Fig. 4.11b-c), porosity increases and the average grain size decreases. Beneath the principal slip surface, the ultracataclasite of the footwall is made of an ultrafine matrix made of dominant < 2 μm in size and with low aspect ratio dolomite grains wrapping only very few < 0.5 mm in size clasts. By comparing Fig. 4.11e with 4.11c, it is possible to appreciate the higher degree of textural evolution of the footwall ultracataclasites with respect to hangingwall cataclasites. Though the composition of the two fault rocks is identical (dolomite), the presence of finer and with lower aspect-ratio

grains in the ultracataclasite matrix suggests that the latter accommodated larger strain and slip. The principal slip surface is open and partly filled by very late precipitation of calcite and sandwiched by a ca. 1 mm thick brownish to reddish in colour aureole (Fig. 4.11a – note that the faint sub-parallel bands in the footwall ultracataclasite are the result of sample preparation and percolation of epoxy along microcracks). EDS maps show that the brownish aureole is enriched in Fe, suggesting the precipitation Fe-oxides and –hydroxides next to the slip surface by late stage fluid percolation (Fig. 4.11b-c; EDS maps in Fig 4.13). In conclusion, the presence of such a texturally evolved ultrafine-grained ultracataclasite with reworked ultracataclasite clasts and a last event of fluid infiltration documented by the formation of the Fe-rich aureole next to the slip surface, suggest multiple slip and fluid infiltration events in the principal slip zone of the thrust.

Sample MM5.6 includes the principal slip zone and the fault core rocks of a minor fault hosted in damage zone at 400m from the Master Fault (station 5.14, see Poster 1). The 3-4 mm thick principal slip zone is cut midway by a sharp (now open) and sub-planar slip surface (Fig. 4.12a). The principal slip zone is made of an ultracataclasite with mm-in-size clasts wrapped by an ultrafine (< 1 μm) matrix; both the clasts and the matrix are dolomitic in composition and they are similar to those found in the slip zone of the thrust (compare Fig. 4.12c with Figs. 4.11c and e). The footwall of the slip zone is a cataclasite-protocataclasite made of re-worked well-cemented cataclasites cut by a series of Riedel and anti-Riedel shears filled by ultracataclasites (R and R' in Fig. 4.11a). With respect to the principal slip zone, the Riedel and anti-Riedel shears are arranged consistently with top to the South ("sinistral" sense of shear in the thin section) of the minor fault.

In conclusion, the slip zones of the few minor and major faults cutting the MMF damage zone studied so far are made of porous cataclasites and ultracataclasites (Fig. 4.11 and 4.12) with, in the case of the minor fault, a relatively evolved process zone (Fig. 4.12a). In the slip zones, the grains are fragmented (often with incipient cracks along cleavage: Figs. 4.11c; 4.12d), locally sub-rounded (Fig. 4.11c), isolated and rotated (it is not possible to reconstruct the original grain by matching the neighbour grains, like most of the grains in Figs. 4.11c, e and 4.12c) in a porous fabric (Fig. 4.11b-d and 4.12b-c). All these characteristics and the absence of pressure-solution seams are consistent with pure cataclastic deformation mechanism which includes grain fragmentation accompanied by frictional grain boundary sliding and dilatancy (e.g., Sibson, 1977).

Regarding the *in-situ* shattered rocks, some characteristics of the Facies 3a (made of cm-in-size fragments) and Facies 3c (which locally preserve meter-in-size lithons) can be appreciated in the cut-and-polished hand specimens (Fig 4.14). Both Facies of the ISRs are cut pervasively by fractures and veins.

The ISR of Facies 3a is a breccia hosted, in the studied sample, in the Green Veined Breccia and cut by thick (> 1 cm) veins filled by dolomite (determined with 10 % HCl aqueous solution) and by a dense network (spacing < 5 mm) of thinner veins with a still undetermined filling (Fig 4.14a). The hand-drawing emphasizes the thick dolomitic veins (coloured in green) and the dense network of minor veins (coloured in black) (Fig. 4.14b). The red arrow in Fig. 4.14b highlights the radial arrangement of the thinner veins, which, in carbonate-built fault zone rocks, may indicate shattering processes active during deformation, possibly associated to shock (seismic-related) events (Fondriest et al., 2015; 2017).

The ISR of Facies 3c was sampled from a meter-in-size lithon and is hosted in massive dolomitized limestones. The breccia is made of dolomitic fragments cut by (1) a dense (spacing < 5mm) network of white in colour carbonate-bearing veins and (2) a less dense (spacing > 1 cm) network of cm- to dm-long quite continuous and black in colour open fractures (Fig 4.14c). The dark colour of the latter is due to epoxy resin impregnation of the specimen (see Fig. 4.14d). These cm- to dm-long open fractures, which are the last deformation event recorded by the breccia, correspond to the main sets of joints along which lithons split when hit by the hammer. Beside this preliminary description, further investigations are required to determine the exact filling of the veins of the two types of ISRs and to understand why the pervasive fracture and vein pattern of the ISRs results in the presence of meter-in-size-lithons (Facies 3c) or in their absence (Facies 3a).

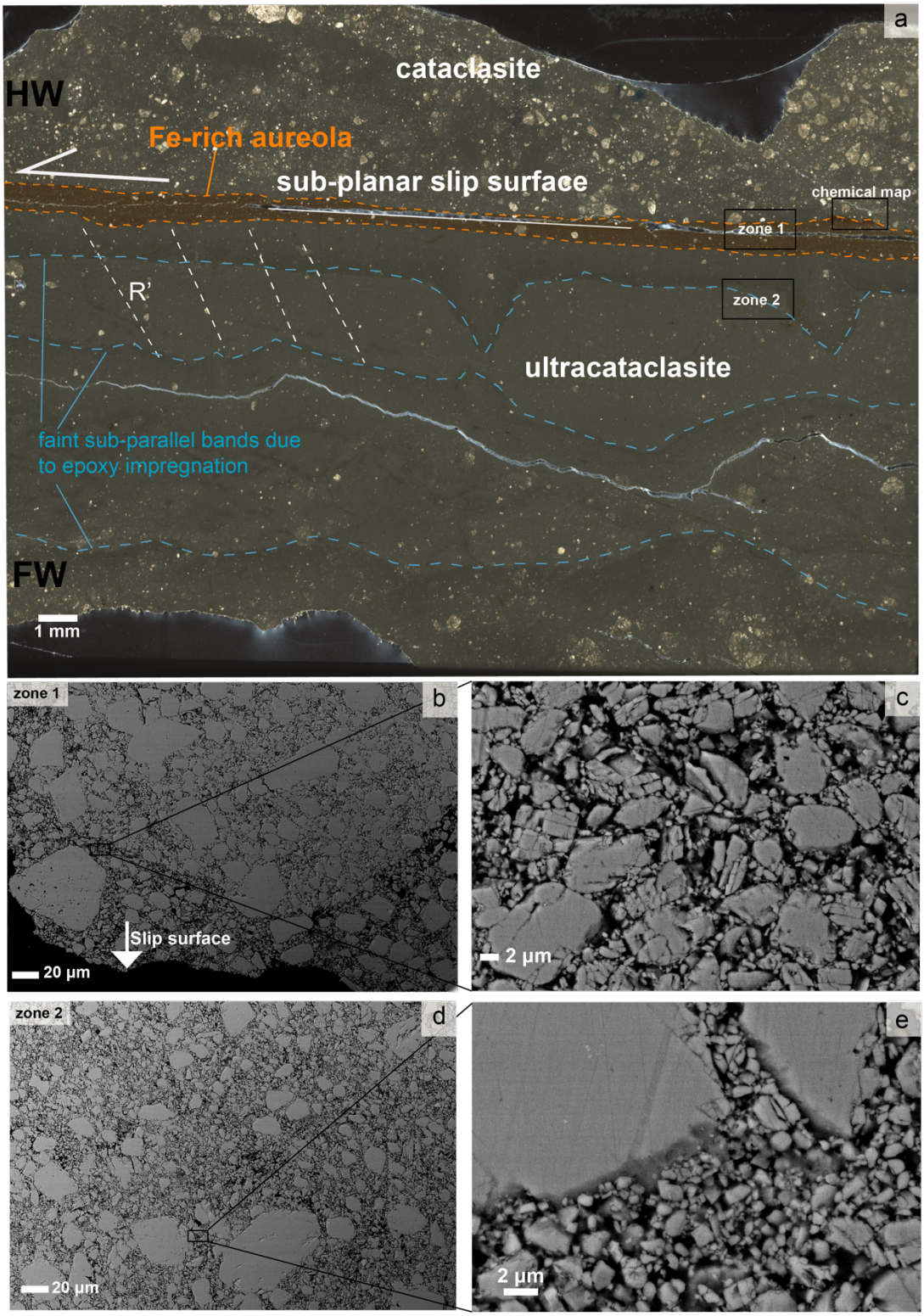


Fig. 4.11 Principal slip zone and slip surface of the low-angle fault at the Station 5.7. (a) Slip zone under the optical microscope. (b) Principal slip zone bordering the slip surface. (c) Fragmented grains along cleavage and porous ultracataclastic fabric in the slip zone (zoom of Fig. b). (d) Ultracataclasite in the footwall. (e) Porous ultracataclastic fabric in the slip zone (zoom of Fig. d). (b) to (d) BSE-FESEM images (see text for discussion)

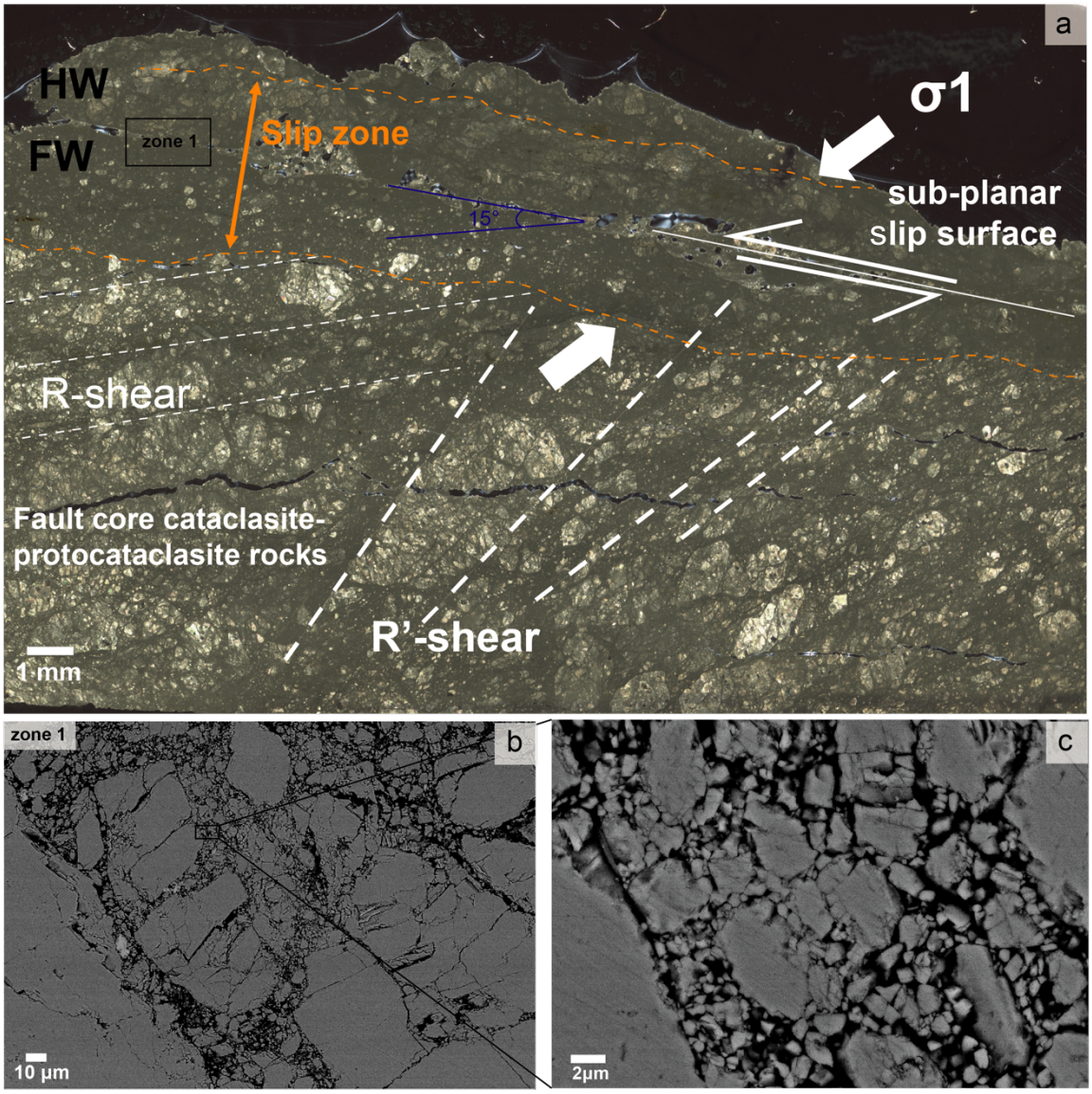


Fig. 4.12 Principal slip zone and slip surface of a minor normal fault cutting the damage zone from station 5.14. (a) The 3-4 mm slip zone cut in the middle by a sharp slip surface (optical microscope image). The array of R-R' shears in the process zone is arranged consistently with a sinistral sense of shear for the slip zone. (b) Principal slip zone bordering the slip surface. (c) Fragmented grains along cleavage and porous cataclastic-ultracataclastic fabric in the slip zone (zoom of Fig. b). Though the average grain size is larger and the slip zone thinner, the overall microstructure is similar to the one found in the low-angle fault (Fig. 4.11) suggesting the activation of purely brittle cataclastic processes in both faults. (b) and (c) BSE-FESEM images (see text for discussion)

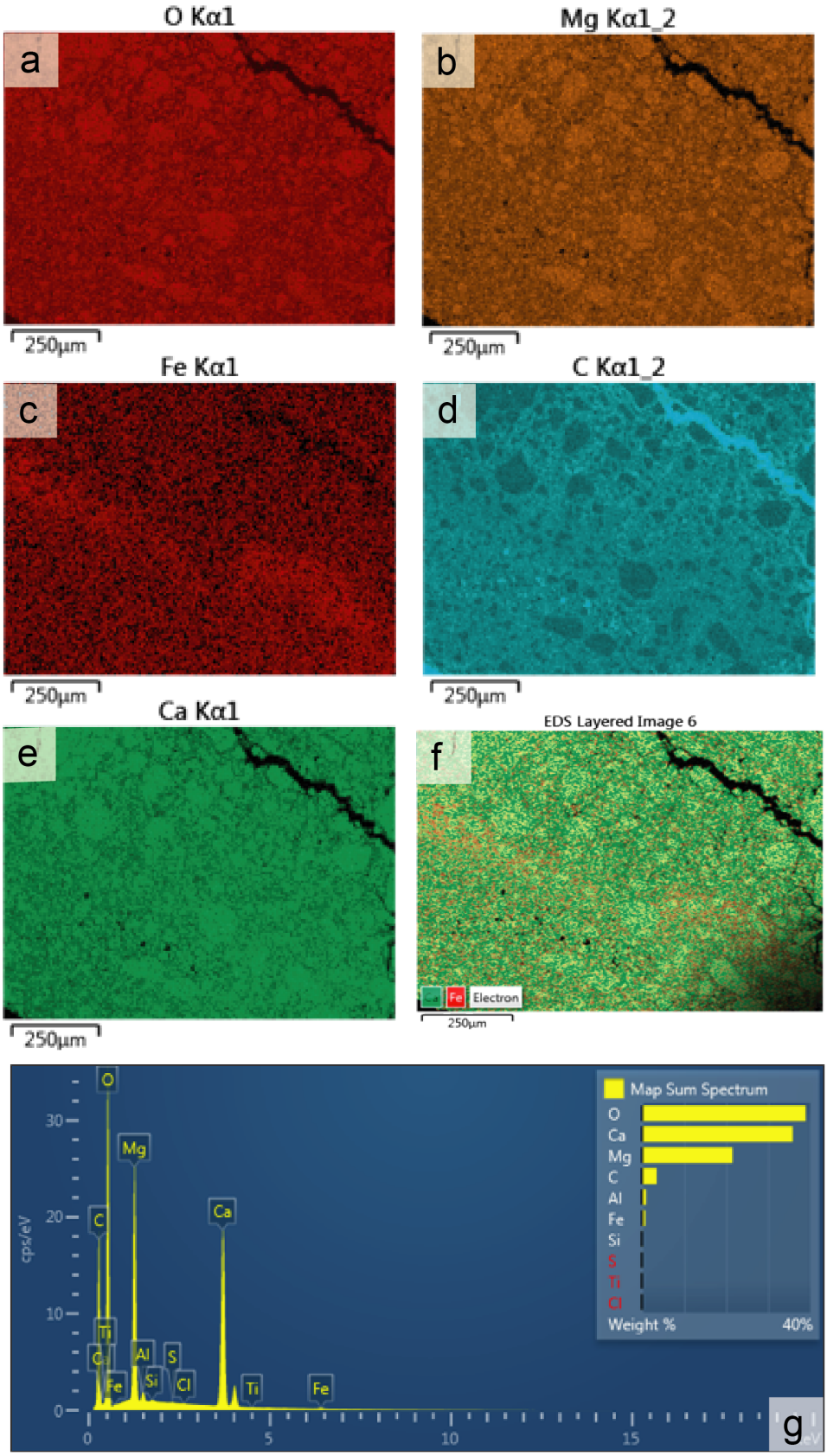


Fig. 4.13 EDS elemental maps of sample MM5.3 (see location in Fig 4.12a). (a to f) The elements measured are O, Mg, Ca, C and Fe. The reddish aureole lining the slipping surface is Fe-Enriched (Fig. 4.11a and Fig. 4.13f). (g) Both clasts and the matrix are dolomitic in composition.

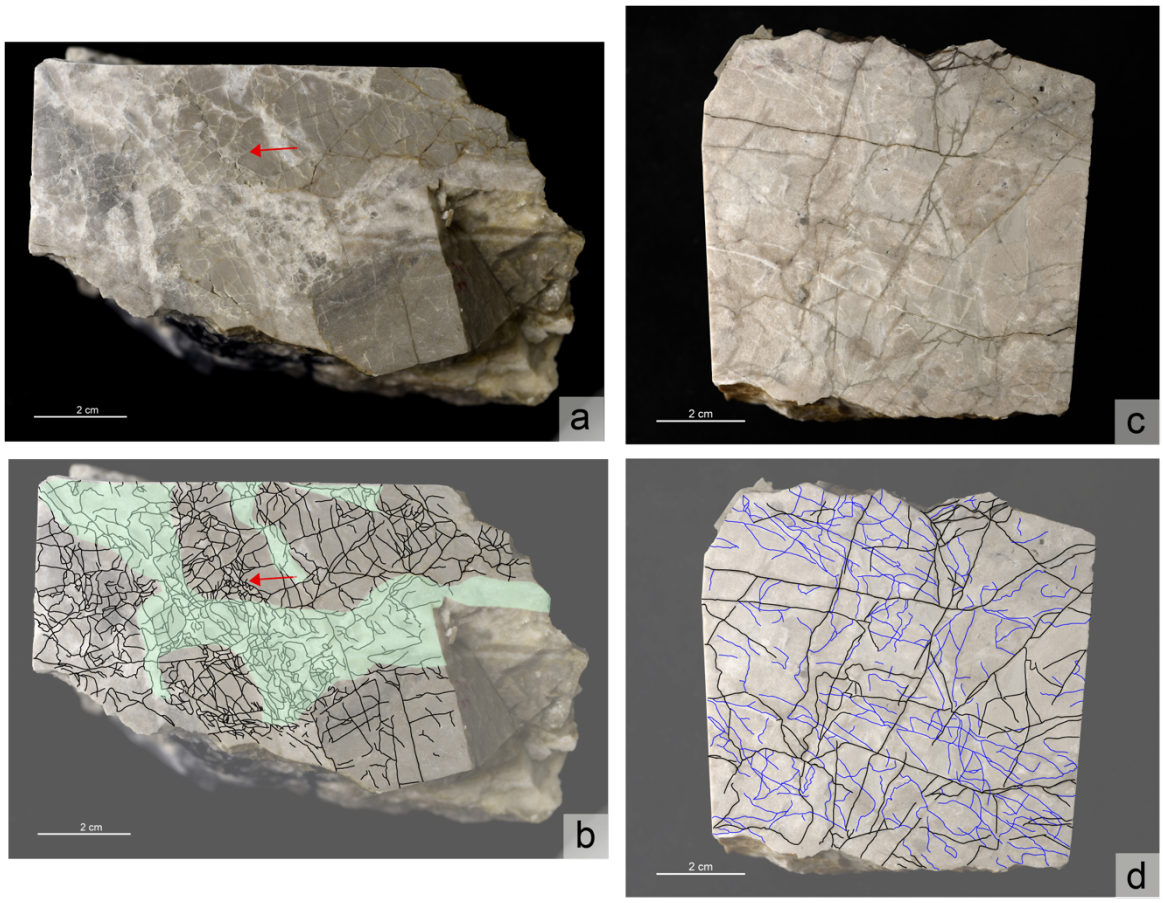


Fig. 4.14 Cut and polished hand specimen of in-situ shattered rocks. (a-b) Facies 3a hosted in Green Veined Breccia, (c-d) Facies 3c hosted in dolomitized massive limestones. In Fig. b hand-drawing emphasizes thick (> 1 cm) veins in green and the radial pattern of narrower veins with black lines (see main text for the description). In Fig. d hand-drawing emphasizes the open fractures with black lines.

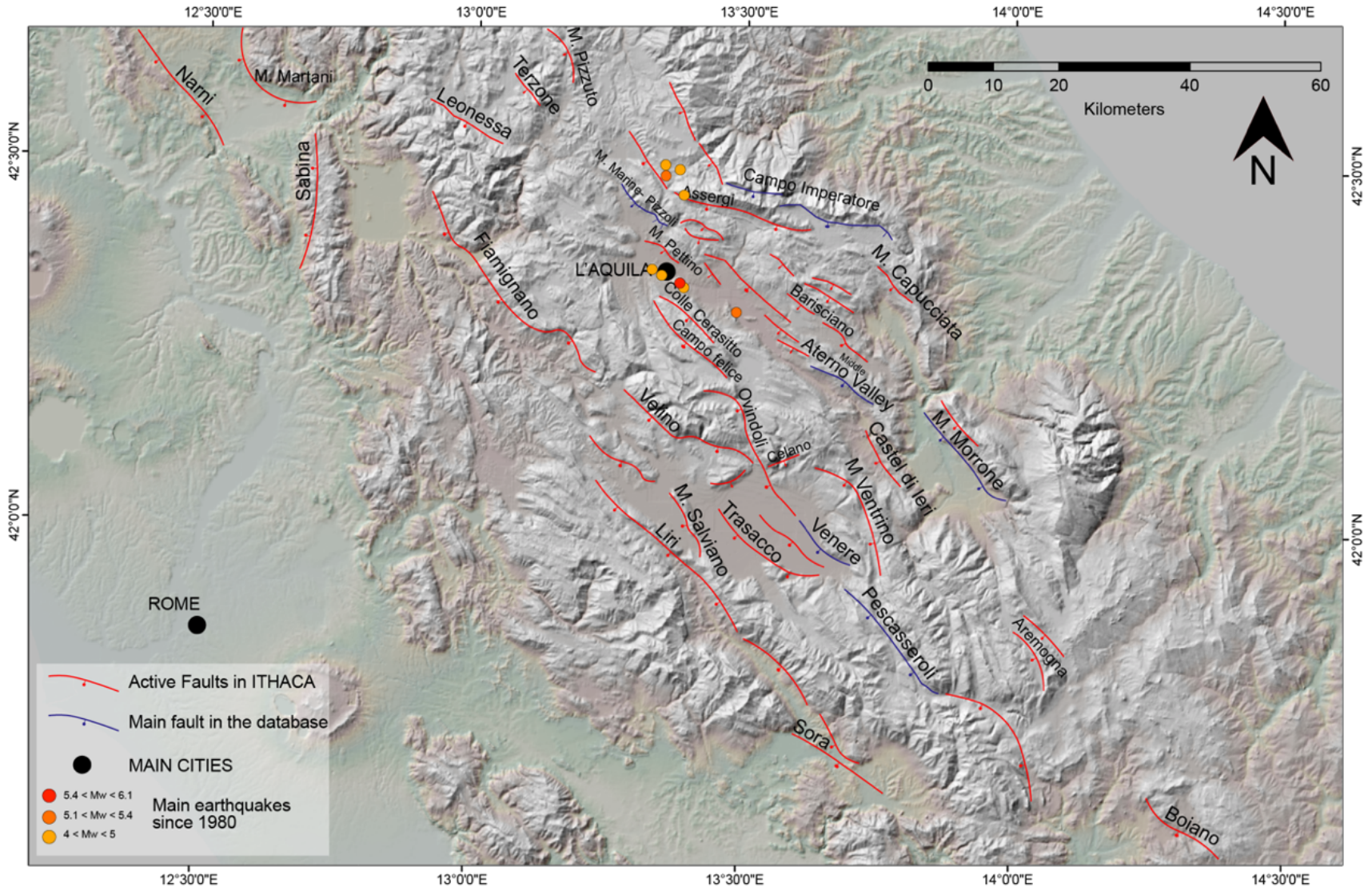


Fig. 4.15 Main carbonate-hosted active normal fault zones of the Central Apennines. In blue the faults included in the catalogue presented in this thesis and characterized by thick damage zones with ISRs.

4.3 *Catalogue of fault damage zones in the Central Apennines*

Thanks to the interpretation of aerial and satellite images, I produced a *catalogue* of carbonate-hosted active normal fault zones of the Central Apennines characterized by thick (up to 100s m) damage zones with *in-situ* shattered carbonates. For each fault zone, the catalogue contains information collected from the literature, while in the field I collected structural data and determined the spatial extent (i.e. thickness) of the *in-situ* shattered rocks. The selected faults are (Fig 4.15):

1. the Monte Marine fault zone (MMF),
2. the Campo Imperatore fault zone (CIF),
3. the Pescasseroli fault zone (PF),
4. the Middle-Aterno Valley fault zone (MAVF),
5. the Morrone fault zone (MF),
6. the Venere fault zone (VF).

The above fault zones were selected among those with the best footwall-block exposure hosted in limestones (i.e., MAVF, MF, VF) and dolostones (i.e., PF, CI, as well as the MMF) also to investigate the role of lithology on the type of damage pattern. Moreover, I selected faults with different lengths and displacements to evaluate *damage zone thickness* vs. *displacement* and *damage zone thickness* vs. *fault length* trends to infer, if any, the presence of scaling laws among these parameters. To produce this dataset, because of time limitations, I have not carried out a collection of structural data with the detail comparable to the one I produced for the Monte Marine Fault damage zone. Nevertheless, the field surveys allowed me to determine, to a first approximation, the distribution of the fault zone rocks and the damage zone thickness. Since intensively fractured and damaged rocks were found also outside the badlands mapped from the aerial and satellite images (e.g. for the MAVF and MF), the measurements of the thickness of the damage zones presented here remain a minimum estimate.

With the exception of the CIF, where I used the high quality structural data, similar to those here presented for the MMF, from Demurtas et al., (2016), I adopted the same fault zone rock classification used for the MMF zone structural map (Fig. 4.4.). The following

sub-sections summarizes the main characteristics of each selected fault zone and the complete dataset can be found in the appendix (Poster 2) and includes:

1. fault data (i.e., strike, dip, displacement, length, etc.) with stereoplots,
2. damage zone data (i.e., thickness, host rock, etc.),
3. outcrop coordinates and map with the structural data collected,
4. geological map of the study area, outcrops photos,
5. references.

4.3.1 Middle-Aterno Valley Fault zone (MAVF)

The Middle Aterno Valley faults pertain to a 21-km-long fault system made of two main segments and it is considered a seismogenic source capable of up to Mw 6.5-7 earthquakes (Falcucci et al., 2015). The absence of large magnitude seismic events reported in the historical catalogues attributable to the MAVF over the past 800-1000 years bring to define the structure as "silent", that is a seismic gap. Faults segments are represented by NW-SE trending and SW dipping synthetic faults and by a major antithetic structure (Falcucci et al., 2015). The structure of the MAVF is well-exposed in the quarry near the Roccapreturo village (Fig 4.16a) and the main fault surface can be followed for kilometers along the Aterno valley. In the quarry, we performed a half-day long structural survey, mapping the main secondary faults and the lithology distribution. In the footwall, made of massive limestone of the Terratta Fm. (Vezzani et al., 1998) we found ISRs until the upper limit of the quarry, without any transition or decrease in the fracture density and measured a damage zone at least **239** m thick. In this damage zone and similarly to what we found in the MMF, few minor low-angle (dip <45°) normal dip-slip faults are cut by high-angle (dip ≥45°) normal faults. Lithons pertaining to the Facies 3c are bordered by faults and, although the morphological relief from their higher resistance to erosion, they have a very high density of fractures comparable to those found in Facies 3a.

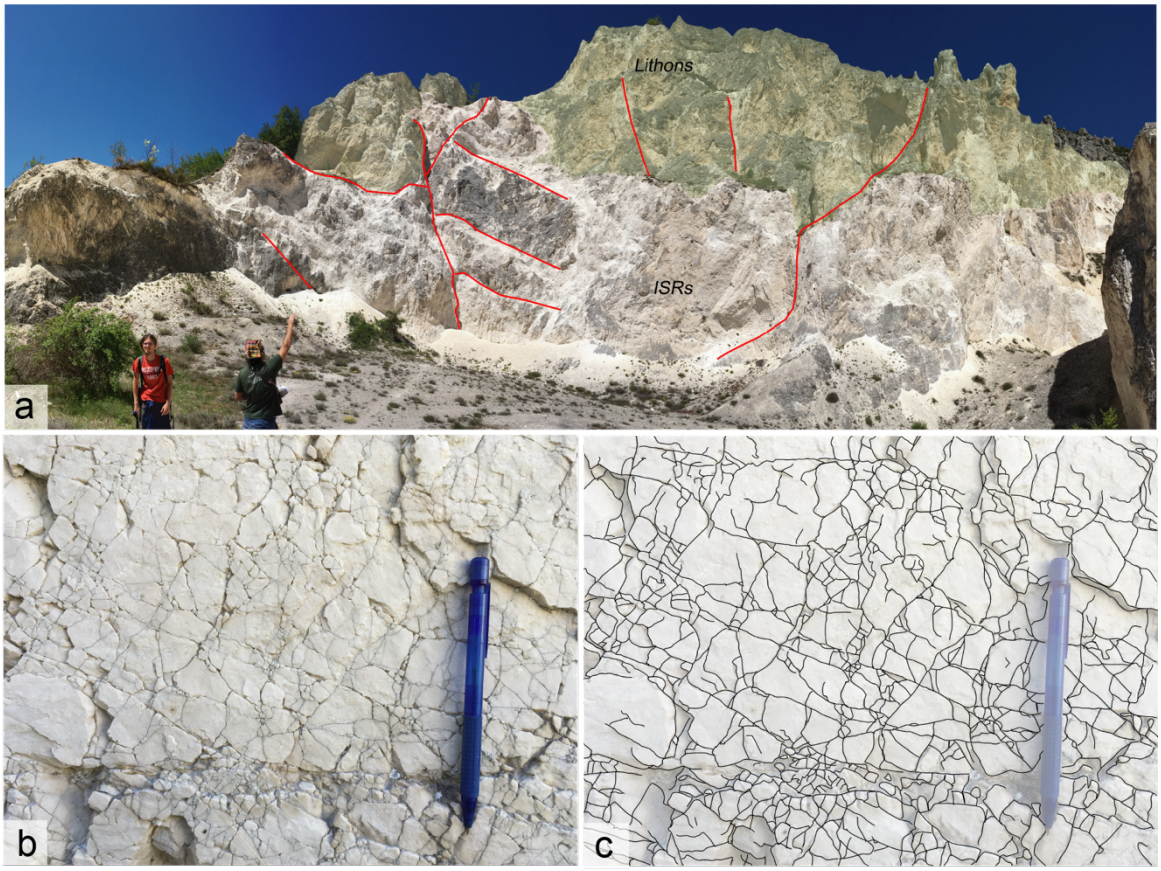


Fig. 4.16 Middle-Aterno Valley Fault zone (MAVF). (a) Wonderful exposure of the damage zone in the footwall at location UTM 392650 E, 4672567 N. (b,c) Mesoscale fracture pattern of ISRs highlighted by hand-drawing.

4.3.2 Morrone Fault zone (MF)

The Morrone fault is part of several hundreds-of-meters wide fault zone crosscutting the western flank of Morrone Mountain and bordering the eastern part of the Sulmona basin (Vezzani et al., 1998). According to historical records, there were no significant earthquakes in this area at least since 1706 (Boschi et al., 1997). The Morrone fault is exposed in two badlands located to the south of the Roccacasale village (Fig 4.17). Here, we performed a half-day long structural survey in the footwall made of the stratified limestone of the Morrone Meridionale Fm. (Vezzani et al., 1998) and measured a damage zone thickness of at least **325** m. Differently from the other damage zones, here a Low strain Damage Zone domain corresponding to the pristine sedimentary fabric is partly preserved and recognizable in the footwall block few meters beneath the surface of the Master Fault. Normal faults in the damage zone are often lined by mm-thick ultracataclasites and cataclasites and cut predominantly ISRs (Fig 4.17d). In the eastern part of the Sulmona Basin and especially near the Roccacasale village, the main fault surface is easily recognizable and the fault core (~1.5m thick) well-exposed in the badlands

(Fig 4.17b). However, because of the thick vegetation, no systematic cross-cutting relations between faults were found, though the majority of the high angle (>45°) faults were sub-parallel to the Master Fault.



Fig. 4.17 The Morrone Fault zone crops out near the village of Roccacasale (UTM 408544 E, 4663742 N). (a) The fault scarp can be followed for km along the western slope of the Morrone mountain. (b) The fault core is about 3 meter thick and (c) just ca. 3 meters away the stromatolitic foliation is well-preserved. (d) Example of normal faults (red lines) which divide the Low strain Damage Zone from the ISRs.

4.3.3 Pescasseroli Fault zone (PF)

The Pescasseroli fault is part of the Upper Sangro Fault System, which is composed by normal and strike-slip NW-SE trending faults. Prevalent normal movement is accommodated by the Pescasseroli fault (Galadini and Galli, 1999) which crops out to the north-east from the Pescasseroli village and its damage zone is well exposed within badlands (Fig 4.18). The fault cut through the Dolomia Principale Fm. and in the footwall block we measured a damage zone at least **227** m thick. The joint sets measured dip toward SW (N230/60 dip azimuth/dip) like the Master Fault.



Fig. 4.18 The Pescasseroli Fault zone (UTM 401990 E, 4630465 N). (a) Panoramic view looking towards the South of the damage zone exposed in the badlands. (b) Detail of the footwall made of highly fragmented rocks cut by pervasive joints.

4.3.4 Venere Fault zone (VF)

The Venere-Gioia dei Marsi fault is part of a NW trending, SW dipping fault zone along the eastern margin of the Fucino Plain. This fault zone is made of three NW striking segments and the central one, south of Venere, is well described by several authors (Agosta and Kirschner, 2003; Agosta and Aydin, 2006 and Ferraro et al., 2018). The footwall block, made of limestones with bird's eyes (Agosta and Kirschner, 2003), is exposed in the Santilli quarry, between the villages of Venere and Gioia dei Marsi (Fig 4.19). This fault ruptured during the 1915 M_s = 7.0 Avezzano earthquake and produced numerous historical earthquakes (Boschi et al., 1997; Michetti et al., 1996; Galadini and Galli, 1999). The Master Fault surface and the fault core crop out in the quarry. The fault core shows, starting from the Master Fault towards the footwall, a gradual transition from ultracataclasite to cataclasite, breccia and eventually ISRs. The damage zone hosts several secondary normal

faults with beautiful mirror-like surfaces (Fig 4.19c). The damage zone goes beyond the outermost quarry front, thus the damage zone thickness is at least ~**77** m.

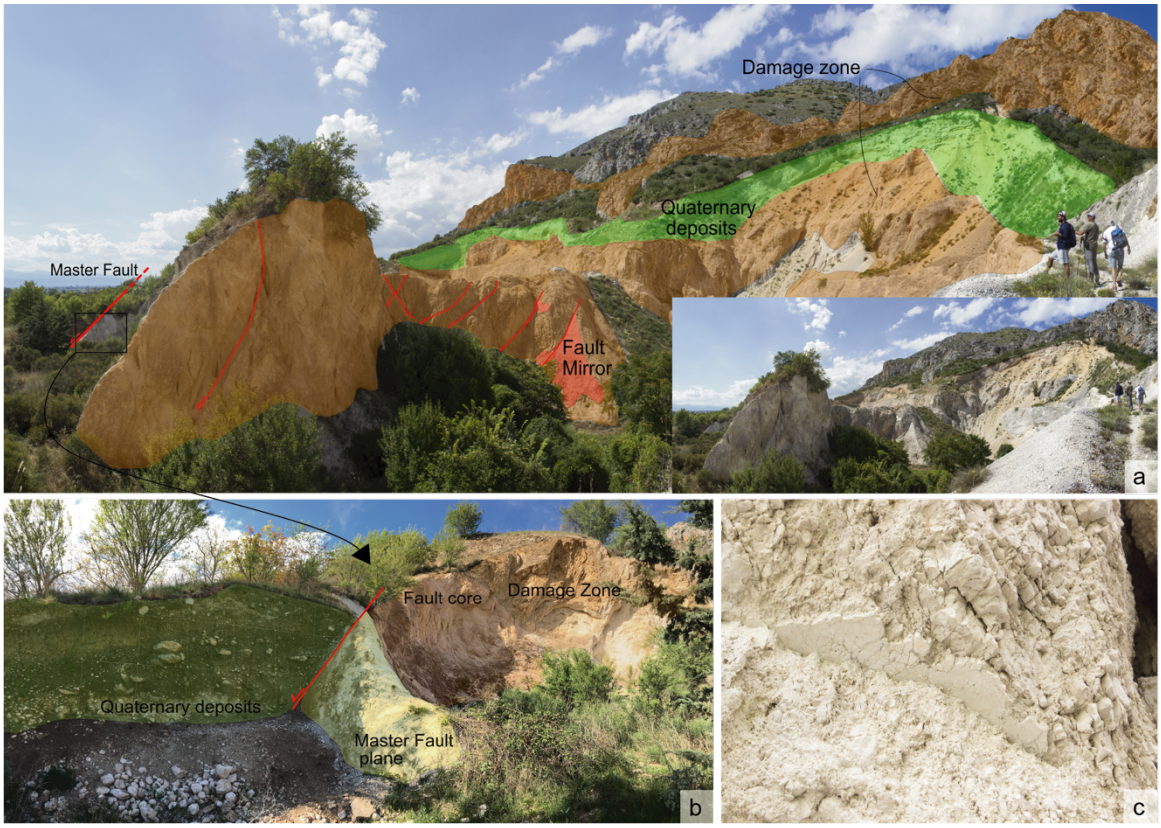


Fig. 4.19 Venere Fault Zone in the Santilli quarry (UTM 389305 E, 4647280 N). (a) The fault core and the damage zone are exposed within the Santilli quarry. (b) Trench made by M. Moro (INGV) showing the lacustrine and slope Quaternary deposits in the hangingwall and the white in colour cataclasites of the fault core. (c) In the damage zone, ISRs and mirror-like surfaces are widespread.

4.3.5 Campo Imperatore Fault zone (CIF)

The Campo Imperatore fault zone delimits the northern margin of the intramountain Quaternary basin of Campo Imperatore in the Gran Sasso Massif area. The CIF damage zone crops out almost continuously for ca. 5 km in about 20 sub-parallel creeks oriented orthogonal to the average strike of the fault zone in the western margin of the Campo Imperatore Plain. The fault belongs to the ~ 20 km long fault system (the Campo Imperatore Fault System) which runs through the Gran Sasso Massif. The CIF zone is described in detail by Demurtas et al. (2016) and most of the data presented here come from that work (Fig 4.20). The exceptional exposure of the damage zone allowed us to quantify in ~**241** m the thickness of the damage zone in footwall block, though, compared to the MMF, the fault structure has a different architecture (see geological and structural map in Demurtas

et al., 2016). The CIF puts in contact the dolomitized (lower part) Calcare Massiccio Fm. at the footwall with the Late-Pleistocene slope deposits at the hangingwall. The stratigraphic displacement measured on the fault is of ca. 2000-3000 m (Adamoli et al., 1997; Vezzani et al., 1998).



Fig. 4.20 The Campo Imperatore fault zone crops out on the eastern side of the Campo Imperatore intramountain basin. (a) Series of badlands exposing the footwall of the fault. (b) Low-angle south dipping fault in the footwall with S-C fabrics indicating top-to-NE movement (= thurst) (see main text and discussion in section 5.2). (c) Secondary normal faults in the footwall cutting the damage zone and lined by cm-thick ultracataclasites.

5 DISCUSSION

The main goals of this thesis are (1) the description of the structure and, (2) the quantification of the thickness of fault damage zones hosted in carbonate-built host rocks and, based on this original dataset, a preliminary discussion about the main factors controlling their thickness. In this section I will exploit:

(1) field structural geology surveys carried out in the Central Apennines of Italy,
(2) remote sensing analysis of satellite and aerial images of fault zones coupled with literature data review and
(3) fault zone rocks macro- and micro-structural observations,

to discuss:

(1) the geometrical complexities of the overstep sector of the MMF zone, including the presence of compressional and extensional fault/fracture networks and the distribution of *in-situ* shattered rocks (ISRs) within the damage zone,
(2) the scaling laws among damage zones thickness and other fault (length, displacement, maximum expected Mw) parameters and,
(3) the role played by the different stages of the seismic cycle in the ISRs formation and distribution.

5.1 *Role of geometrical complexities in controlling the ISRs distribution*

A striking first order field observation regarding the distribution of ISRs along the MMF zone, is that the thickness of the ISR increases from few meters in the northern sector, near Barete, where the Master Fault is ca. planar and strikes NW-SE, to ca. 1000 m in the central sector where the Master Fault strike rotates towards the West (Fig. 4.4). The central sector of the MMF is located in an area in which the footwall block is exposed within badlands morphology while the Master Fault surface is poorly exposed because it runs through the village of Pizzoli (Fig. 4.1c). The Ithaca database reports the MMF as a single NW-SE trending fault surface, bending to the West in the area near Pizzoli. Conversely, geomorphic features (i.e., small scarps) and indirect evidences of coseismic deformation obtained from paleosismological investigation suggest the presence of at least two principal

fault strands, linking or overstepping in this area (Moro et al., 2002; Moro, 2016; Galli, 2011) (see Poster 1). As a consequence, in the surveyed area, we infer the presence of the Master Fault surface mainly on the basis of small morphological scarps resulting from historical seismic surface ruptures (e.g., 1703 Mw 6.7 L'Aquila earthquake). Instead, in the overstep sector of the MMF, the damage zone is well exposed in badlands and it shows such a high density of secondary faults, joints and complicated distribution and abundance of ISRs that according to me is not possible to associate such a complex fault zone architecture to a single fault. As a consequence, I interpret the structure of the MMF in the area of Pizzoli village as the result of the interaction of two main fault segments (the Barete-Pizzoli and Pizzoli-Arischia segments).

Gupta and Scholz (2000) distinguished between ***hard linkage***, where the fault segments are physically linked, and ***soft linkage*** where the fault segments interact only through the associated stress perturbation. In the absence of good quality outcrops of the Master Fault it is hard to infer how the two main fault strands are linked. In fact, information about displacement accumulation in the overlap zone is required to distinguish between hard and soft linkages (Fig 5.1 a-h; Gupta and Scholz, 2000).

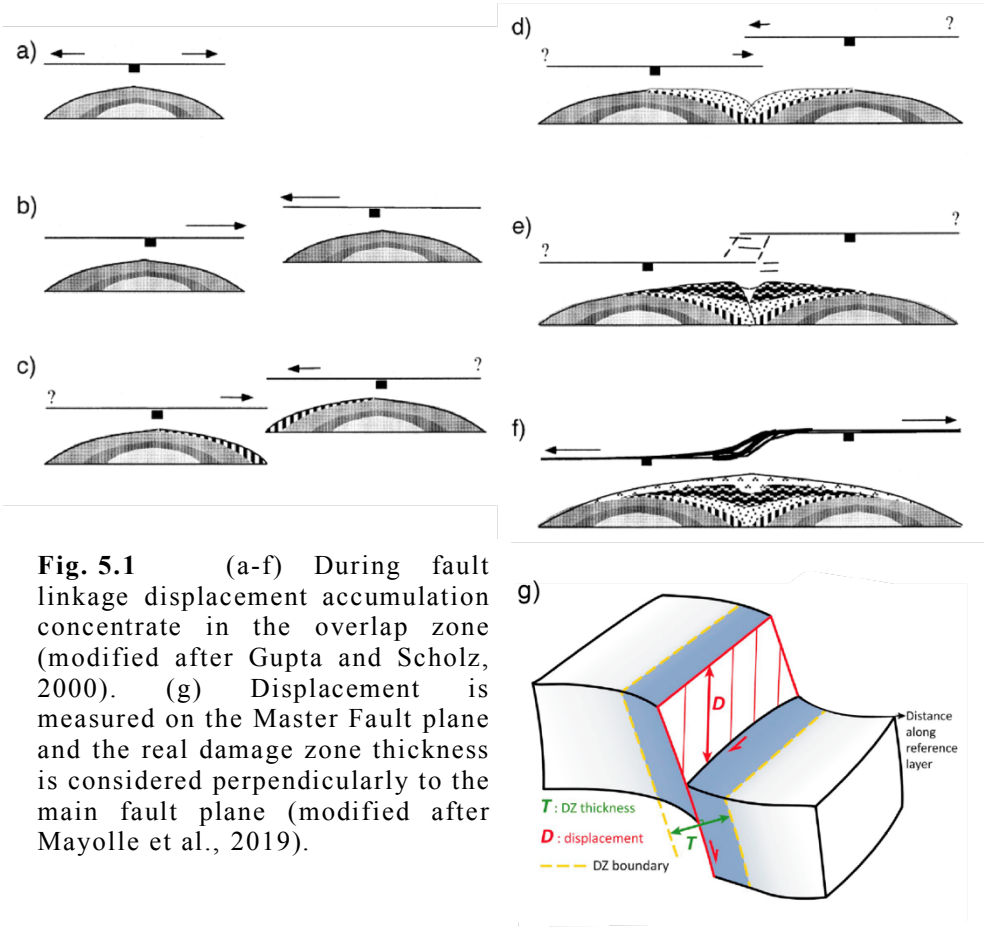


Fig. 5.1 (a-f) During fault linkage displacement accumulation concentrate in the overlap zone (modified after Gupta and Scholz, 2000). (g) Displacement is measured on the Master Fault plane and the real damage zone thickness is considered perpendicularly to the main fault plane (modified after Mayolle et al., 2019).

Importantly, one of the most critical aspects of step-over zones is their role as physical barriers to earthquake rupture and seismic waves propagation (Sibson, 1985; Wesnousky, 2006). In fact, a significant fault bend or step-over can act as *stress concentrator* (Aki, 1989). For example, in the case of the 1966 M_L 5.5 Parkfield earthquake and in several other strike-slip earthquakes, the propagation of seismic ruptures terminated in the vicinity of dilational jogs (Sibson, 1985). In fact, when the seismic rupture propagating at kilometres per second reaches the fault tip, the abrupt rupture deceleration results in large stress dissipation spread over a broad zone of rocks around the fault tip, and in the reduction of the stress transferred to nearby fault segments (e.g., see models by Fang and Andrews and discussion in Fondriest et al., 2015). The complex damage pattern and the presence of very thick domains of ISRs in the step-over region could result from the geometrical role as *stress concentrator* and as seismic barrier during earthquakes.

5.2 *Role of compressive structures in controlling the ISRs distribution*

An original and relevant finding of this field survey, is the occurrence in the central sector of the MMF zone of low-angle (dip <45°) fault structures cut by the normal high angle (dip ≥45°) faults (Figs. 4.4, 4.7, 4.9). Previously published geological maps did not report the presence of low angle faults, here interpreted as compressional structures (see discussion below), in the MMF zone overstepping area (e.g., Vezzani et al., 1998; Carta Geologica d'Italia, 1955, Carta Geologica d'Italia, foglio 359 L'Aquila).

As discussed in chp. 3, the Central Apennines underwent a polyphasic tectonic evolution. The formation and activity of continental scale extensional faults during the Permo-Triassic rifting stages of Tethys ocean and their post-rifting Jurassic and early Cretaceous sin-sedimentary activity, was followed, starting from the Late Miocene, by a compressional phase and, from the Early Pleistocene, by an extensional phase. This geodynamic evolution led the fault structures formed in extension (the crustal-scale Permo-Triassic to Jurassic-Early Cretaceous fault zones) to be (1) re-activated as reverse faults when favourably oriented or cut by thrusts in the Miocene-Pliocene and (2) the Miocene-Pliocene reverse faults and thrusts to be re-activated as low angle normal faults or cut by newly formed high-angle normal fault in the Middle Pleistocene-Holocene (i.e., tectonic inversion, Barchi et al., 1998).

High-resolution hypocentral locations of aftershocks of moderate to large in magnitude earthquakes in the Central Apennines illuminate both high angle structures

clearly associated to extensional faulting but also low angle and shallow-seated (3-6 km depth) tectonic structures (Fig 5.2a-b) (Chiaraluce et al., 2011; Valoroso et al., 2013). This high-quality seismological data set was exploited also to obtain high-resolution velocity models (Vp and Vp/Vs distributions) of the upper crust of the Central Apennines (Fig 5.2c). For example, in the case of the Paganica Fault (a 18 km long fault striking NW-SE and dipping ~55° to the SW) and responsible of the mainshock of the 2009 M_w 6.1 L'Aquila earthquake, both aftershock distribution and P-waves velocity models shows that at 3-5 km depth the normal fault zone cuts a well-defined low-angle (~15°) dipping seismogenic volume (Fig. 5.2b). This seismogenic volume is interpreted as the shallow flat portion of a thrust inherited from the Miocene-Pliocene compressional phase (Chiaraluce et al., 2011, Valoroso et al., 2013). Similarly, Vp anomaly volume distributions (Buttinelli et al., 2018) can be related to flat and ramp thrust structures that originated during compression and were reactivated as normal faults during the Quaternary extension (Fig. 5.2c). In particular, seismic velocity anomalies revealed the presence in the central Apennines domain of three main E-verging thrust systems, in accordance with the geological interpretation of ENI-AGIP seismic profiles made by Bigi et al. (2011).

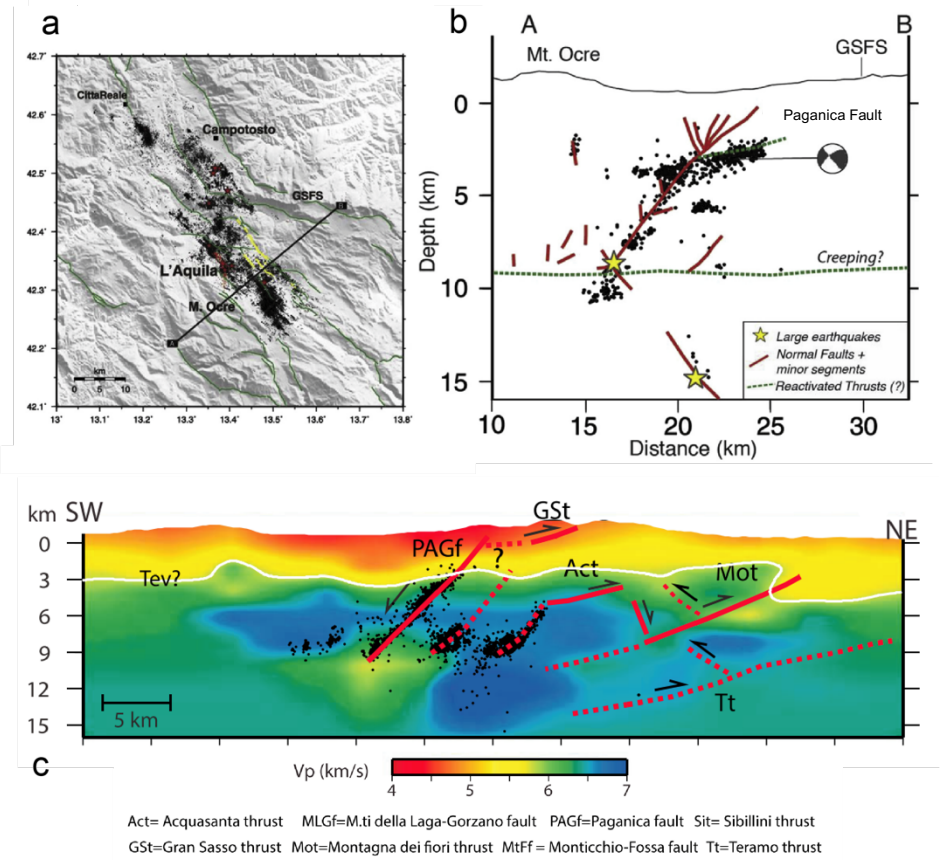


Fig. 5.2 High resolution epicentral and hypocentral locations and Vp distribution in the Central Apennines. (a) Epicentres of the aftershocks of the 2009 Mw 6.1 L'Aquila earthquake. (b) NE-SW trending vertical section near the town of L'Aquila with the hypocentral distribution of the aftershocks associated to 2009 seismic sequence. Below the Paganica fault, aftershocks highlight a low-angle structure (from Valoroso et al., 2013). (c) Vp anomaly distribution in tomograms suggest the occurrence of flat and ramp thrust structures (from Buttinelli et al., 2018).

Since the compressional and extensional tectonic phases were coaxial (Fig 3.3c), faults trending NNE, E(SE) and SE are likely to be reactivated with different kinematics, in particular, thrusts were cut or reactivated as a low-angle extensional faults during the Present extension (Pizzi and Galadini, 2009; Leah et al., 2018). In several outcrops of the damage zone of the MMF zone, high-angle SW-dipping faults cut and offset with displacements < 1m low-angle and probably older SW-dipping faults. For instance, we interpreted the low-angle faults at the stations 5.7 and 5.9 as thrusts of the Miocene-Pliocene compressional phase based on the following evidences:

- the attitude of these minor low-angle faults agrees with the general top-to-the-NE vergence of the Apenninic compressional structures (Fig. 4.5b);
- multiple sets of joints and low order faults associated to the low-angle faults can be interpreted as R and R' Riedel-type shear fractures and are consistent with a top-to-the-NE compressional kinematics (station 5.9, Fig. 4.7e);
- the kinematic inversion of the fault slip data show predominance of compression in some localities (station 5.9, Fig. 4.8).

Moreover, the presence of at least one Miocene in age thrust in the area is also suggested by the occurrence of the Green Veined Breccia (section 4.1). The lithological features of this breccia are very similar to the fault breccia defined as "Breccia Unit" by Demurtas et al., (2016) in the Vado di Corno fault damage zone (Campo Imperatore Fault System) as follows:

> *"... grey, green to brownish in colour fault rocks which can be classified mostly as cohesive crush breccias (Sibson, 1977) or "mosaic- crackle breccias" (Mort and Woodcock, 2008) which typically outcrops (i) at the bottom of the creeks, (ii) associated with NNE-SSW striking low-angle (dip angle 20-40°) oblique faults with contractional S-C cleavages and R- shear fractures (Riedel fractures) or (iii)*

related with low-angle normal faults characterized by an older-on-younger "stratigraphy"."

In the so-called Breccia Unit described by Demurtas et al., (2016), secondary dolostones and dolomitic veins developed in the Calcare Massiccio Fm. during a syn- to post-thrusting event. This Miocene in age dolomitization event was driven by Mg-rich fluids percolating along the damage zones of these thrusts (Clemenzi et al., 2015). Similarly to Breccia Unit of the Vado di Corno Fault Zone, the dolomite-rich Green Veined Breccia of the MMF is associated to low-angle faults (dip < 40°) and could be related to thrust-related fluid circulation, thus emphasizing the record of the Miocene-Pliocene compressional phase in the damage zone of the MMF.

The important role of the tectonic inversion for the MMF architecture and for the damage zone thickness is further highlighted by the increase of ISRs volumes where compressional fault structures intersect extensional ones. In fact, Facies 1 ultra-cataclasites and Facies 2 cataclasites are present only in the fault cores (thickness up to 30 m) of the normal Master Fault and in the fault cores (few cm thick) of minor faults cutting the damage zone (Fig. 4.6d). Nevertheless, in correspondence of the low-angle faults interpreted as thrusts (stations 5.9 and 5.7), (1) cataclasites are up to 70 cm thick (Fig 4.7b) and (2) the Facies 3a broadens in thickness (see geological map of Fig. 4.9). Clearly, the presence of low-angle faults, perhaps a second order geometrical feature when compared to the first order along strike geometrical complexity (presence of step-over discussed in section 5.1), results in further increase of the ISR and fault damage zone. Two possible and perhaps naïve models on how the presence of low-angle faults in the overstep sector of the MMF result in increased thickness of ISRs are:

1. The thrust and the high-angle normal faults belong respectively to the Miocene-Pliocene compressional phase and to the Pleistocene extensional phase. The fault related damage developed in the extensional phase would be added to the damage zone of the previous compressional phase, causing the thickness of the damage zones to increase.

2. Low-angle (dip < 45) faults and associated fault/fracture network represent a geometrical complexity with respect to the sole normal faulting. Indeed, the geometrical complexity of the fault is a factor that influences the arrest of the

seismic rupture and the energy radiation. For example, a model proposed by Okubo et al. (2018) suggests that when preexisting secondary fractures are activated in the off-fault medium, they behave as secondary sources of radiate waves, which contribute to the enhancement of high-frequency components in the near-field ground motion. Thus, the complex damage pattern and the presence of very thick domains of ISRs in the overstep region of the MMF could result from the enhanced radiated and scattered seismic waves due to the fracture network of the preexisting low-angle faults.

5.3 *Seismogenic behaviour of the Monte Marine Fault and simple model for the formation of ISRs*

The historical and recent seismicity derived from seismological data and paleosismological analysis, testify the seismogenic behaviour of the MMF. For example, trench excavations of the MMF report evidences for the re-activations of the Upper Aterno Fault System in the historical seismic sequences of the 1315, 1349, 1461, 1762 (IX-X of the Mercalli Intensity Scale) (Moro et al., 2002, 2016; Galli et al., 2011). Moreover, the most recent faulting event recognized from paleosismology is ascribable to the Mw 6.7 February 02, 1703 event (Moro et al., 2016) which was generated by a ca. 30-km long fault rupture (including the Upper Aterno and L'Aquila faults system). Both historical and recent earthquakes in the Central Apennines relate to the Quaternary extensional phase of the inner Apenninic domain and deformation is mainly accommodated through normal faulting. Similarly, in the overstep sector of the MMF, the extensional faults are the most recurrent structures. The NW-SE strike and slip direction towards SW of these normal faults (Fig. 4.5b) are in accord with the NE trending σ3 axis of the present-day active extension (Pizzi and Galadini, 2009, Pace et al., 2014).

The historical and recent seismicity together with field and microstructural observations of faults and fault zone rocks suggest the propagation of seismic ruptures within the MMF. For example, cataclastic slip zones are made of clasts with pervasive and radial fractures and *in-situ* shattered grains (i.e., lacking significant shear deformation, Fig 4.12a). Indeed, *in-situ* shattering seems to be the main process which also led to the formation of the great volume of the damage zone of the MMF.

The occurrence of ISRs up to 1000 m from the Master Fault in the overstep sector (Poster 1) recalls the fact that most fault zones have a complex internal structure within

which seismic ruptures nucleate, propagate and arrest (Andrews, 2005). In fact, abrupt stress changes related to rupture propagation are not confined to the slip zone of the fault, but they spread in a volume of meters to tens of meters and more around the rupture front. Thus, stress perturbations induced by rupture propagation will be much higher than the ambient tectonic stress and they are likely to be the highest stresses the rock could experience (Scholz et al., 1993). In this context, the formation of *in-situ* shattered rocks may be the result of intense fragmentation in the host rocks due to repeated passage of ruptures along the Master Fault during the main shock, and along the minor nearby faults during the aftershock sequence (Andrews 2005, Fondriest et al., 2015). Aftershock activity may contribute to the thickening of the damage zone up to hundreds of meters from the Master Fault.

In the case of the MMF, *in-situ* rock shattering is also due to the sudden deceleration or arrest of the seismic rupture along the step-over. The latter acts as a physical barrier to earthquake rupture propagation, resulting in a large dissipation of kinetic energy of the rupture in the wall rocks and intense rock shattering (Sibson, 1985; Wesnousky, 2006). Moreover, the presence of low-angle and high-angle faults influences the propagation of seismic waves. In fact, seismic waves released by the propagation of seismic ruptures both along the Master Fault (main shocks) and minor faults cutting the damage zone (aftershocks) remain trapped (Li and Leary, 1990). Waves trapping result in energy dissipation in the wall rocks. In particular, during the extensional phase of wave propagation and because of (i) the low tensile strength of rocks and (ii) the low confining stress at these shallow crustal depths, wall rocks are split and fragmented, resulting in the formation of *in-situ* shattered rocks (Fig 5.3).

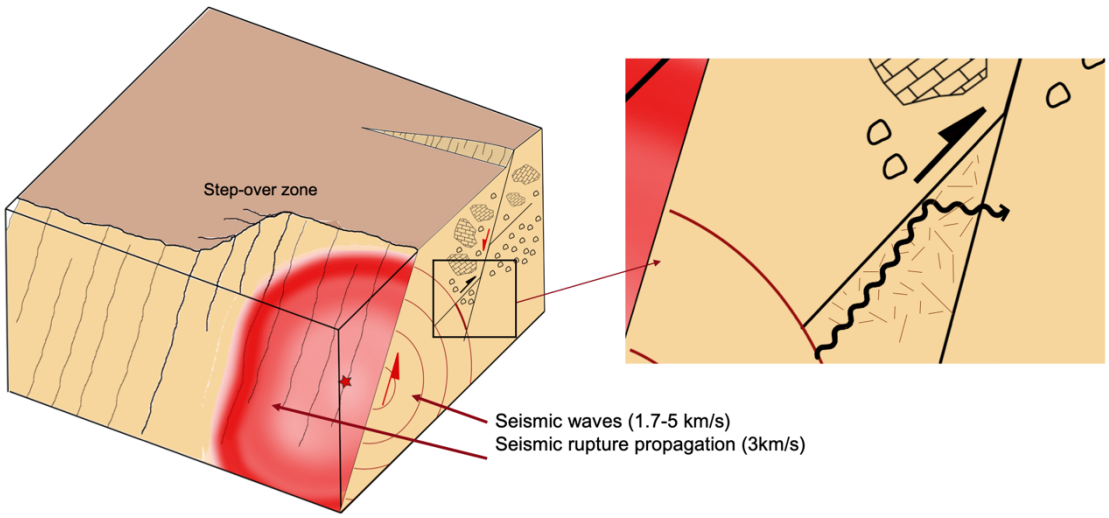


Fig. 5.3 Simple model for the formation of ISRs related to the propagation of the seismic rupture (red halo) in a step-over region. Seismic waves propagate in the damage zone and remain trapped due to the presence of low-angle and high-angle faults and damaged rocks. Contrast of impedance in the wall rocks of the Master Fault result in generation of trapped waves which contributes to the *in-situ* shattering of the rocks (From Miriana Chinello B.Sci. Thesis 2019)

5.4 *Scaling laws of fault damage zones in the Central Apennines*

In this thesis I present a catalogue of six carbonate-hosted active normal faults zones in the Central Apennines exhumed from similar crustal depth (2-4 km, at least the Campo Imperatore, Venere and Morrone Faults) and whose damage zones include ISRs and are up to 100s m thick (see list of the selected faults in section 4.3). As stated in section 4.3, the fault zones were selected based on their exposure (badlands and quarries ca. orthogonal to fault strike), fault length and displacement, and type (dolostones, limestones, etc.) of footwall host rock.

A common feature found in the dedicated field surveys of the selected faults, is their structural complexity. Starting from the Master Fault towards the footwall, the first tens of meters are made by a thick band of cataclasites and ultracataclasites (e.g., Facies 1 in section 4.1) and then by a several tens of meters to hundreds meter thick damage zones including ISRs (Facies 3a & 3c in section 4.1) cut by (1) tens to hundreds of minor faults lined by ultra-cataclasites and cataclasites and (2) multiple and pervasive set of joints (see Poster 2).

In general, the structure of the damage zones of the selected faults is quite similar to the one described in the MMF zone and discussed in section 4.1. However, in map view,

the thickness and distribution of the damage zones are highly variable along fault strike (Fig. 5.5a for a map view). Damage zone thickness values were measured along the badlands, recalculated perpendicular to the Master Fault strike and eventually plotted, in log-log plot vs. fault displacement (Fig 5.4a). The values of the damage zone thickness presented here must be considered as a minimum estimate, since fault-related damage is inferred to go beyond, at least in some cases, to the exposures in the badlands and in the quarries. For comparison purposes with previously published data which report the entire thickness of the fault damage zone, we made the strong assumption that in the studied faults the thickness of the damage zone is symmetric with respect to the Master Fault. In fact, in our study, we measured only the thickness of the footwall because the hangingwall was buried beneath thick quaternary deposits and does not crop out in these large displacement normal faults. Because of this, in Fig. 5.4a I report both the estimated thickness of the damage zone in the footwall (orange in colour dots) and the thickness of the entire damage zone by doubling the value of the footwall thickness to include also the damage zone in the hangingwall (black dots). I also briefly discuss the relations between fault damage zone thickness vs. fault length and fault displacement vs. fault length.

Fault zone thickness vs. fault displacement. The relation between these two fault parameters is (see section 1.2.4 and Shipton et al., 2006b; Childs et al., 2009; Faulkner et al., 2011; Savage and Brodsky, 2011; Mayolle et al., 2019.):

$$y = Cx^a$$

with y the fault damage zone thickness, C a pre-exponential factor, x displacement and a the power law exponent. In the log-log plot of Fig. 5.4a, the relation between fault displacement and total fault zone thickness is almost linear:

$$\log y = \log C + a \log x$$

with the slope of the best fit curve $a \sim 0.18$. With respect to the best fit line, our data set has a scattering limited to only one order of magnitude, with respect to scattering of ~2-3 orders of magnitude in previous compilations which include a large collection of faults from different mode of faulting, lithologies and geodynamic settings (e.g., Savage and Brodsky, 2011, Childs et al., 2009). This might also due to the higher uniformity of the

selected faults in our study regarding their kinematics (normal faults) and lithology of their host rocks (limestones and dolostones). In addition, the best fit of our faults dataset maintains a linear regression also for displacement values greater than 100m (Fig 5.4d). This is in contrast with the published dataset where, for displacement > 100 m, the thickness of the damage zone saturates to ca. 100 m (Mayolle et al., 2019). However, the data from Mayolle et al., (2019) refer to the damage zones of individual Master Faults, whereas, for instance, the MMF consists of at least two main fault segments (Fig. 4.1c). Thus, the occurrence of structural complexities like the overstep sector of the MMF could result in the great increase in the damage zone thickness as discussed in sections 5.1 and 5.3.

Fault zone thickness vs. fault length. The conclusion (section 5.1) that the presence of first order structural complexities (e.g., fault bends, step-overs) may result in the increase in the damage zone thickness, seems suggested by the preliminary observation that the thickness of the damage zone decreases with fault length (Fig. 5.5). Now, earthquake magnitude increases with fault length (Fig 5.4f), and the elastic strain energy released by the earthquake increases with fault length (Scholz, 2019). As a consequence, for seismic faults with similar kinematics, hosted in similar rocks and exhumed from similar depths, we would expect, in the absence of geometrical irregularities, the thickness of the damage zone to increase with fault length (which corresponds to an increase in earthquake magnitude). This is confirmed by the increase of seismological breakdown work or shear fracture energy (which is also associated to the fault damage during seismic rupture propagation in the fault core) with seismic slip (e.g., Abercrombie and Rice, 2005; Nielsen et al., 2016). Instead, though biased by the limited amount of field exposures, our dataset indicates a very poor dependence of damage zone thickness with fault length (Fig. 5.5) and a slight decrease of damage zone thickness with expected maximum earthquake magnitude (Fig. 5.4g), suggesting that is the fault geometrical complexity rather than the earthquake magnitude to play a pivotal role in the distribution and amount of fault damage.

Maximum fault displacement vs. fault length. Our dataset regards normal faults hosted in carbonates. Instead, fault zone parameters from the literature relations (fault length, displacement, damage thickness) are about

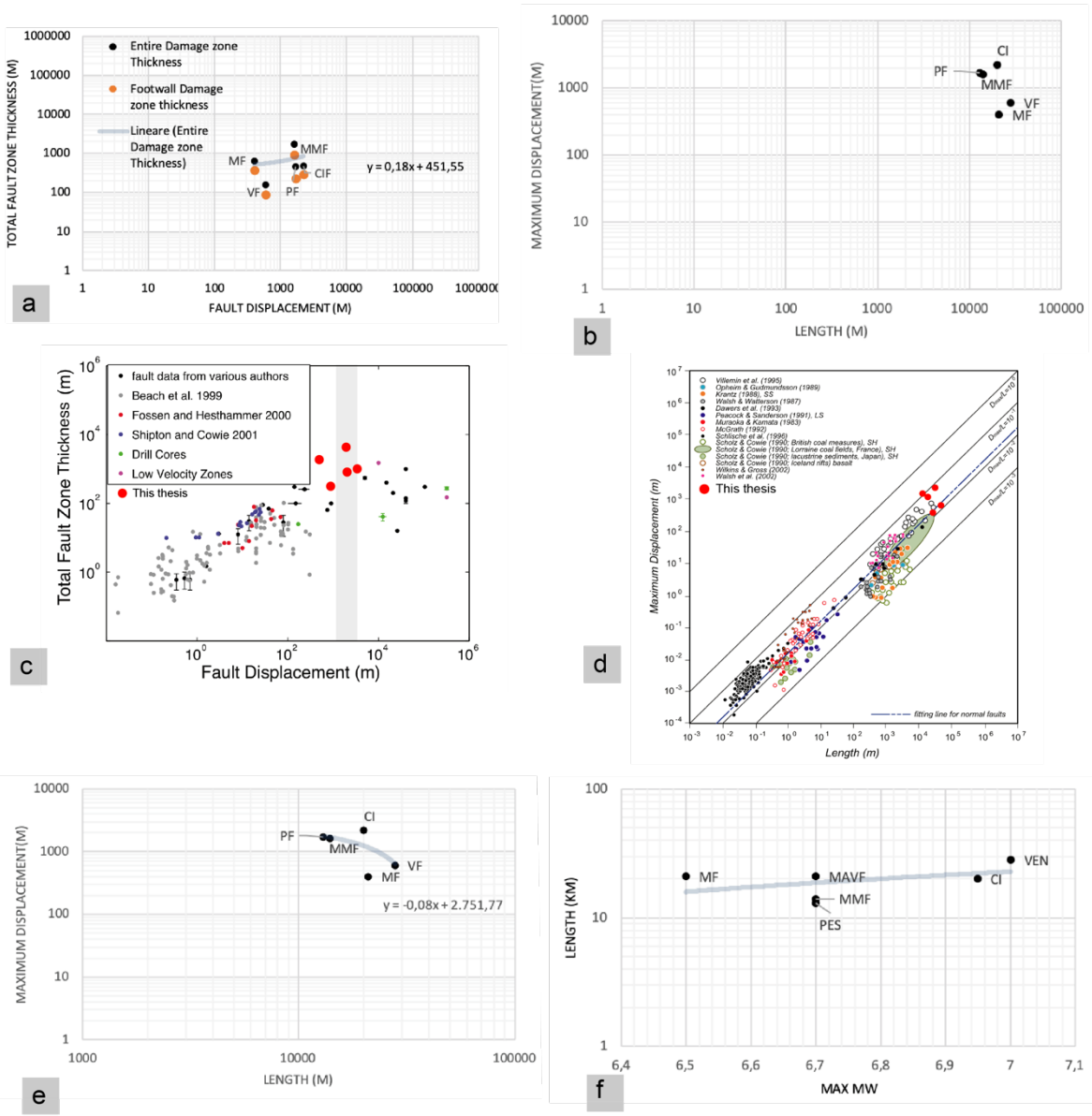


Fig. 5.4 Log-log diagram showing relations among (a, c) total fault zone thickness vs. fault displacement, (b, d) maximum displacement vs. fault length (modified after Mayolle et al., 2019 and after Kim, 2005, (e) maximum displacement vs. length (trend line in blue). Diagram showing (f) the increase of the maximum Mw with increasing fault length and (g) the decreasing of Maximum Mw with increasing damage zone

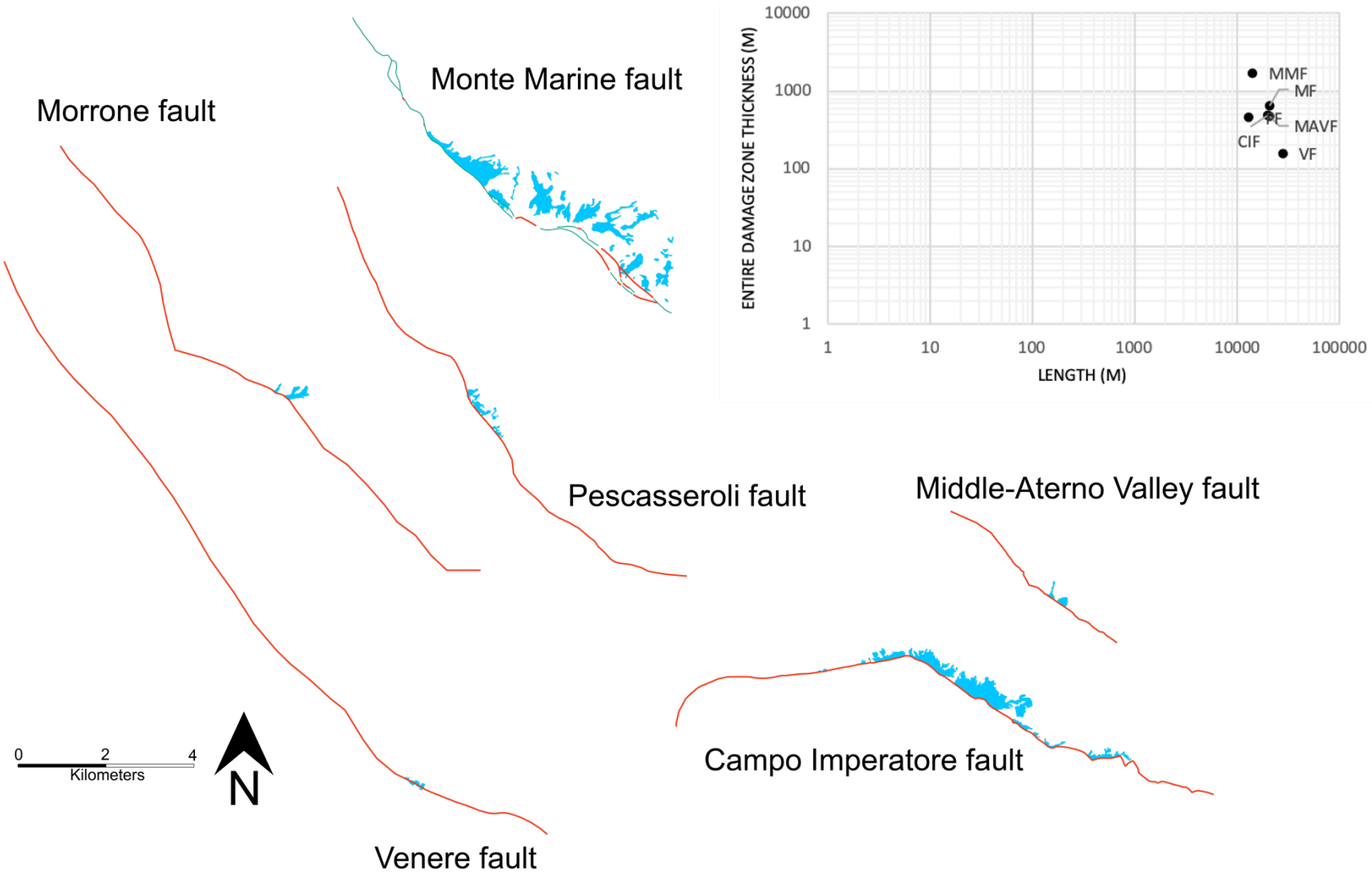


Fig. 5.5 Trace of the fault of the catalogue at the same scale with map view of the fault damage zone. Damage zone thickness vs. fault length data indicate a decrease of damage zone thickness with increasing fault length. However, data are limited and biased by the outcrops availability and exposures. A wider dataset in needed to derive a more accurate trend.

faults hosted in terrigenous deposits, igneous rocks, etc. (Savage and Brodsky, 2011; Childs et al., 2009; Kim et al., 2004). Because of this, we checked if our fault data fit the systematic increase of displacement with fault length. The relation is in the form:

$$y = Cx^n$$

with *y* the displacement of the fault, *C* a pre-exponential factor, *x* the length and *n* the power law exponent usually in the range from 0.5 to 2 (Fig 5.4d, the best fit is a power law with an exponent ca. 1, which indicate a linear scaling law; Kim and Sanderson, 2005).

Our dataset includes normal faults with lengths comparable to the longest faults of the dataset from the literature (10^4 -10^5 m, Kim and Sanderson, 2005). In particular, our selected group of faults roughly follows both the general trend of increasing fault displacement with fault length. However, with regards for the best fit line for normal faults (blue in colour dashed line), our data set is up to one order of magnitude larger (i.e., for a given fault length of ca. 10 km, the displacement in the studied faults can be up to one order in magnitude larger than the one of normal faults hosted in different lithologies, Figs. 5.4 b, d). Ultimately, even though our six-faults dataset confirms the power law between *Maximum Fault Displacement vs. Length* and *Thickness vs. Displacement* (e.g., Kim and Sanderson, 2005, Savage and Brodsky, 2011) and extends the validity of the scaling laws also for faults longer and with greater Displacement than those in the literature, if taken alone this six-faults dataset is not self-reliant. Indeed, to derive *Displacement vs. Length* and *Thickness vs. Displacement* trends that can be attributed to the only normal active faults in carbonates it is necessary to implement the dataset with faults with smaller lengths and displacements. Since the scattering of the data is strongly related to the fault lithology and kinematic, in a new implemented dataset the uniformity of these factors could maintain a low scattering of the data and yield more accurate scaling law trends.

6 CONCLUSIONS

The thesis is focused on the quantitative determination of the thickness of damage fault zones in carbonates by means of (1) detailed field structural geology surveys of the well-exposed Monte Marine fault zone (Central Apennines) and (2) the production of a first *catalogue* of active normal faults with thick damage zones (including *in-situ* shattered carbonates) and their relations with host lithology, fault length and displacement. These data are used for a preliminary discussion about the main factors that control damage zone formation and thickness in carbonate hosted faults.

In-situ shattered rocks (ISRs) are fault breccias with exploded jigsaw textures and with evidence of no shear strain (pristine sedimentary structures such as bedding, stromatolitic foliations, etc., might be locally preserved: Fondriest et al., 2015). The occurrence of ISRs is common within exhumed carbonate-hosted fault zones of various kinematics and becomes almost ubiquitous in seismically active regions such as the Central Apennines of Italy. Despite their impact on the understanding of earthquake mechanics (see sections 1.1 and 1.2.1) till today the spatial distribution of ISRs has never been investigated in detail and the origin of this fault zone rock remains largely unknown.

The normal Monte Marine Fault zone (ca. 10 km NE of the town of L'Aquila, Abruzzo, Fig. 4.1c) strikes ca. NW-SE on average, is about 14 km long and accommodates ca. 1700 m of displacement. Thanks to (1) remote sensing analysis of satellite and aerial photos, (2) detail field structural geology surveys and (3) microstructural investigations, I obtained the following findings:

1) The Monte Marine Fault zone in the area from the village of Barete (northern sector) to Arischia (southern sector) strikes NW-SE and bends ca. E-W in the sector near the village of Pizzoli (central sector in Fig. 4.1c). The fault zone has a 30 m thick main fault core and a up to 1000 m thick damage zone. The **fault core** consists of ultracataclasites and cataclasite (*Facies 1 and 2,* section 4.1), whereas the **damage zone** is made of (a) *in-situ* shattered rocks (*Facies 3a and 3c*), (b) *Low strain Damage Zone* and (c) *Green Veined Breccia* (Fig. 4.4). The latter is associated to the presence of inherited thrust faults and associated fluid-rock interaction and late stage, probably Miocene-Early Pliocene in age, fluid circulation (discussion in section 5.2; Demurtas et al., 2016);

2) the detailed structural and geological map of the central sector (Pizzoli sector) of the MMF (Poster 1) and geological cross sections (Fig. 4.9), show first and second order geometrical complexities. The first order complexity is due to the presence of a step-over or of a relay ramp in the Central Sector between the Barete-Pizzoli and Pizzoli-Arischia fault segments; the second order complexity is related to the presence of the Miocene-Pliocene inherited thrust faults (section 4.1.1). The maximum thickness of the damage zone of the Monte Marine Fault zone is achieved in this central sector;

3) *In-situ* shattered rocks are interpreted as the result of "explosion" of the wall rocks during earthquakes (section 5.3 and Fondriest et al., 2015) based also on:
   (a) microstructural observations (breccia with intense intragranular fragmentation often with radial patterns and no evidence of shear Fig. 4.14),
   (b) their spatial distribution along the fault (Fig. 4.4: the *in-situ* shattered rocks bound the fault core);

4) *In-situ* shattering of the wall rocks may occur up to hundreds of meters far from the Master Fault due to the stress perturbations and the near field elastic waves induced and released by the propagation of repeated ruptures both along the Master Fault (main shocks) and minor faults cutting the damage zone (foreshocks and especially aftershocks) (section 5.3). The evidence that most of the displacement and strain concentrates in the Master Fault core (section 4.1.1.2 and Fig. 4.10), confirms that tensile *in-situ* shattering (compression followed by decompression during the propagation of elastic waves or associated to the abrupt stress perturbations associated to the propagation of seismic ruptures) should be responsible for ISRs formation rather than shear-dominated deformation;

5) The exceptional thickness (c. 1000 m) of the damage zone achieved in the central sector of the seismogenic Monte Marine Fault zone (e.g., source of historical earthquakes including the 1703 Mw 6.7), is probably due to the combination of:
   (a) the first order geometrical complexity (step-over or relay ramp between the two main fault-segments) which would act as a fault barrier during moderate to large in magnitude earthquakes propagating along the Master Fault. The stress shock and energy dissipated by the abrupt deceleration of the seismic ruptures at the

step or relay structures would result in the formation of large *in-situ* shattered rock volumes (section 5.1),

(b) the presence of inherited Miocene-Pliocene compressional thrust faults with their respective damage zones may had contributed to the total damage rock volume measured in the intersection areas between extensional and compressional structures (section 5.1),

(c) the second order geometrical complexity associated to (1) the presence of inherited thrust faults reactivated as normal faults or (2) the newly formed minor normal and strike slip faults may have been the seismogenic source of local but intense foreshock and aftershock seismic activity which, through the generation of trapped seismic waves, contributed to the generation of *in-situ* shattered rocks.

6) Together with the Monte Marine Fault zone, other five active normal faults of the Central Apennines exhumed from similar depth (2-4 km) were selected based on their exposure and available data from the literature regarding their length, displacement, maximum expected magnitude of the earthquakes. The thickness of the damage fault zone was estimated from aerial and satellite images and checked in the field with dedicated field surveys. All the selected fault zones were hosted in carbonate-built rocks and characterized by up to 100s m thick damage zones (Fig. 5.4, Poster 2). By exploiting this original but still limited fault zone catalogue, I find power-law relations between *fault damage zone thickness, fault displacement* and *fault length* which follow relatively well and extend to higher displacements and fault thicknesses the trends presented for fault zones cutting other lithologies (Mayolle et al., 2019, Kim and Sanderson, 2005). However, and consistently with the other field observations listed above, the thickness of the damage zone increases with fault displacement and slightly decreases with fault length suggesting that first order geometrical complexities (e.g., presence of step-overs or relay ramps) is probably the main factor controlling the thickness of *damage zones* in seismogenic faults in carbonates.

6.1 *Future research*

In this thesis I emphasized the role that ISRs could have in the understanding of the mechanics of earthquakes. I presented original field work results that were meant to describe how the ISRs distribute within a fault zone and how the damage zone thickness is

related to some fundamental fault properties, such as fault length and fault displacement. However, this thesis remains a very first, sometimes naïve, contribution to the topic of off-fault damage associated to the propagation of seismic ruptures, and especially for the case of faults hosted in carbonate rocks. In fact, despite the impressive volumes and thicknesses of damage fault zone in carbonates, this topic has been overlooked in the literature yet.

By writing this thesis, I realized that there are several limitations in my work, also due to the limited time (6 months) to be dedicated according to Academic rules to the preparation of a M.Sci. thesis in Geology. In the future, **first** I would like to expand the time-consuming structural survey I did to the entire exposure of the Monte Marine Fault footwall-block. In fact, the central sector of the fault hosts so many geometrical complexities that render very difficult the understanding of the processes involved in the formation of the *in-situ* shattered rocks. **Second**, I would like to implement the catalogue about the thickness of fault damage zones in the Central Apennines by expanding the data collection to other active faults exhumed from similar depths or shallower depths (also to understand better the dependence of fault zone thickness with depth) but with smaller lengths and displacements. This enrichment of the population of the dataset would make any scaling-law trend clearer. **Third,** I would like to relate quantitatively the roughness of the Master Fault to the average thickness of the damage zone to better define the role, if any, of first order geometrical complexities to the volume of the damage zones. **Fourth,** experimental work and the microstructural and petrophysical characterization of the ISRs would also provide additional constraint to their possible formation mechanisms. Together with the field work, this experimental (and microstructural) approach would also allow me to estimate the energy dissipated in the formation of damage zones and perhaps constrain the energy budget (e.g., how much of the elastic strain energy released during earthquakes is partitioned into on-fault vs. off-fault processes?) of earthquakes hosted in carbonate-built rocks.

References

Abercrombie, R.E., and Rice, J.R., 2005, Can observations of earthquake scaling constrain slip weakening? In Geophysical Journal International, v. 162, p. 406–424.

Adamoli, L., Calamita, F., Pierantoni, P.P., Pizzi, A., Ridolfi, M., Rusciadelli, G., and Scisciani, V., 1997, Miocene pre-thrusting normal faults in the Central Apennines (Italy) in Tectonic Studies Group Annual General Meeting.

Agosta, F., and Aydin, A., 2006, Architecture and deformation mechanism of a basin-bounding normal fault in Mesozoic platform carbonates, central Italy: Journal of Structural Geology, v. 28, p. 1445–1467, doi:10.1016/J.JSG.2006.04.006.

Agosta, F., and Kirschner, D.L., 2003, Fluid conduits in carbonate-hosted seismogenic normal faults of central Italy: Journal of Geophysical Research: Solid Earth, v. 108.

Agosta, F., Prasad, M., and Aydin, A., 2007, Physical properties of carbonate fault rocks, fucino basin (Central Italy): Implications for fault seal in platform carbonates: Geofluids, v. 7, p. 19–32, doi:10.1111/j.1468-8123.2006.00158.x.

Agosta, F., Wilson, C., and Aydin, A., 2015, The role of mechanical stratigraphy on normal fault growth across a Cretaceous carbonate multi-layer, central Texas (USA): Italian Journal of Geosciences, v. 134, p. 423–441, doi:10.3301/IJG.2014.20.

Aki, K., 1989, Geometric features of a fault zone related to the nucleation and termination of an earthquake rupture, in Proceedings of Conference XLV. Fault Segmentation Controls of Rupture Initiation and Termination, p. 1–9.

Allmendinger, R., Cardozo, N., and Fisher, D., 2011, Structural geology algorithms: Vectors and tensors: Cambridge University Press.

Alvarez, W., 1976, A former continuation of the Alps: Bulletin of the Geological Society of America, v. 87, p. 891–896.

Alvarez, W., Cocozza, T., and Wezel, F.C., 1974, Fragmentation of the Alpine orogenic belt by microplate dispersal: Nature, v. 248, p. 309.

Ambrosetti, P., 1983, Neotectonic map of Italy.

Andrews, D.J., 2005, Rupture dynamics with energy loss outside the slip zone: Journal of Geophysical Research: Solid Earth, v. 110, p. 1–14, doi:10.1029/2004JB003191.

Ballas, G., Soliva, R., Benedicto, A., and Sizun, J.-P., 2014, Control of tectonic setting and large-scale faults on the basin-scale distribution of deformation bands in porous sandstone (Provence, France): Marine and Petroleum Geology, v. 55, p. 142–159.

Barchi, M.R., De Feyter, A., Magnani, M.B., Minelli, G., Pialli, G., and Sotera, B.M., 1998, The structural style of the Umbria-Marche fold and thrust belt: Mem. Soc. Geol. It, v. 52, p. 38.

Barchi, M., Galadini, F., Lavecchia, G., Messina, P., Michetti, A.M., Peruzza, L., Pizzi, A., Tondi, E., and Vittori, E., 2000, Sintesi delle conoscenze sulle faglie attive in Italia Centrale: GNDT, Gruppo Nazionale per la Difesa dai Terremoti, p. 62.

Basili, R., Valensise, G., Vannoli, P., Burrato Pierfrancesco, Umberto Fracassi, Mariano, S., Monica Tiberti Maria, and Boschi Enzo, 2008, The Database of Individual Seismogenic Sources (DISS), version 3: Summarizing 20 years of research on Italy's earthquake geology: Tectonophysics, v. 453, p. 20–43, doi:10.1016/j.tecto.2007.04.014.

Ben-Zion, Y., and Shi, Z., 2005, Dynamic rupture on a material interface with spontaneous generation of plastic strain in the bulk: Earth and Planetary Science Letters, v. 236, p. 486–496, doi:10.1016/j.epsl.2005.03.025.

Ben-Zion, Y., and Zaliapin, I., 2019, Spatial variations of rock damage production by earthquakes in southern California: Earth and Planetary Science Letters, v. 512, p. 184–193.

Berg, S.S., and Skar, T., 2005, Controls on damage zone asymmetry of a normal fault zone: Outcrop analyses of a segment of the Moab fault, SE Utah: Journal of Structural Geology, v. 27, p. 1803–1822, doi:10.1016/j.jsg.2005.04.012.

Bigi, S., Casero, P., and Ciotoli, G., 2011, Seismic interpretation of the Laga basin; constraints on the structural setting and kinematics of the Central Apennines: Journal of the Geological Society, v. 168, p. 179–190.

Bigi, S., and Pisani, P., 2003, The" pre-thrusting" Fiamignano normal fault: Bollettino della Società Geologica Italiana , v. 122, p. 267–276.

Billi, A., Salvini, F., and Storti, F., 2003, The damage zone-fault core transition in carbonate rocks: Implications for fault growth, structure and permeability: Journal of Structural Geology, v. 25, p. 1779–1794, doi:10.1016/S0191-8141(03)00037-3.

Billi, A., and Di Toro, G., 2008, Fault-related Carbonate rocks and earthquakes indicators: recent advances and future trends: Structural Geology: New Research, p. 1–24.

Billi, A., 2010, Microtectonics of low-P low-T carbonate fault rocks: Journal of Structural Geology, v. 32, p. 1392–1402.

Blumetti, A.M., 1995, Neotectonic investigations and evidence of paleoseismicity in the epicentral area of the January–February 1703, Central Italy, earthquakes: Perspectives in paleoseismology, v. 6, p. 83–100.

Blumetti, A.M., and Guerrieri, L., 2007, Fault-generated mountain fronts and the identification of fault segments: Implications for seismic hazard assessment: Bollettino Società Geologica Italiana, v. 126, p. 307–322.

Boschi, E., 1996, New trends in active faulting studies for seismic hazard assessment: Annals of Geophysics v. 39, p.6

Boschi, E., Guidoboni, E., Ferrari, G., Valensise, G., and Gasperini, P., 1997, Catalogue of the strong earthquakes in Italy from 461 BC to 1990: ING and SGA, Bologna, Italy, p. 973.

Bosi, C., 1975, Osservazioni preliminari su faglie probabilmente attive nell'Appennino centrale: Bollettino della Società Geologica Italiana, v. 94, p. 827–859.

Bosi, V., Funiciello, R., and Montone, P. Fault inversion: an example in central appennines (Italy): Il Quaternario, v. 7 p.577-588. Bosi, C., Galadini, F., Giaccio, B., Messina, P., and Sposato, A., 2003, Plio-Quaternary continental deposits in the Latium-Abruzzi Apennines: the correlation of geological events across different intermontane basins: Il Quaternario, v. 16, p. 55–76.

Brune, J.N., and N., J., 2001, Fault-normal dynamic unloading and loading: An explanation for" non-gouge" rock powder and lack of fault-parallel shear bands along the San Andreas Fault: American Geophysical Union, Fall Meeting Abstracts.

Bubeck, A., Wilkinson, M., Roberts, G.P., Cowie, P.A., McCaffrey, K.J.W., Phillips, R., and Sammonds, P., 2015, The tectonic geomorphology of bedrock scarps on active

normal faults in the Italian Apennines mapped using combined ground penetrating radar and terrestrial laser scanning: Geomorphology, v. 237, p. 38–51, doi:10.1016/j.geomorph.2014.03.011.

Buttinelli, M., Pezzo, G., Valoroso, L., De Gori, P., and Chiarabba, C., 2018, Tectonics Inversions, Fault Segmentation, and Triggering Mechanisms in the Central Apennines Normal Fault System: Insights From High-Resolution Velocity Models: Tectonics, v. 37, p. 4135–4149, doi:10.1029/2018tc005053.

Caine, Jonathan, S., Evans, James, P., Forster, Craig, B., Caine, J.S., Evans, J.P., and Forster, C.B., 1996, Fault zone architecture and permeability structure (supplemental data): Geology, v. 24, p. 1049.

Cardozo, N., and Allmendinger, R.W., 2013, Spherical projections with OSXStereonet: Computers & Geosciences, v. 51, p. 193–205, doi:10.1016/J.CAGEO.2012.07.021.

Carminati, E., Lustrino, M., and Doglioni, C., 2012, Geodynamic evolution of the central and western Mediterranean: Tectonics vs. igneous petrology constraints: Tectonophysics, v. 579, p. 173–192, doi:10.1016/j.tecto.2012.01.026.

Carta Geologica d'Italia, 1955. 1:100000, 139, L'Aquila. Servizio Geologico d'Italia

Centamore, E., Fumanti, F., and Nisio, S., 2002, The Central-Northern Apennines geological evolution from Triassic to Neogene time: Bollettino della Società Geologica Italiana, Volume Speciale, v. 1, p. 181–197.

Chiarabba, C., Amato, A., Anselmi, M., Baccheschi, P., Bianchi, I., Cattaneo, M., ... & De Luca, G., The 2009 L'Aquila (Central Italy) MW6. 3 earthquake: Main shock and aftershocks: Geophysical Research Letters, v. 36, p. 1–6, doi:10.1029/2009GL039627.

Chiaraluce, L., 2012, Unravelling the complexity of Apenninic extensional fault systems: A review of the 2009 L'Aquila earthquake (Central Apennines, Italy): Journal of Structural Geology, v. 42, p. 2–18, doi:10.1016/j.jsg.2012.06.007.

Chiaraluce, L., Valoroso, L., Piccinini, D., Di Stefano, R., and De Gori, P., 2011, The anatomy of the 2009 L'Aquila normal fault system (Central Italy) imaged by high resolution foreshock and aftershock locations: Journal of Geophysical Research: Solid Earth, v. 116, p. 1–25, doi:10.1029/2011JB008352.

Childs, C., Manzocchi, T., Walsh, J.J., Bonson, C.G., Nicol, A., and Scho, M.P.J., 2009, A geometric model of fault zone and fault rock thickness variations: v. 31, p. 117–127, doi:10.1016/j.jsg.2008.08.009.

Choi, J.H., Edwards, P., Ko, K., and Kim, Y.S., 2016, Definition and classification of fault damage zones: A review and a new methodological approach: Earth-Science Reviews, v. 152, p. 70–87, doi:10.1016/j.earscirev.2015.11.006.

Clemenzi, L., Storti, F., Balsamo, F., Molli, G., Ellam, R., Muchez, P., and Swennen, R., 2015, Fluid pressure cycles, variations in permeability, and weakening mechanisms along low-angle normal faults: The Tellaro detachment, Italy: Bulletin, v. 127, p. 1689–1710.

Cortinovis, S., Balsamo, F., Storti, F., La Valle, F., Fondriest, M., and Di Toro, G., 2018, Architecture and fault rocks of the seismogenic Monte Marine fault zone (Central Appennines, Italy), in *Gruppo Nazionale di Geofisica della Terra Solida abstract*, *(GNGTS)* 2018.

Cowan, D.S., 1999, Do faults preserve a record of seismic slip? A field geologist's opinion: Journal of Structural Geology, v. 21, p. 995–1001, doi:10.1016/j.jsg.2015.06.006.

Cowie, P.A. et al., 2017, Orogen-scale uplift in the central Italian Apennines drives episodic behaviour of earthquake faults: Scientific Reports, v. 7, doi:10.1038/srep44858.

D'agostino, N., Giuliani, R., Mattone, M., and Bonci, L., 2001, Active crustal extension in the central Apennines (Italy) inferred from GPS measurements in the interval 1994–1999: Geophysical Research Letters, v. 28, p. 2121–2124.

Delle Piane, C., Clennell, M. Ben, Keller, J.V.A., Giwelli, A., and Luzin, V., 2017, Carbonate hosted fault rocks: A review of structural and microstructural characteristic with implications for seismicity in the upper crust: Journal of Structural Geology, v. 103, p. 17–36, doi:10.1016/j.jsg.2017.09.003.

Demurtas, M., Fondriest, M., … F.B.-J. of S., and 2016, undefined Structure of a normal seismogenic fault zone in carbonates: the Vado di Corno Fault, Campo Imperatore, Central Apennines (Italy): Elsevier, https://www.sciencedirect.com/science/article/pii/S0191814116301067 (accessed March 2019).

Demurtas, M., Fondriest, M., Balsamo, F., Clemenzi, L., Storti, F., Bistacchi, A., Di Toro, G., 2016, Structure of a normal seismogenic fault zone in carbonates: Structure of a normal seismogenic fault zone in carbonates: the Vado di Corno Fault, Campo Imperatore, Central Apennines (Italy): Journal of Structural Geology, v. 90, p. 185–206, doi:10.1016/j.jsg.2016.08.004.

Demurtas, M., Smith, S.A.F., Prior, D.J., Spagnuolo, E., and Di Toro, G., 2019a, Development of crystallographic preferred orientation during cataclasis in low-temperature carbonate fault gouge: Journal of Structural Geology, v. 126, p. 37–50, doi:https://doi.org/10.1016/j.jsg.2019.04.015.

Demurtas M., Smith S., Prior D., Brenker F., Di Toro G., 2019b. Grain size sensitive creep during simulated seismic slip in nanogranular fault gouges: constraints from Transmission Kikuchi Diffraction (TKD). Journal of Geophysical Research 10.1029/2019JB018071. In press

De Paola, N., Hirose, T., Mitchell, T., Di Toro, G., Viti, C., and Shimamoto, T., 2011, Fault lubrication and earthquake propagation in thermally unstable rocks: Geology, v. 39, p. 35–38, doi:10.1130/G31398.1.

De Paola, N., Holdsworth, R.E., Viti, C., Collettini, C., and Bullock, R., 2015, Can grain size sensitive flow lubricate faults during the initial stages of earthquake propagation? Earth and Planetary Science Letters, v. 431, p. 48–58, doi:https://doi.org/10.1016/j.epsl.2015.09.002.

Di Toro, G., Han, R., Hirose, T., De Paola, N., Nielsen, S., Mizoguchi, K., Ferri, F., Cocco, M., and Shimamoto, T., 2011, Fault lubrication during earthquakes: Nature, v. 471, p. 494, https://doi.org/10.1038/nature09838.

Doan, M.L., Gary, G., and Andreas, S., 2009, Rock pulverization at high strain rate near the San Andreas Fault: Nature Geoscience, v. 2 p.709.

Doglioni, C., 1991, A proposal for the kinematic modelling of W-dipping subductions - possible applications to the Tyrrhenian-Apennines system: Terra Nova, v. 3, p. 423–434, doi:10.1111/j.1365-3121.1991.tb00172.x.

Doglioni, C., Gueguen, E., Harabaglia, P., and Mongelli, F., 1999, On the origin of west-directed subduction zones and applications to the western Mediterranean: Geological Society, London, Special Publications, v. 156, p. 541–561, doi:10.1144/gsl.sp.1999.156.01.24.

Doglioni, C., Mongelli, F., and Pieri, P., 1994, Doglioni et al, 1994, The Puglia uplift (SE Italy). An anomoly in the foreland of the Apenninic subduction due to buckling of a thick continental lithosphere.pdf: v. 13, p. 1309–1321.

Dor, O., Ben-Zion, Y., Rockwell, T.K., and Brune, J., 2006a, Pulverized rocks in the Mojave section of the San Andreas Fault Zone: Earth and Planetary Science Letters, v. 245, p. 642–654, doi:10.1016/j.epsl.2006.03.034.

Dor, O., Rockwell, T.K., and Ben-Zion, Y., 2006b, Geological observations of damage asymmetry in the structure of the San Jacinto, San Andreas and Punchbowl faults in Southern California: a possible indicator for preferred rupture propagation direction: Pure and Applied Geophysics, v. 163, p. 301–349.

Dor, O., Chester, J.S., Ben-Zion, Y., Brune, J.N., and Rockwell, T.K., 2009, Characterization of Damage in Sandstones along the Mojave Section of the San Andreas Fault: Implications for the Shallow Extent of Damage Generation, in Mechanics, Structure and Evolution of Fault Zones, Basel, Birkhäuser Basel, p. 1747–1773, doi:10.1007/978-3-0346-0138-2_10.

Evans, J.P., 1990, Thickness-displacement relationships for fault zones: Journal of structural geology, v. 12, p. 1061–1065.

Faccenna, C., Becker, T.W., Lucente, F.P., Jolivet, L., and Rossetti, F., 2001, History of subduction and back-arc extension in the central Mediterranean: Geophysical Journal International, v. 145, p. 809–820, doi:10.1046/j.0956-540X.2001.01435.x.

Falcucci, E. et al., 2015, Deep reaching versus vertically restricted Quaternary normal faults: Implications on seismic potential assessment in tectonically active regions: Lessons from the middle Aterno valley fault system, central Italy: Tectonophysics, v. 651–652, p. 186–198, doi:10.1016/j.tecto.2015.03.021.

Fang, Z., and Dunham, E.M., 2013, Additional shear resistance from fault roughness and stress levels on geometrically complex faults: Journal of Geophysical Research: Solid Earth, v. 118, p. 3642–3654.

Faulkner, D.., Lewis, A.., and Rutter, E.., 2003, On the internal structure and mechanics of large strike-slip fault zones: field observations of the Carboneras fault in southeastern Spain: Tectonophysics, v. 367, p. 235–251, doi:10.1016/S0040-1951(03)00134-3.

Faulkner, D.R., Mitchell, T.M., Rutter, E.H., and Cembrano, J., 2008, On the structure and mechanical properties of large strike-slip faults: Geological Society, London, Special Publications, v. 299, p. 139 LP – 150, doi:10.1144/SP299.9.

Faulkner, D.R., Mitchell, T.M., Jensen, E., and Cembrano, J., 2011, Scaling of fault damage zones with displacement and the implications for fault growth processes: Journal of Geophysical Research: Solid Earth, v. 116, p. 1–11, doi:10.1029/2010JB007788.

Faulkner, D.R., Jackson, C.A.L., Lunn, R.J., Schlische, R.W., Shipton, Z.K., Wibberley, C.A.J., and Withjack, M.O., 2010, A review of recent developments concerning the structure, mechanics and fluid flow properties of fault zones: Journal of Structural Geology, v. 32, p. 1557–1575, doi:10.1016/j.jsg.2010.06.009.

Faure Walker, J.P., Roberts, G.P., Sammonds, P.R., and Cowie, P., 2010, Comparison of earthquake strains over 102 and 104 year timescales: Insights into variability in the seismic cycle in the central Apennines, Italy: Journal of Geophysical Research: Solid Earth, v. 115, p. 1–26, doi:10.1029/2009JB006462.

Ferraro, F., Grieco, D.S., Agosta, F., and Prosser, G., 2018, Space-time evolution of cataclasis in carbonate fault zones: Journal of Structural Geology, v. 110, p. 45–64, doi:10.1016/j.jsg.2018.02.007.

Ferraro, F., Agosta, F., Ukar, E., Grieco, D.S., Cavalcante, F., Belviso, C., and Prosser, G., 2019, Structural diagenesis of carbonate fault rocks exhumed from shallow crustal depths: An example from the central-southern Apennines, Italy: Journal of Structural Geology, v. 122, p. 58–80, doi:10.1016/j.jsg.2019.02.008.

Fondriest, M., Aretusini, S., Di Toro, G., and Smith, S.A.F., 2015, Fracturing and rock pulverization along an exhumed seismogenic fault zone in dolostones: The Foiana Fault Zone (Southern Alps, Italy): Tectonophysics, v. 654, p. 56–74, doi:10.1016/j.tecto.2015.04.015.

Fondriest, M., Doan, M.L., Aben, F., Fusseis, F., Mitchell, T.M., Voorn, M., Secco, M., and Di Toro, G., 2017, Static versus dynamic fracturing in shallow carbonate fault zones: Earth and Planetary Science Letters, v. 461, p. 8–19, doi:10.1016/j.epsl.2016.12.024.

Fondriest, M., Smith, S.A.F., Mair, K., Nielsen, S.B., Candela, T., and Di Toro, G., 2013, Mirror-like faults and power dissipation during earthquakes: Geology, v. 41, p. 1175–1178, doi:10.1130/g34641.1.

Fondriest, M., Smith, S.A.F., Di Toro, G., Zampieri, D., and Mittempergher, S., 2012, Fault zone structure and seismic slip localization in dolostones, an example from the Southern Alps, Italy: Journal of Structural Geology, v. 45, p. 52–67, doi:10.1016/J.JSG.2012.06.014.

Fossen, H., 2016, Structural geology: Cambridge University Press.

Fracassi, U., 2001, Morphotectonic signature of the Campo Imperatore Quaternary basin (Central Apennines): implications for the seismotectonics of Central Italy, Unpublished Ph. D. thesis

Galadini, F., and Galli, P., 2000, Active tectonics in the Central Appennines (Italy) - Input data for seismic hazard assessment: Natural Hazards, v. 22, p. 225–270, doi:10.1023/A:1008149531980.

Galadini, F., and Galli, P., 1999, The Holocene paleoearthquakes on the 1915 Avezzano earthquake faults (central Italy): Implications for active tectonics in the central Apennines: Tectonophysics, v. 308, p. 143–170, doi:10.1016/S0040-1951(99)00091-8.

Galadini, F., and Messina, P., 2001, Plio-Quaternary changes of the normal fault architecture in the central Apennines (Italy): Geodinamica Acta, v. 14, p. 321–344.

Galli, P.A.C., Giaccio, B., Messina, P., Peronace, E., and Zuppi, G.M., 2011, Palaeoseismology of the L'Aquila faults (central Italy, 2009, Mw 6.3 earthquake): Implications for active fault linkage: Geophysical Journal International, v. 187, p. 1119–1134, doi:10.1111/j.1365-246X.2011.05233.x.

Gasperi, G., 1995, Geologia regionale: geologia dell'Italia e delle regioni circummediterranee: Pitagora editrice.

Ghisetti, F., and Vezzani, L., 1999, Depth and modes of Pliocene-Pleistocene crustal extension of the Apennines (Italy): Terra Nova, v. 11, p. 67–72, doi:10.1046/j.1365-3121.1999.00227.x.

Ghisetti, F., and Vezzani, L., 2002, Normal faulting, extension and uplift in the outer thrust belt of the central Apennines (Italy): Role of the Caramanico fault: Basin Research, v. 14, p. 225–236, doi:10.1046/j.1365-2117.2002.00171.x.

Green, A.A., and Craig, M.D., 1985, Analysis of aircraft spectrometer data with logarithmic residuals.

Green II, H.W., Shi, F., Bozhilov, K., Xia, G., and Reches, Z., 2015, Phase transformation and nanometric flow cause extreme weakening during fault slip: Nature Geoscience, v. 8, p. 484, https://doi.org/10.1038/ngeo2436.

Gudmundsson, A., Simmenes, T.H., Larsen, B., and Philipp, S.L., 2010, Effects of internal structure and local stresses on fracture propagation, deflection, and arrest in fault zones: Journal of Structural Geology, v. 32, p. 1643–1655.

Gueguen, E., Doglioni, C., and Fernandez, M., 1998, On the post-25 Ma geodynamic evolution of the western Mediterranean: Tectonophysics, v. 298, p. 259–269, doi:10.1016/S0040-1951(98)00189-9.

Gupta, A., and Scholz, C.H., 2000, A model of normal fault interaction based on observations and theory: Journal of Structural Geology, v. 22, p. 865–879, doi:10.1016/S0191-8141(00)00011-0.

Han, R., Hirose, T., and Shimamoto, T., 2010, Strong velocity weakening and powder lubrication of simulated carbonate faults at seismic slip rates: Journal of Geophysical Research: Solid Earth, v. 115, doi:10.1029/2008JB006136.

Han, R., Shimamoto, T., Hirose, T., Ree, J.-H., and Ando, J., 2007, Ultralow Friction of Carbonate Faults: Science, v. 316, p. 878–880.

Hunstad, I., Selvaggi, G., D'Agostino, N., England, P., Clarke, P., and Pierozzi, M., 2003, Geodetic strain in peninsular Italy between 1875 and 2001: Geophysical Research Letters, v. 30, p. 1–4, doi:10.1029/2002GL016447.

Jackson, J., and McKenzie, D., 1999, A hectare of fresh striations on the Arkitsa fault, central Greece: Journal of Structural Geology, v. 21, p. 1–6, doi:10.1016/S0191-8141(98)00091-1.

Kamb, W.B., 1959, Ice petrofabric observation from blue glacier, Washington, in relation to theory and experiment: Journal of geophysical research, v. 54.

Kim, Y.S., Peacock, D.C.P., and Sanderson, D.J., 2004, Fault damage zones: Journal of Structural Geology, v. 26, p. 503–517, doi:10.1016/j.jsg.2003.08.002.

Kim, Y.S., and Sanderson, D.J., 2005, The relationship between displacement and length of faults: A review: Earth-Science Reviews, doi:10.1016/j.earscirev.2004.06.003.

Lavecchia, G., de Nardis, R., Cirillo, D., Brozzetti, F., and Boncio, P., 2012, The May-June 2012 Ferrara Arc earthquakes (northern Italy): structural control of the spatial evolution of the seismic sequence and of the surface pattern of coseismic fractures: Annals of Geophysics, v. 55.

Leah, H., Fondriest, M., Lucca, A., Storti, F., Balsamo, F., and Di Toro, G., 2018, Coseismic extension recorded within the damage zone of the Vado di Ferruccio Thrust Fault, Central Apennines, Italy: Journal of Structural Geology, v. 114, p. 121–138, doi:10.1016/j.jsg.2018.06.015.

Li, Y.-G., and Leary, P.C., 1990, Fault zone trapped seismic waves: Bulletin of the Seismological Society of America, v. 80, p. 1245–1271.

Lustrino, M., Morra, V., Fedele, L., and Franciosi, L., 2009, Beginning of the Apennine subduction system in central western Mediterranean: Constraints from Cenozoic "orogenic" magmatic activity of Sardinia, Italy: Tectonics, v. 28, p. 1–23, doi:10.1029/2008TC002419.

Ma, S., and Andrews, D.J., 2010, Inelastic off-fault response and three-dimensional dynamics of earthquake rupture on a strike-slip fault: Journal of Geophysical Research, v. 115, p. 1–16, doi:10.1029/2009jb006382.

Maceroni, D., Racano, S., Falcucci, E., and Gori, S., 2018, Application of quaternary studies for the assessment of active and capable faults in the central Apennines : Implications for microzonation and seismotectonic analyses.

Machette, M.N., 2000, Active, capable, and potentially active faults - a paleoseismic perspective: Journal of Geodynamics, v. 29, p. 387–392, doi:10.1016/S0264-3707(99)00060-5.

Malinverno, A., and Ryan, W.B.F., 1986, Exthension in the Tyrrhenian sea and shortening in the Apennines as result of arc migration driven by sinking of the lithosphere: Tectonics, v. 5, p. 227–245.

Manighetti, I., King, G., and Sammis, C.G., 2004, The role of off-fault damage in the evolution of normal faults: Earth and Planetary Science Letters, v. 217, p. 399–408, doi:10.1016/S0012-821X(03)00601-0.

Marrett, R., and Allmendinger, R.W., 1990, Kinematic analysis of fault-slip data: Journal of Structural Geology, v. 12, p. 973–986, doi:10.1016/0191-8141(90)90093-E.

Mayolle, S., Soliva, R., Caniven, Y., Wibberley, C., Ballas, G.G., Milesi, G., and Dominguez, S.S., 2019, Scaling of fault damage zones in carbonate rocks: Journal of Structural Geology, v. 124, p. 35–50, doi:10.1016/j.jsg.2019.03.007.

Micarelli, L., Benedicto, A., and Wibberley, C.A.J., 2006, Structural evolution and permeability of normal fault zones in highly porous carbonate rocks: Journal of Structural Geology, v. 28, p. 1214–1227, doi:10.1016/j.jsg.2006.03.036.

Michetti, A.M., Brunamonte, F., Serva, L., and Vittori, E., 1996, Trench investigations of the 1915 Fucino earthquake fault scarps (Abruzzo, Central Italy): geological evidence of large historical events: Journal of Geophysical Research: Solid Earth, v. 101, p. 5921–5936.

Michetti, A.M., Serva, L., and Vittori, E., 2000, ITHACA (Italy hazard from Capable Faulting), a database of active capable faults of the Italian onshore territory: Database on CD-ROM, Int. Rep. of ANPA (Agenzia Nazionale Protezione Ambiente).

Michie, E.A.H. et al., 2014, Influence of carbonate facies on fault zone architecture: Journal of Structural Geology, v. 65, p. 82–99, doi:10.1016/j.jsg.2014.04.007.

Mitchell, T.M., Ben-Zion, Y., and Shimamoto, T., 2011, Pulverized fault rocks and damage asymmetry along the Arima-Takatsuki Tectonic Line, Japan: Earth and Planetary Science Letters, v. 308, p. 284–297, doi:10.1016/j.epsl.2011.04.023.

Mitchell, T.M., and Faulkner, D.R., 2009, The nature and origin of off-fault damage surrounding strike-slip fault zones with a wide range of displacements: A field study from the Atacama fault system, northern Chile: Journal of Structural Geology, v. 31, p. 802–816, doi:10.1016/j.jsg.2009.05.002.

Morelli, L.A., Bonardi, G., Colonna, V., and Dietrich, D., 1976, L'arco calabro-peloritano nell'orogene appenninico-maghrebide.

Morewood, N.C., and Roberts, G.P., 2000, The geometry, kinematics and rates of deformation within an en echelon normal fault segment boundary, central Italy: Journal of Structural Geology, v. 22, p. 1027–1047, doi:10.1016/S0191-8141(00)00030-4.

Moro, M., Bosi, V., Galadini, F., Galli, P., Giaccio, B., Messina, P., and Sposato, A., 2002, Analisi paleosismologiche lungo la faglia del M. Marine (alta Valle dell'Aterno): risultati preliminari: Il Quaternario, v. 15, p. 267–278.

Moro, M., Moro, M., Falcucci, E., Gori, S., Saroli, M., and Galadini, F., 2016, New paleoseismic data across the Mt. Marine Fault between the 2016 Amatrice and 2009 L'Aquila seismic sequences (central Apennines): Annals of Geophysics, v. 59, p. 1–7, doi:10.4401/ag-7260.

Nielsen, S., Spagnuolo, E., Smith, S.A.F., Violay, M., Di Toro, G., and Bistacchi, A., 2016, Scaling in natural and laboratory earthquakes: Geophysical Research Letters, v. 43, p. 1504–1510.

Okubo, K., Bhat, H.S., Rougier, E., Marty, S., Schubnel, A., Lei, Z., Knight, E.E., and Klinger, Y., 2019, Dynamics, radiation and overall energy budget of earthquake rupture with coseismic off-fault damage: Journal of Geophysical Research: Solid Earth, p. 1–43, doi:10.1029/2019jb017304.

Pace, P., Domenica, A. Di, and Calamita, F., 2014, Summit low-angle faults in the Central Apennines of Italy: Younger-on-older thrusts or rotated normal faults? Constraints for defining the tectonic style of thrust belts: Tectonics, v. 33, p. 756–785, doi:10.1002/2013TC003385.

Papanikolaou, I.D., Roberts, G.P., and Michetti, A.M., 2005, Fault scarps and deformation rates in Lazio-Abruzzo, Central Italy: Comparison between geological fault slip-rate and GPS data: Tectonophysics, v. 408, p. 147–176, doi:10.1016/j.tecto.2005.05.043.

Patacca, E., Sartori, R., and Scandone, P., 1990, Tyrrhenian basin and Apenninc arcs: kinematic relations since Late Tortonian times.: Mem. Soc. Geol. It, v. 45, p. 425–451.

Peacock, D.C.P., Dimmen, V., Rotevatn, A., and Sanderson, D.J., 2017, A broader classification of damage zones: Journal of Structural Geology, v. 102, p. 179–192, doi:10.1016/j.jsg.2017.08.004.

Peacock, D.C.P., Knipe, R.J., and Sanderson, D.J., 2000, Glossary of normal faults: Journal of Structural Geology, v. 22, p. 291–305, doi:10.1016/S0191-8141(00)80102-9.

Perrin, C., Manighetti, I., and Gaudemer, Y., 2016, Off-fault tip splay networks: A genetic and generic property of faults indicative of their long-term propagation: Comptes Rendus - Geoscience, v. 348, p. 52–60, doi:10.1016/j.crte.2015.05.002.

Pizzi, A., and Galadini, F., 2009, Pre-existing cross-structures and active fault segmentation in the northern-central Apennines (Italy): Tectonophysics, v. 476, p. 304–319, doi:10.1016/j.tecto.2009.03.018.

Power, W., and Tullis, T., 1989, The relationship between slickenside surfaces in fine-grained quartz and the seismic cycle: Journal of Structural Geology, v. 11, p. 879–893.

Pozzi, G., De Paola, N., Nielsen, S.B., Holdsworth, R.E., and Bowen, L., 2018, A new interpretation for the nature and significance of mirror-like surfaces in experimental carbonate-hosted seismic faults: Geology, v. 46, p. 583–586, doi:10.1130/G40197.1.

Rempe, M., Mitchell, T.M., Renner, J., Smith, S.A.F., Bistacchi, A., and Di Toro, G., 2018, The Relationship Between Microfracture Damage and the Physical Properties of Fault-Related Rocks: The Gole Larghe Fault Zone, Italian Southern Alps: Journal of Geophysical Research: Solid Earth, v. 123, p. 7661–7687.

Roberts, G.P., and Michetti, A.M., 2004, Spatial and temporal variations in growth rates along active normal fault systems: An example from The Lazio-Abruzzo Apennines, central Italy: Journal of Structural Geology, v. 26, p. 339–376, doi:10.1016/S0191-8141(03)00103-2.

Rovida, A., Locati, M., Camassi, R., and Lolli, B., 2016, CPTI15, the 2015 version of the Parametric Catalogue of Italian Earthquakes.

Rowe, C.D., and Griffith, W.A., 2015, Do faults preserve a record of seismic slip: A second opinion: Journal of Structural Geology, v. 78, p. 1–26, doi:10.1016/j.jsg.2015.06.006.

Salvini, F., Billi, A., and Wise, D.U., 1999, Strike-slip fault-propagation cleavage in carbonate rocks: the Mattinata Fault Zone, Southern Apennines, Italy: Journal of Structural Geology, v. 21, p. 1731–1749.

Saroli, M. et al., 2008, Nuovi Dati Paleosismologici Dal Settore Orientale Del Bacino Del Fucino (Italia Centrale): Italian Journal of Quaternary Sciences, v. 21, p. 383–394.

Savage, H.M., and Brodsky, E.E., 2011, Collateral damage: Evolution with displacement of fracture distribution and secondary fault strands in fault damage zones: Journal of Geophysical Research: Solid Earth, v. 116, p. 1–14, doi:10.1029/2010JB007665.

Scholz, C.H., 2019, The mechanics of earthquakes and faulting: Cambridge university press.

Scholz, C.H., Dawers, N.H., Yu, J., Anders, M.H., and Cowie, P.A., 1993, Fault growth and fault scaling laws: preliminary results: Journal of Geophysical Research: Solid Earth, v. 98, p. 21951–21961.

Schröckenfuchs, T., Bauer, H., Grasemann, B., and Decker, K., 2015, Rock pulverization and localization of a strike-slip fault zone in dolomite rocks (Salzach-Ennstal-Mariazell-Puchberg fault, Austria): Journal of Structural Geology, v. 78, p. 67–85, doi:10.1016/j.jsg.2015.06.009.

Shipton, Z.K., and Cowie, P.A., 2001, Damage zone and slip-surface evolution over μm to km scales in high-porosity Navajo sandstone, Utah: Journal of Structural Geology, doi:10.1016/S0191-8141(01)00035-9.

Shipton, Z.K., and Cowie, P.A., 2003, A conceptual model for the origin of fault damage zone structures in high-porosity sandstone: Journal of Structural Geology, v. 25, p. 333–344, doi:https://doi.org/10.1016/S0191-8141(02)00037-8.

Shipton, Z.K., Evans, J.P., Abercrombie, R.E., and Brodsky, E.E., 2006a: The missing sinks slip localization in faults, damage zones, and the seismic energy budget.

Shipton, Z.K., Evans, J.P., and Thompson, L.B., 2005, The geometry and thickness of deformation-band fault core and its influence on sealing characteristics of deformation-band fault zones:

Shipton, Z.K., Soden, A.M., Kirkpatrick, J.D., Bright, A.M., and Lunn, R.J., 2006b, How thick is a fault? Fault displacement-thickness scaling revisited.

Sibson, R.H., 1977, Fault rocks and fault mechanisms: Journal of the Geological Society, v. 133, p. 191–213, doi:10.1144/gsjgs.133.3.0191.

Sibson, R.H., 1985, Stopping of earthquake ruptures at dilational fault jogs: Nature, v. 316, p. 248–251, doi:10.1038/316248a0.

Sibson, R.H., 1986, Brecciation processes in fault zones: Inferences from earthquake rupturing: Pure and Applied Geophysics PAGEOPH, v. 124, p. 159–175, doi:10.1007/BF00875724.

Sibson, R.H., 2003, Thickness of the seismic slip zone: Bulletin of the Seismological Society of America, v. 93, p. 1169–1178, doi:10.1785/0120020061.

Siman-Tov, S., Aharonov, E., Boneh, Y., and Reches, Z., 2015, Fault mirrors along carbonate faults: Formation and destruction during shear experiments: Earth and Planetary Science Letters, v. 430, p. 367–376, doi:10.1016/j.epsl.2015.08.031.

Siman-Tov, S., Aharonov, E., Sagy, A., and Emmanuel, S., 2013, Nanograins form carbonate fault mirrors: Geology, v. 41, p. 703–706, doi:10.1130/G34087.1.

Smith, S.A.F., Billi, A., di Toro, G., and Spiess, R., 2011, Principal Slip Zones in Limestone: Microstructural Characterization and Implications for the Seismic Cycle (Tre Monti Fault, Central Apennines, Italy): Pure and Applied Geophysics, v. 168, p. 2365–2393, doi:10.1007/s00024-011-0267-5.

Smith, S.A.F., Di Toro, G., Kim, S., Ree, J.H., Nielsen, S., Billi, A., and Spiess, R., 2013, Coseismic recrystallization during shallow earthquake slip: Geology, v. 41, p. 63–66, doi:10.1130/G33588.1.

Smith, S.A.F., Nielsen, S., and Di Toro, G., 2015, Strain localization and the onset of dynamic weakening in calcite fault gouge: Earth and Planetary Science Letters, v. 413, p. 25–36, doi:https://doi.org/10.1016/j.epsl.2014.12.043.

Soliva, R., Benedicto, A., and Maerten, L., 2006, Spacing and linkage of confined normal faults: importance of mechanical thickness: Journal of Geophysical Research: Solid Earth, v. 111.

Spagnuolo, E., Plümper, O., Violay, M., Cavallo, A., and Di Toro, G., 2015, Fast-moving dislocations trigger flash weakening in carbonate-bearing faults during earthquakes: Scientific Reports, v. 5, p. 16112, https://doi.org/10.1038/srep16112.

Tarasewicz, J.P.T., Woodcock, N.H., and Dickson, J.A.D., 2005, Carbonate dilation breccias: Examples from the damage zone to the Dent Fault, northwest England: Bulletin of the Geological Society of America, doi:10.1130/B25568.1.

Torabi, A., and Berg, S.S., 2011, Scaling of fault attributes: A review: Marine and Petroleum Geology, v. 28, p. 1444–1460, doi:10.1016/j.marpetgeo.2011.04.003.

Traforti, A., Mari, G., Carli, C., Demurtas, M., Massironi, M., and Di Toro, G., 2017, VNIR reflectance spectroscopy of natural carbonate rocks: implication for remote sensing identification of fault damage zones: EGU General Assembly, v. 19, p. 7935.

Valoroso, L., Chiaraluce, L., Piccinini, D., Di Stefano, R., Schaff, D., and Waldhauser, F., 2013, Radiography of a normal fault system by 64,000 high-precision earthquake locations: The 2009 L'Aquila (central Italy) case study: Journal of Geophysical Research: Solid Earth, v. 118, p. 1156–1176, doi:10.1002/jgrb.50130.

Verberne, B.A., de Bresser, J.H.P., Niemeijer, A.R., Spiers, C.J., de Winter, D.A.M., and Plümper, O., 2013, Nanocrystalline slip zones in calcite fault gouge show intense crystallographic preferred orientation: Crystal plasticity at sub-seismic slip rates at 18–150 C: Geology, v. 41, p. 863–866.

Verberne, B.A., Spiers, C.J., Plümper, O., De Winter, D.A.M., and Spiers, C.J., 2014, Supplementary Materials for Superplastic nanofibrous slip zones control seismogenic fault friction: Science, v. 346, p. 1342–1344, doi:10.1126/science.1259003.

Vermilye, J.M., and Scholz, C.H., 1998, The process zone: A microstructural view of fault growth: Journal of Geophysical Research: Solid Earth, v. 103. p. 12223-12237.

Vezzani, L., Festa, A., and Ghisetti, F.C., 2010, Geology and Tectonic Evolution of the Central-Southern Apennines, Italy: Geological Society of America, p. 1–58, doi:10.1130/2010.2469.

Vezzani, L., Ghisetti, F., Bigozzi, A., Follador, U., and Casnedi, R., 1998, Carta geologica dell'Abruzzo: scala 1: 100.000: Selca.

Walsh, J.J., and Watterson, J., 1988, Analysis of the relationship between displacements and dimensions of faults: Journal of Structural Geology, v. 10, p. 239–247, doi:10.1016/0191-8141(88)90057-0.

Wechsler, N., Allen, E.E., Rockwell, T.K., Girty, G., Chester, J.S., and Ben-Zion, Y., 2011, Characterization of pulverized granitoids in a shallow core along the San Andreas Fault, Littlerock, CA: Geophysical Journal International, v. 186, p. 401–417, doi:10.1111/j.1365-246X.2011.05059.x.

Wesnousky, S.G., 2006, Predicting the endpoints of earthquake ruptures: Nature, v. 444, p. 358–360, doi:10.1038/nature05275.

Wibberley, C.A.J., Yielding, G., and Di Toro, G., 2008, Recent advances in the understanding of fault zone internal structure: a review: Geological Society, London, Special Publications, v. 299, p. 5–33, doi:10.1144/sp299.2.

Wilkinson, M., Roberts, G.P., McCaffrey, K., Cowie, P.A., Walker, J.P.F., Papanikolaou, I., Phillips, R.J., Michetti, A.M., Vittori, E., and Gregory, L., 2015, Slip distributions on active normal faults measured from LiDAR and field mapping of geomorphic offsets: an example from L'Aquila, Italy, and implications for modelling seismic moment release: Geomorphology, v. 237, p. 130–141.

Woodcock, N.H., and Mort, K., 2008, Classification of fault breccias and related fault rocks: Geological Magazine, v. 145, p. 435–440, doi:10.1017/S0016756808004883.

Yuan, F., Prakash, V., and Tullis, T., 2011, Origin of pulverized rocks during earthquake fault rupture: Journal of Geophysical Research: Solid Earth, v. 116, p. 1–18, doi:10.1029/2010JB007721.

References of the catalogue

Carta geologica d'Italia alla scala 1:50.000, foglio 368 Avezzano.

Carta geologica d'Italia alla scala 1:50.000, foglio 369 Sulmona.

Carta geologica d'Italia alla scala 1:50.000, foglio 378 Scanno.

Carta geologica d'Italia alla scala 1:50.000, foglio 359 L'Aquila

Agosta F. and Aydin A., Architecture and deformation mechanism of a basin-bounding normal fault in mesozoic platform carbonates, central Italy. Journal of Structural Geology, 28(8):1445–1467, **2006**.

Agosta F. and Kirschner, Fluid conduits in carbonate-hosted seismogenic normal faults of central Italy. Journal of Geophysical Research: Solid Earth, 108(B4), **2003**.

Barchi M., Lavecchia G. , Galadini F., Messina P., Michetti A., Peruzza L., Pizzi A., Tondi E., Vittori E., Sintesi delle conoscenze sulle faglie attive in italia Centrale: parametrizzazione ai fini della caratterizzazione della pericolosita` sismica. **2000**.

Billi A., Di Toro G., Landowe S.J., Hammlerp G.M., Fault-related carbonate rocks and earthquake indicators: recent advances and future trends. Structural Geology: New Research, pages 63–86, **2008**.

Blumetti A.M., Guerrieri L., Fault-generated mountain fronts and the identification of fault segments: implications for seismic hazard assessment. Bollettino della Società Geologica Italiana, 126(2):307, **2007**.

Bubeck A.,Wilkinson M., Roberts G.P., Cowie P.A., McCaffrey K.J.W., Phillips R., Sammonds P., The tectonic geomorphology of bedrock scarps on active normal faults in the italian apennines mapped using combined ground penetrating radar and terrestrial laser scanning. Geomorphology, 237:38–51, **2015**.

Cavinato G.P., Carusi C., Dall'Asta M., Miccadei E., Piacentini T., Sedimentary and tectonic evolution of plio–pleistocene allu- vial and lacustrine deposits of fucino basin (Central Italy). Sedimentary Geology, 148(1-2):29–59, **2002**.

Chiarabba C., Amato A., Anselmi M., Baccheschi P., Bianchi I., Cattaneo M., Cecere G., Chiaraluce L., Ciaccio M.G., De Gori P., et al., The 2009 l'aquila (Central Italy) mw6. 3 earthquake: Main shock and aftershocks. Geophysical Research Letters, 36(18), **2009**.

Cortinovis S., Balsamo F., Storti F., Di Toro G., Architecture and microstructural properties of the seismogenetic monte marine extensional fault affecting partially dolomitized

carbonate rocks, Central Apennines (Italy). In EGU General Assembly Conference Abstracts, 20:12655, **2018**.

Demurtas M., Fondriest M., Balsamo F., Clemenzi L., Storti F., Bistacchi A., Di Toro G., Structure of a normal seismoge- nic fault zone in carbonates: the vado di corno fault, campo imperatore, Central Apennines (Italy). Journal of Structural Geology, 90:185–206, **2016**.

Galadini F. and Galli P., Active tectonics in the Central Apennines (Italy)– input data for seismic hazard assessment. Natural Hazards, 22(3):225–268, **2000**.

Falcucci E., Gori S., Moro M., Fubelli G., Saroli M., Chiarabba C., Galadini F., Deep reaching versus vertically restricted quaternary normal faults: Implications on seismic potential assessment in tectonically active regions: Lessons from the middle aterno valley fault system, Central Italy. Tectonophysics, 651:186– 198**, 2015**.

Faure Walker J.P., Roberts G.P., Sammonds P.R., Cowie P., Comparison of earthquake strains over 102 and 104 year timescales: Insights into variability in the seismic cycle in the Central apennines, Italy. Journal of Geophysical Research: Solid Earth, 115(B10), **2010**.

Ferraro F., Grieco D.S., Agosta F., Prosser G., Space-time evolution of cataclasis in carbonate fault zones. Journal of Structural Geology, 110:45–64, **2018**.

Galadini F., Archaeoseismology in Italy: case studies and implications on long-term seismicity. Journal of Earthquake Engineering, 5:35–68, **2001**.

Galadini F. and Galli P., The holocene paleoearthquakes on the 1915 Avezzano earthquake faults (Central Italy): implications for active tectonics in the Central apennines. Tectonophysics, 308(1-2):143–170, **1999**.

Galli P., Galadini F., Moro M., Giraudi C., New paleoseismological data from the gran sasso d'italia area (Central apennines). Geophysical Research Letters, 29(7):38–1, **2002**.

Galli P., Giaccio B., Messina P., Peronace E., Zuppi G.M., Palaeoseismology of the L'Aquila faults (Central Italy, 2009, Mw 6.3 earthquake): Implications for active fault linkage. Geophysical Journal International, 187(3):1119–1134, **2011.**

Ghisetti F. and Vezzani L., Thrust belt development in the Central apen- nines (Italy): Northward polarity of thrusting and out-of-sequence deformations in the gran sasso chain. Tectonics, 10(5):904–919, **1991**.

Gori S., Giaccio B., Galadini F., Falcucci E., Messina P., Sposato A., Dramis F., Active normal faulting along the mt. morrone south-western slopes (Central apennines, Italy). International journal of earth sciences, 100(1):157–171, **2011**.

Miccadei E., Paron P, Piacentini T., The sw escarpment of the montagna del morrone (abruzzi, Central Italy): geomorphology of a faulted- generated mountain front. Geografia Fisica e Dinamica Quaternaria, 27(1):55–87, **2004**.

Morewood N. and Roberts G., The geometry, kinematics and rates of defor- mation within an en echelon normal fault segment boundary, Central Italy. Journal of Structural Geology, 22(8):1027–1047, **2000**.

Moro M., Falcucci E., Gori S., Saroli M., Galadini F., New paleoseismic data across the mt. marine fault between the 2016 amatrice and 2009 l'aquila seismic sequences (Central apennines). Annals of geophisycs, **2016**.

Papanikolaou I.D., Roberts G.P., Michetti A.M., Fault scarps and deformation rates in lazio–abruzzo, Central Italy: Comparison between geological fault slip-rate and gps data. Tectonophysics, 408(1-4):147–176, **2005**.

Piccardi P., Gaudemer Y., Tapponnier P., Boccaletti M., Active oblique extension in the Central apennines (Italy): Evidence from the fucino region. Geophysical Journal International, 139:499 – 530, 11 **1999**.

Roberts G.P., and Michetti A.M., Spatial and temporal variations in growth rates along active normal fault systems: an example from the lazio–abruzzo apennines, Central Italy. Journal of Structural Geology, 26(2):339–376, **2004**.

Vezzani L. and Ghisetti F., Carta geologica dell'Abruzzo: scala 1: 100,000. **1998**.

Working Group DISS. Database of individual seismogenic sources (DISS), version 3.2.1: A compilation of potential sources for earthquakes larger than M 5.5 in Italy and surrounding areas, **2018**.

Appendix

A. *Table of samples*

B. *Poster 1*

C. *Poster 2*

Locality	UTM (WGS 84) Coordinates	Sample	Structural Domain	Type	Attitude			Thin Section	SEM	Polished sec.
					Dip az.	Dip	Pitch			
Station 5.7	361839 E 4699757 N	**MM 5.0**	Slip zone	Thrust	270	19	110	X		
Station 5.3	362313 E 4699524 N	**MM 5.1**	Slip zone	Normal Fault	190	75	75	X		
	362524 E 4699655 N	**MM 5.2**	Slip zone	N. Fault	246	81				
Station 5.9	362538 E 4699717 N	**MM 5.3**	Slip zone	Thrust	220	38	100	X	X	
Station 5.9	362538 E 4699717 N	**MM 5.4**		Loose cataclasite (Thrust)						
Station 5.13	362827 E 4699900 N	**MM 5.5**	Host Rock					X		
Station 5.14	362697 E 4699349 N	**MM 5.6**	Slip zone	N. Fault	232	50	75	X	X	
Station 5.14	362754 E 4699391 N	**MM 5.7**	Slip zone	N. fault	184	59	90	X		
Station 5.16	363346 E 4999047 N	**MM 5.8**	Slip zone	N. fault	348	55		X		
Station 5.16	363346 E 4999047 N	**MM 5.9**	Slip zone	N. fault	257	40		X		
Station 5.16	363346 E 4999047 N	**MM 5.10**		Loose cataclasite						
Station 6.4	362988 E 4699368 N	**MM 6.0**	Green Veined Breccia	Fault Breccia						
Station 5.14	362697 E 4699349 N	**MM 6.1**	Green Veined Breccia	Dolostone with Oncoids						
Station 5.14	362697 E 4699349 N	**MM 6.2**	Green Veined Breccia	Fault Breccia				X		X
Station 5.4	362210 E 4699608 N	**MM 6.3**	Facies 3c	ISRs	195	55				
Station 5.4	362210 E 4699608 N	**MM 6.4**	Facies 3c	ISRS	232	80		X		X
Station 5.4	362224 E 4699608 N	**MM 6.5**	Facies 3c	ISRs	010	86				
Station 5.6	361997 E 4699616 N	**MM 6.6**	Facies 3c	ISRs	190	71				
Station 5.6	361997 E 4699616 N	**MM 6.7**	Facies 3c	ISRs	049	88				
Station 5.7	362306 E 4699580 N	**MM 6.8**	Facies 3a	ISRs	149	40		X		8
Station 5.7	362306 E 4699580 N	**MM 6.9**	Facies 3a	ISRs				X		
Station 5.7	362306 E 4699580 N	**MM 6.10**	Facies 3a	ISRs	242	88				
Station 5.7	362330 E 4699541 N	**MM 6.11**	Facies 3a	ISRs	259	73				

Acknowledgments

Ringrazio le figure che mi sono stati Maestri, coloro cioè che con la trascinante forza dell'esempio mi hanno accompagnato nelle salite, sempre solo fino all'anticima.
La mia famiglia innanzitutto, per la costante mano sulla spalla, e per l'appoggio incondizionato datomi in ogni scelta.
Il Prof Giulio Di Toro, per le possibilità offerte, per la fiducia, per la passione tumultuosa per la Geologia e la scienza che spesso esonda e contagia.
Michele Fondriest, per la leggerezza da mettere nelle cose, per gli incoraggiamenti e per la grande esperienza nel lavoro di campagna dalla quale ho potuto prendere esempio.
Il prof. Cannonieri, per la mente critica e spirito umanistico che gli è riuscito di inculcarci.
I libri che leggo e l'aria fresca che portano.

Ringrazio gli amici. Matteo una volta ha detto: "Fabio, l'amicizia sta negli occhi di chi guarda", e, aggiungo ora io, anche negli occhi di chi ti guarda *da lontano*, tenendoti d'occhio ma non per mano.
A Michele e Matteo (quello degli *occhi di chi guarda*), con cui il tempo ha stretto sempre di più i nodi della rete che ci rende amici.
A Marco e Mattia, per il loro essere Maestri e, non esaurendosi in questo, essere soprattutto molto amici, di quelli che sull'amicizia potrebbero tenere un corso universitario.
Al Gruppo Animatori, per la grande parte di cammino affrontata insieme in questi anni, nell'amicizia e nella fatica dei tanti appuntamenti, nel dormire in tenda e nello stare seduti in cerchio a condividere.

Ringrazio i vecchi e meno vecchi coinquilini che in questi anni universitari hanno provato cosa significa vedere un "ubriaco di studio" e per averlo sopportato.

Ringrazio chi altro per questa tesi è stato in "calanco" assieme a me: Silvia Cortinovis, il prof. Fabrizio Balsamo, Miriana e Luca.

Ringrazio Leonardo Tauro per la supervisione durante la preparazione dei campioni e sezioni sottili e ringrazio Andrea Cavallo per averci seguito durante le sessioni al FE-SEM.

Ringrazio Donato Sigolo, per aver seguito con solerzia il "ritardo nella procedura di conseguimento titolo".

Ringrazio, infine, il geotermometro a granato e biotite [1] che mi ha insegnato come due minerali, proprio perché ricchi di elementi diversi, se sono vicini rimangono all'equilibrio nonostante le avversità di pressione e temperatura. Granato e Biotite si scambiano reciprocamente Ferro e Magnesio: basta così poco per renderli felici (i.e., in equilibrio). Li vedessi in sezione sottile! Non diresti mai che questi due si sono fatti una tirata di 300 °C perchè hanno l'aspetto di due innamorati che escono a braccetto dalla sauna, di certo sudati, ma felici perchè insieme. Un po' come me e Irene. Di questo paragone Irene sapeva già, ma ho voluto ripeterglielo (1) per sottolineare che la geologia sa essere anche poetica e (2) per avere nuovamente l'occasione di dirle che la amo.

[1] Ferry, Spear 1978, Experimental calibration of the partitioning of Fe and Mg between biotite and garnet, Contributions to Mineralogy and Petrology, Volume 66, Issue 2, pp 113–117